

LISBON UNIVERSITY  
FACULTY OF SCIENCES  
CENTRO DE MATEMÁTICA E  
APLICAÇÕES FUNDAMENTAIS

VRIJE UNIVERSITY AMSTERDAM  
FACULTY OF EARTH AND LIFE  
SCIENCE  
DEPARTMENT OF THEORETICAL  
BIOLOGY



**UNIVERSIDADE  
DE LISBOA**



RICH DYNAMICS IN MULTI-STRAIN MODELS:  
NON-LINEAR DYNAMICS AND DETERMINISTIC  
CHAOS IN DENGUE FEVER EPIDEMIOLOGY

MAÍRA AGUIAR FREIRE DOS SANTOS

PHD THESIS IN ASSOCIATION  
TO OBTAIN THE DOCTORAL DEGREE IN BIOLOGY WITH SPECIALIZATION IN  
POPULATION BIOLOGY OF LISBON UNIVERSITY, AND TO OBTAIN THE  
DOCTORAL DEGREE IN LIFE SCIENCES OF VRIJE UNIVERSITEIT AMSTERDAM

2012

LISBON UNIVERSITY  
FACULTY OF SCIENCES  
CENTRO DE MATEMÁTICA E  
APLICAÇÕES FUNDAMENTAIS

VRIJE UNIVERSITY AMSTERDAM  
FACULTY OF EARTH AND LIFE  
SCIENCE  
DEPARTMENT OF THEORETICAL  
BIOLOGY



**UNIVERSIDADE  
DE LISBOA**



**RICH DYNAMICS IN MULTI-STRAIN MODELS:  
NON-LINEAR DYNAMICS AND DETERMINISTIC  
CHAOS IN DENGUE FEVER EPIDEMIOLOGY**

**MAÍRA AGUIAR FREIRE DOS SANTOS**

PHD THESIS IN ASSOCIATION  
TO OBTAIN THE DOCTORAL DEGREE IN BIOLOGY WITH SPECIALIZATION IN  
POPULATION BIOLOGY OF LISBON UNIVERSITY, AND TO OBTAIN THE  
DOCTORAL DEGREE IN LIFE SCIENCES OF VRIJE UNIVERSITEIT AMSTERDAM  
THESIS SUPERVISED BY PROFESSOR DOCTOR BOB W. KOOI AND  
PROFESSOR DOCTOR FRANCISCO DIONÍSIO

2012

Acknowledgments: This thesis was done in association with Amsterdam University. The research in this thesis has been supported by the Fundação para a Ciência e a Tecnologia, FCT grant SFRH/BD/43236/2008, and has been further supported by the Portuguese FCT project PTDC/MAT/115168/2009 and by the EU project DENFREE under Framework Program 7. The work was carried out at Centro de Matemática e Aplicações Fundamentais, Science Faculty, Lisbon University, Portugal.

**Note:** For interpretation of the references to color in the figures and figure legends, the reader is referred to the electronic version of this thesis and or to the web version of each article.

“In the middle of difficulty lies  
opportunity.”

---

Albert Einstein





# Contents

<b>Resumo</b>	<b>7</b>
<b>Samenvatting</b>	<b>13</b>
<b>English summary</b>	<b>19</b>
<b>1 Introduction</b>	<b>25</b>
1.1 The SIR Epidemic Model . . . . .	27
1.2 Dengue fever Epidemiology . . . . .	31
1.3 Multi-strain models motivated by dengue fever epidemiology: a review . . . . .	36
1.4 Discussion and conclusions . . . . .	50
<b>2 Epidemiology of dengue fever: A model with temporary cross-immunity and possible secondary infection shows bifurcations and chaotic behavior in wide parameter regions</b>	<b>53</b>
2.1 Introduction . . . . .	54
2.2 Basic two-strain epidemic model . . . . .	56
2.3 Time series analysis . . . . .	58
2.3.1 Time series simulations . . . . .	59
2.3.2 State space plots . . . . .	60
2.3.3 Maxima return map of $I$ from state space plot . . . . .	61
2.3.4 Numerical bifurcation diagram . . . . .	61
2.3.5 Quantifying unpredictability: Lyapunov exponents . . . . .	64
2.4 Bifurcation analysis by continuation . . . . .	66
2.4.1 Stationary states for the symmetric case . . . . .	66
2.4.2 Bifurcations analysis beyond equilibria . . . . .	68
2.5 Conclusion . . . . .	74
<b>3 Torus bifurcations, isolas and chaotic attractors in a simple dengue fever model with ADE and temporary cross-immunity</b>	<b>77</b>
3.1 Introduction . . . . .	77
3.2 Dynamical system . . . . .	80

3.2.1	Symmetries . . . . .	80
3.3	Bifurcation diagrams for various $\alpha$ values . . . . .	82
3.3.1	Bifurcation diagram for $\alpha = 3y^{-1}$ . . . . .	82
3.3.2	Bifurcation diagram for $\alpha = 2y^{-1}$ . . . . .	83
3.3.3	Bifurcation diagram for $\alpha = 1y^{-1}$ . . . . .	84
3.4	Two-parameter diagram . . . . .	86
3.5	Lyapunov spectra for various $\alpha$ values . . . . .	87
3.6	Conclusions . . . . .	88
	Appendix . . . . .	88
3.A	Epidemic model equations . . . . .	88
<b>4</b>	<b>The role of seasonality and import in a minimalistic multi-strain dengue model capturing differences between primary and secondary infections: complex dynamics and its implications for data analysis</b>	<b>91</b>
4.1	Introduction . . . . .	92
4.2	The seasonal multi-strain epidemic model . . . . .	94
4.3	Analysis techniques . . . . .	97
4.4	Bifurcation analysis . . . . .	99
4.4.1	Bifurcation analysis of the non-seasonal model . . . . .	100
4.4.2	Bifurcation analysis of the seasonal models . . . . .	102
4.5	Time series . . . . .	106
4.5.1	Lyapunov exponents and predictability: . . . . .	108
4.5.2	Implications for data analysis: . . . . .	110
4.6	Discussion and conclusions . . . . .	110
	Appendix . . . . .	113
4.A	Seasonal forcing . . . . .	113
4.B	Attractors in state space . . . . .	114
4.B.1	Attractors in state space for the non-seasonal multi-strain dengue model . . . . .	114
4.B.2	Attractors in state space for the low seasonal multi-strain dengue model . . . . .	117
4.B.3	Attractors in state space for the seasonal multi-strain dengue model with import of infected . . . . .	118
4.C	Bifurcation diagram comparison . . . . .	119
4.D	Lyapunov exponents and import factor . . . . .	119
<b>5</b>	<b>Scaling of stochasticity in dengue hemorrhagic fever epidemics</b>	<b>123</b>
5.1	Introduction . . . . .	123
5.2	Modeling dengue fever epidemiology . . . . .	124
5.3	The stochastic model . . . . .	125
5.4	The role of import . . . . .	129
5.5	Scaling of stochasticity . . . . .	132

5.6	Conclusions . . . . .	134
<b>6</b>	<b>Irregularity in dengue fever epidemics: difference between first and secondary infections drives the rich dynamics more than the detailed number of strains</b>	<b>137</b>
6.1	Introduction . . . . .	138
6.2	Two competing multi-strain models: a dimensional problem . . .	139
6.2.1	The two-strain model versus the four-strain model . . . . .	141
6.3	Numerical analysis . . . . .	143
6.4	Discussion and Remarks . . . . .	148
	Appendix . . . . .	149
6.A	Unpacking the n-strain model into a four-strain model . . . . .	149
	<b>Bibliography</b>	<b>153</b>
	<b>Acknowledgments</b>	<b>161</b>
	<b>Curriculum vitae</b>	<b>163</b>



# Resumo

**Palavras chaves: modelos matemáticos, dengue, multi-estirpe, imunidade cruzada temporária, caos determinístico**

Ao longo da história, as doenças infecciosas veem causado o enfraquecimento e morte prematura de grandes parte da população humana, gerando sérias preocupações sociais e econômicas. Muitos são os fatores quem têm contribuído para a persistência e o aumento na ocorrência de doenças infecciosas, tais como factores demográficos, mudanças políticas, sociais e econômicas, mudanças ambientais, adaptação microbiana, etc. Segundo a Organização Mundial de Saúde (OMS), as doenças infecciosas são a segunda principal causa de morte no mundo, depois das doenças cardiovasculares (WHO, 2010).

Dentre as doenças transmissíveis mais preocupantes, o dengue é, de acordo com a OMS, um problema de saúde pública internacional, com mais de 55% da população mundial vivendo em áreas com risco de transmissão da infecção. O dengue, uma infecção viral transmitida por mosquitos, é uma das principais causas de doença e morte nos trópicos e subtropicais. A infecção pelo vírus do dengue pode ser causada por qualquer uma das quatro cepas existentes, designadas por serotipos  $DEN - 1$ ,  $DEN - 2$ ,  $DEN - 3$  e  $DEN - 4$ . Estes serotipos são distintos, porém, antígenicamente relacionados. A infecção gerada por um determinado serotipo confere imunidade total e permanente (ao longo da vida) para apenas aquele serotipo, e também imunidade cruzada temporária para os outros serotipos. A imunidade cruzada temporária tem uma duração estimada que varia de três a nove meses, e está relacionada com os níveis de anticorpos gerados durante a resposta imune a uma primeira infecção pelo vírus do dengue. Afirma-se que o alto nível destes anticorpos seria suficiente para a proteção contra outras infecções causadas por patógenos antígenicamente relacionados.

O dengue pode se manifestar em duas formas clínicas: dengue clássico (DC), uma forma não-fatal da doença, e dengue hemorrágica (DH), que pode evoluir para uma forma muito grave conhecida como síndrome do choque do dengue (DSS). Estudos epidemiológicos associam os casos graves da doença (DH) com a

segunda infecção do dengue. Existem boas evidências relacionando as infecções sequenciais pelos vírus do dengue e o aumento para os riscos do desenvolvimento do dengue hemorrágico. Esta associação se deve a um processo imunológico chamado de antibody-dependent enhancement (ADE). O antibody-dependent enhancement ocorre quando os anticorpos pré-existentes, provenientes de uma primeira infecção do dengue, não neutralizam mas sim realçam a nova infecção pelo vírus do dengue.

Não existe uma medicação específica para a infecção do dengue. O tratamento dos casos de dengue clássico é apenas de suporte e para os casos de dengue hemorrágico a hospitalização é frequentemente necessária para obtenção de um tratamento adequado. A vacina contra o dengue ainda não está disponível, uma vez que terá que simular proteção para todos os quatro serotipos existentes. Atualmente, algumas vacinas candidatas encontram-se em diversos estágios de desenvolvimento. Até o presente momento, a prevenção na exposição e o controle dos vetores são as únicas alternativas para a prevenção da transmissão do dengue.

A modelação matemática tornou-se uma ferramenta importante para a compreensão da epidemiologia e da dinâmica das doenças infecciosas. Uma série de modelos determinísticos, tais como o modelo Susceptível-Infetado (SI) e o modelo Susceptível-Infetado-Recuperado (SIR), por exemplo, têm sido propostos com base nos padrões de fluxo para cada um dos compartimentos representando os estágios da doença. O modelo epidemiológico SIR divide a população de indivíduos em três classes: Susceptíveis ( $S$ ), Infetados ( $I$ ) e Recuperados ( $R$ ). Este tipo de modelo pode ser utilizado para representar, por exemplo, as doenças infecciosas que não conferem imunidade permanente, possibilitando a reinfeção. Assumindo que a transmissão da doença se faz de pessoa para pessoa, os indivíduos susceptíveis tornam-se infetados e infecciosos (capazes de transmitir a doença), se curam e se tornam recuperados (com imunidade temporária ao patógeno causador da doença). Depois de um determinado período tempo, acontece a perda desta imunidade e o indivíduo tornar-se novamente susceptível, podendo se reinfetar. A dinâmica multi-estirpe é geralmente modelada utilizando extensões dos modelos do tipo SIR. Para capturar as diferenças entre a primeira e a segunda infecção é preciso considerar pelo menos dois serotipos diferentes na composição do modelo do tipo SIR.

A dinâmica da epidemiologia do dengue é particularmente complexa, com grandes flutuações (variações em quantidade ao longo do tempo) na incidência da doença. Modelos matemáticos recentes para a transmissão do vírus do dengue se concentram no efeito ADE e na imunidade cruzada temporária. Estes modelos apresentam resultados de flutuações críticas com distribuição em lei de potência para os casos da doença, caos determinístico e dessincronização caótica, devido a sua estrutura multi-estirpe. O comportamento caótico é obtido quando assumindo infectividade muito alta para a segunda infecção do dengue, isto é, assumindo que os indivíduos na segunda infecção pelo vírus do dengue transmitem a doença com uma taxa muito mais elevada do que os indivíduos na primeira

infecção. Considerações da imunidade cruzada temporária associada ao efeito ADE gera uma nova janela caótica inesperada e biologicamente mais realistas, onde a infectividade dos indivíduos na segunda infecção do dengue é reduzida devido a severidade da doença e a provável hospitalização causada pelo processo imunológico do ADE.

Nesta tese apresentamos a análise e os resultados obtidos em diferentes extensões do modelo clássico SIR. Estes modelos foram motivado pela epidemiologia do dengue e a sua peculiar característica imunológica causada pelo antibody-dependent enhancement. O nosso estudo se concentra em um modelo minimalístico, em que pelo menos dois serotipos diferentes são necessários para descrever as diferenças entre as infecções primária e secundária causadas pelas diferentes cepas do vírus do dengue. Os modelos dividem a população humana em susceptíveis, infectados e recuperados, e utiliza índices para diferenciar cada um dos serotipos. Os indivíduos podem ser: (1) susceptíveis sem nenhuma infecção prévia pelo vírus do dengue, (2) infectados e recuperados pela primeira vez, (3) susceptíveis com um histórico de infecção prévia e (4) infectados pela segunda vez (por uma cepa diferente da primeira infecção) e, provavelmente hospitalizados devido ao processo de ADE. O modelo minimalístico apresenta uma dinâmica estrutural rica ao incorporar aos modelos já existentes para a transmissão do dengue, o período de imunidade cruzada temporária associada ao processo de antibody-dependent enhancement capaz de gerar diferenças nas taxas de transmissão para as infecções primárias e secundárias da doença.

No Capítulo 1 apresentamos as propriedades do modelo básico SIR aplicado ao estudo das doenças transmissíveis. A análise da dinâmica apresentada, identificando os limites e os pontos de equilíbrio, com o objectivo de introduzir a notação e a terminologia utilizada. Estes resultados são posteriormente generalizados para os modelos motivados pela epidemiologia do dengue. No Capítulo 2, o modelo básico do tipo SIR para dois serotipos diferentes é apresentado e analisado. Este capítulo enfatiza o aspecto multi-estirpe e seus efeitos sobre a população humana. Os efeitos da dinâmica dos vetores e ou da sazonalidade não são modelados explicitamente, sendo levados em conta apenas pelos parâmetros efetivos do modelo. No Capítulo 3 apresentamos uma análise detalhada dos pontos de bifurcações encontrados para os parâmetros de ADE ( $\phi$ ) e de imunidade cruzada temporária ( $\alpha$ ).

No Capítulo 4, o modelo sazonal do dengue é apresentado. Com base nos dados disponíveis de monitoramento do dengue, o papel da força sazonal e os casos importados da doença foram considerados como efeitos biologicamente relevantes para a determinação do comportamento dinâmico do sistema. O comparativo entre três cenários distintos (não-sazonal, sazonal e sazonal com casos importados da doença) é apresentado neste capítulo. A adição da sazonalidade e de possíveis casos importados da doença institui complexidade á dinâmica e apresenta boa concordância qualitativa entre os dados empíricos dos casos graves da doença (DH) e o output do modelo.



Até o momento, apenas esses modelos minimalísticos têm a possibilidade de ser qualitativamente bem compreendido e, eventualmente testados contra os dados existentes. A simplicidade do modelo (poucos parâmetros e poucas variáveis de estado) oferece uma perspectiva promissora na inferência dos valores dos parâmetros, utilizando os dados referentes ao numerero de casos de dengue hemorrágico. A estimação de parêmetros em séries temporais caóticas é notoriamente difícil devido á imprevisibilidade a longo prazo versus previsibilidade a curto prazo. Recentemente, esta previsibilidade a curto prazo tem sido usada em inferência estatística para para abordagens temporalmente localizadas encontrandi dificuldades na obtenção de uma resposta final definitiva para a melhor estimativa dos parâmetros.

A capacidade de prever os futuros surtos do dengue na ausência de intervenção humana tem como objetivo compreender o efeitos das medidas de controle da doença, incluindo a implementação de programas de vacinação, quando esta estiver disponível e acessível. Os ensaio com esta vacina deverão ser realizados em um ano em que o numero de casos da doença for suficientemente altos (e não em um ano em que o número de casos da doença fossem naturalmente baixos) afim de facilitar os teste estatísticos para a eficácia da vacina. Desta maneira, a previsão do número de casos da doença com base no balanço determinístico do número de indivíduos infectados e indivíduos susceptíveis seria de grande utilidade prática.

A propagação de doenças é um fenômeno inerentemente estocástico, mas os modelos para a propagação do dengue são em sua maioria expressos matematicamente por um conjunto equações diferenciais deterministicas, que são mais fáceis de analisar. A aproximação do campo médio, uma aproximação utilizada em processos estocásticos para a obtenção de dinâmicas deterministicas, é uma boa aproximação para ser utilizada a fim de compreender melhor o comportamento dos sistemas estocásticos em determinadas regiões de parâmetro. No entanto, apenas os modelos estocásticos, ao contrário dos modelos deterministicos, podem captar as flutuações observadas em algumas das séries temporais de dados empíricos. No Capítulo 5, a versão estocástica do modelo multi-estirpe minimalístico é apresentado. Neste capítulo investigamos a interação entre estocasticidade, sazonalidade e casos importados da doença. A introdução de estocasticidade é capaz de explicar as flutuações observadas em algumas série temporais de dados para os casos graves do dengue, revelando um cenário onde o ruído e o esqueleto determinístico se interagem fortemente. Para uma população suficientemente grande, o modelo estocástico é bem descrito pelo esqueleto determinístico, capturando a dinâmica essencial da doença. O modelo estocástico gera, a partir das informaes topológicas da dinâmica, a percepção sobre os valores relevantes dos parâmetros do modelo.

O modelo minimalístico do dengue é um sistema com 9 dimensões e, tem boas chances de poder se utilizado em uma futura inferência estatística, para estimar todas as condições iniciais e os poucos parâmetros do modelo. Os dados empíricos disponíveis para os casos de dengue hemorrágico consistem na incidência mensal

de casos hospitalizados e, para este tipo de dados, o modelo capaz de gerar infecções primária e secundária causadas por diferentes serotipos do dengue (sem a necessidade de se considerar diferenças nas dinâmicas para cada um dos diferentes serotipos existentes), apresenta uma boa concordância qualitativa entre os dados empíricos e o output do modelo (ver Capítulo 4 e Capítulo 5). Diferentemente do modelo minimalístico multi-estirpe para a transmissão do dengue, o modelo incluindo os quatro serotipos é matematicamente representado por um sistema com 26 equações diferenciais. Este sistema apresenta uma dimensão elevada (25 dimensões) e dificilmente poderá ser utilizado em inferência estatística, devido ao elevado número de variáveis e condições iniciais.

No Capítulo 6, o modelo para a transmissão do dengue incluindo todos os serotipos existentes é apresentado. Com os quatro serotipos,  $DEN - 1$ ,  $DEN - 2$ ,  $DEN - 3$  e  $DEN - 4$ , as classes SIR são identificadas por índices para cada um dos serotipos. A assimetria epidemiológica entre as cepas continua a não ser considerada. Os dados serológicos existentes para cada um dos serotipos em separado são recentes e escassos, não sendo capazes de fornecer informações fidedignas às possíveis diferenças existentes entre os parâmetros biológicos (tais como as taxas de infecção e taxas de recuperação) para cada uma das quatro cepas do vírus do dengue. Neste capítulo apresentamos a comparação entre os diagramas de bifurcação para os dois modelos multi-estirpe, assumindo respectivamente 2 e 4 serotipos diferentes na transmissão da doença. Para a região de interesse biológico (onde os indivíduos infectados pela segunda vez transmitem menos do que os indivíduos infectados pela primeira vez, devido a severidade da doença) os pontos de bifurcação acontecem em regiões similares para o parâmetro do efeito ADE.

A lei da parcimônia favorece o mais simples dos dois modelos concorrentes e desta forma, concluímos que o modelo minimalístico para a transmissão do dengue (dois serotipos), na sua simplicidade, é um bom modelo para ser analisado. O modelo minimalístico do dengue é capaz de produzir a complexidade esperada para explicar as flutuações observadas nos dados empíricos da doença e apresenta, dentro da possibilidade, baixa dimensionalidade. A Inferência estatística utilizando os dados empíricos para estimar os parâmetros básicos de transmissão, infectividade, a gravidade da doença (parâmetro ADE) e período de imunidade cruzada temporária, é de extrema importância e definitivamente necessária para identificar os eventuais desvios do caso mais simples de simetria, que foram investigados aqui. O estudo da estimação dos parâmetros utilizando o modelo minimalístico do dengue está em andamento.

A dinâmica vetorial também pode desempenhar um papel importante na compreensão da epidemiologia do dengue. As investigações descritas nesta tese surtem uma série de possíveis direções para a continuidade desta pesquisa e, em termos de trabalho futuro, a investigação de extensões do modelo minimalístico poderá abordar as seguintes questões e problemas: (1) Qual é a real contribuição das infecções primárias e secundárias para a fora de infecção? Indivíduos na

segunda infecção transmitem mais ou menos do que a indivíduos na primeira infecção? (2) Existem diferenças significativas entre as taxas de infecção para cada um dos serotipos existentes? Até que ponto a estrutura de bifurcação pode explicar a real contribuição da diversidade viral? (3) Formular hipóteses usando o mecanismo adequado de imunidade cruzada temporária e a proteção gerada em infecções recorrentes. (4) Modelar ensaios de vacinas, com base na previsibilidade a curto prazo em sistemas caóticos, para futura implementação de programas de imunização, quando a(s) vacina(s) tetravalente estiver disponível e acessível. E finalmente (5) propor alvos para a intervenção e para o planejamento de medidas controle, baseando-se no impacto esperado da doença. O Meu interesse especial se concentra na possível parametrização do modelo a partir dos dados referentes á incidência da doença grave e na prevalência de infecção. Esta ferramenta epidemiológica ajudaria a compreender os efeitos das medidas de controle e, poderia ser utilizada para orientar as políticas de prevenção e controle da transmissão do vírus do dengue, gerando uma percepção sobre a previsão dos surtos futuros do dengue.

# Samenvatting

Sinds mensenheugenis hebben infectie ziekten geleid tot slepende ziektes en vroegtijdige sterfte onder grote delen van de wereld bevolking, leidend tot grote sociale en economische problemen. Vele factoren hebben bijgedragen tot het in stand houden en de toename van infectie ziekten: demografisch factoren, politieke, sociale en economische veranderingen, verandering van de gezondheidszorg, enz. Volgens de Wereldgezondheidsorganisatie (WHO), zijn ze wereldwijd de tweede doodsoorzaak na hart en vaat ziektes (WHO, 2010). De laatste jaren zijn wiskundige modellen belangrijke gereedschappen geworden voor het verkrijgen van kennis over infectieziekten en hebben ze bijgedragen aan de grote vooruitgang in het maken van strategieën voor het beheersen van ziektes, bijvoorbeeld bij het opzetten van vaccinatie programma's.

Knokkelziekte (Eng. dengue) is een door muggen, de tijgermug, overgedragen virale infectieziekte. Deze ziekte is in de laatste jaren een groot internationaal gezondheidsprobleem geworden en een belangrijke ziekte en sterfte bron in (sub)tropische gebieden. Knokkelkoorts wordt veroorzaakt door vier antigeen verschillende virussen, bekend als dengue-varianten DENV 1, DENV 2, DENV 3 en DENV 4. Infectie met één serotype geeft levenslange immuniteit voor slechts dat serotype en maar tijdelijke immuniteit voor de andere serotypes. Tijdens de reactie op de infectie worden antilichamen gegenereerd. Het duurt drie tot negen maanden voordat het niveau van die antilichamen voldoende is om bescherming te bieden tegen infectie door een ander, maar gerelateerd, serotype.

Er zijn twee varianten van de ziekte: knokkelkoorts (dengue fever (DF)) een vorm zonder fatale afloop en hemorrhagische knokkelkoorts (dengue hemorrhagic fever (DHF)) die tot een shock kunnen leiden, bekend als een “dengue shocksyndroom” (DSS) vaak met fatale afloop.

Epidemiologische studies wijzen erop dat de hemorrhagische dengue eerder optreedt door een tweede infectie bij iemand die eerder een knokkelkoorts-aanval door een ander knokkelkoorts-virus heeft doorgemaakt. Een proces beschreven als “antibody-dependent enhancement” (ADE) is hiervoor verantwoordelijk. Daarbij kunnen de antilichamen die tijdens een eerdere infectie door een ander serotype aangemaakt zijn, niet neutraliseren maar zelfs de nieuwe infectie verergeren.

De behandeling van de milde vorm is alleen symptomatisch en ondersteunend. De ernstige vorm vereist daarentegen veel aandacht waarbij de patiënt voldoende moet drinken, en eventueel extra vocht moet krijgen via een infuus. Er bestaat nog geen vaccin tegen knokkelkoorts omdat een beschermende immuunreactie gestimuleerd moet worden voor de vier serotypes. Meerdere kandidaten, zoals tetravalent vaccines, zijn op dit moment in verschillende stadia van ontwikkeling.

Tot nu toe is voorkoming van muggenbeten de enige mogelijke preventieve bestrijdingsmaatregel tegen verspreiding van de ziekte. Muggenbeten kunnen worden voorkomen door bijvoorbeeld het dragen van bedekkende kleding, het verwijderen van mogelijke besmettingshaarden zoals schoon stilstaand water waar de muggen bij voorkeur hun eitjes in leggen en het gebruik van verdelgingsmiddelen tegen de muggen.

Wiskundige modellen zijn een interessant gereedschap geworden voor het leren begrijpen van de epidemiologie en dynamica van infectieziekten. Er een aantal deterministische compartimentsmodellen, zoals de SI en SIR modellen, voor het beschrijven van het verloop van ziektes in een populatie. In het SIR model wordt onderscheid gemaakt tussen drie klassen: vatbaar (Susceptible), besmettelijk (Infected) en genezen (Recovered). Dit model kan gebruikt worden als er levenslange immuniteit is en waarbij de infectiebesmetting overgedragen wordt van mens op mens: de vatbaren worden geïnfecteerd en besmettelijk en daarna weer beter. Men kan dit model ook zo uitbreiden dat na een immuniteitsperiode tijdelijk genezen personen weer vatbaar worden.

Bij meerdere vormen van de ziekte worden in het algemeen andere uitbreidingen van de SIR-modellen gebruikt. Bijvoorbeeld de verschillen tussen de eerste knokkelkoorts infectie veroorzaakt door één variant van de virus en een tweede infectie door een andere variant te bestuderen zijn twee-varianten SIR-modellen gebruikt. Modellen voor interacties tussen meerdere varianten met ADE maar zonder een tijdelijke immuniteitsperiode hebben deterministisch chaotisch gedrag laten zien waarbij de infectiviteit van de tweede infectie. De uitbreiding met een tijdelijke cross-immuniteitsperiode geeft een nieuw type chaotische gedrag bij onverwachte maar biologisch realistische parameterwaarden voor de infectiviteit voor de tweede infectie.

In dit proefschrift worden meerdere uitbreidingen van de klassieke enkel-variant SIR populatie model bestudeerd. Deze modellen zijn van toepassing voor het bestuderen van een knokkelkoorts epidemiologie met het kenmerkende ADE fenomeen. We zijn geïnteresseerd in een minimalistisch model waarbij tenminste twee varianten nodig zijn om de verschillen tussen de eerste en een tweede infectie te kunnen beschrijven. In het model worden voor twee populaties de volgende klassen onderscheiden. Personen kunnen vatbaar zijn zonder ooit geïnfecteerd geweest te zijn, besmettelijk van de eerste infectie, vatbaar terwijl de persoon al een keer besmet geweest is voor een tweede infectie, en besmettelijk en genezen voor de tweede infectie nu door een andere variant en tenslotte volledig genezen. De personen die voor de tweede keer besmet zijn hebben meer kans in het zieken-

huis te belanden vanwege het ADE effect en dat leidt tot de ernstige vorm van de ziekte. De uitbreiding van bestaande knokkelkoorts modellen met een tijdelijke cross-immuniteit laat een rijk dynamisch gedrag zien met deterministische chaos voor biologisch meer realistische parameterwaarden.

In Hoofdstuk 1 worden de eigenschappen van het basale SIR epidemiologisch model voor infectie ziekten beschreven met daarbij een overzicht van de analyse van het dynamisch gedrag, zoals het identificeren van drempels voor het uitbreken van de ziekte en evenwichten. Daarbij wordt ook meteen de terminologie ingevoerd. Deze resultaten worden daarna gegeneraliseerd voor geavanceerdere knokkelkoorts epidemiologie modellen.

In Hoofdstuk 2 wordt het twee-varianten SIR-type model gegeven voor knokkelkoorts epidemiologiën. Hoofdstuk 3 geeft een gedetailleerde bifurcatie analyse van de basale multi-varianten knokkelkoorts model in termen van de ADE parameter  $\phi$  en de parameter voor de tijdelijke immuniteit voor een andere variant  $\alpha$ .

Hoofdstuk 4 behandelt de invloed van seizoensinvloeden waarbij tweede infecties met tijdelijke cross-immuniteit mogelijk zijn. Waarnemingen van incidenties van knokkelkoorts suggereren dat seizoensinvloeden maar ook de import van ziektes via geïnfecteerde personen mede bepalend zijn voor het dynamisch gedrag van knokkelkoorts incidenties. Verschillende scenario's: resp. geen, lage en sterke seizoensinvloeden met daarbij een beperkte import via geïnfecteerde personen worden bestudeerd. Deze uitgebreide modellen laten complexe dynamiek zien die kwalitatief goed overeenstemmen met empirische waarnemingen over DHF gevallen.

Tegenwoordig is het mogelijk alleen van twee-varianten modellen het gedrag kwalitatief goed te doorgronden en waarvan de voorspellingen vergeleken kunnen worden met waarnemingen. De eenvoud van het model (lage aantal parameters en toestandsvariabelen) maakt het mogelijk parameterwaarden te schatten waarbij gebruik gemaakt wordt van waargenomen aantallen DHF gevallen. Deze schattingstechnieken zijn nootore moeilijk toe te passen op tijdsreeksen met chaotisch gedrag. Maar korte termijn voorspellingen zijn mogelijk. Als men de effecten van beleidsmaatregelen wil begrijpen is het belangrijk toekomstige uitbraken van knokkelkoorts te kunnen voorspellen. Ook al zou een virus vaccin beschikbaar komen, dan blijft dit relevant voor de implementatie van vaccinatie programma's. Om een voorbeeld te geven: als een proef voor het bepalen van de effectiviteit van vaccinaties gedaan wordt in een jaar waarin de ziekte alleen voorkomt bij een beperkt aantal personen dan zijn deze waarnemingen statistische gezien veel moeilijker te interpreteren dan wanneer de proef in een jaar uitgevoerd zou worden waarin de ziekte veel vaker voorkomt. Het kunnen voorspellen wanneer de volgende knokkelkoorts epidemie optreed en hoe groot die is, is dus van groot praktisch belang.

Ofschoon de overdracht van ziektes een inherent stochastisch fenomeen is zijn knokkelkoorts modellen meestal geformuleerd met deterministische differentiaal-

vergelijkingen. De gemiddelde veldbeschrijving (“mean field approximation”) geeft vaak een goede benadering en kan gebruikt worden om een beter begrip te krijgen van het gedrag van stochastische systemen voor bepaalde situaties. Daarbij worden de gemiddelde hoeveelheden benaderd door correlaties te verwaarlozen. Echter, in sommige gevallen kunnen alleen stochastische in tegenstelling tot deterministische modellen waargenomen fluctuaties beschrijven.

In Hoofdstuk 5 wordt een stochastische versie van het multi-varianten model beschreven. Deze formulering houdt rekening met essentiële verschillen tussen de eerste en de tweede besmettingen in knokkelkoorts epidemiologie. De interactie tussen stochasticiteit, seizoenen en import wordt onderzocht. Het introduceren van stochasticiteit is noodzakelijk om waargenomen fluctuaties in beschikbare gegevens bestanden laat een scenario zien waarbij ruis en de complexe deterministisch gedrag elkaar sterk beïnvloeden. Wanneer de populatie groot genoeg is kan het stochastisch systeem goed benaderd worden met een deterministisch model met behoud van de essentiële dynamiek. Daarmee krijgt men inzicht in de relevante parameterwaarden op grond van enkel topologische informatie over de dynamiek.

Het twee-varianten knokkelkoorts model is een 9 dimensionaal systeem (d.w.z. dat er 9 toestandsvariabelen zijn) en daarmee lijken toekomstige parameterschattingen haalbaar waarbij alle beginvoorwaarden (hier 9) naast een beperkt aantal parameters vastgelegd kunnen worden. Lange termijn epidemiologische waarnemingen van maandelijkse ziekenhuisopnamen met DHF zijn beschikbaar. Om dit soort gegevens te kunnen analyseren zijn modellen noodzakelijk die zowel eerste als tweede besmettingen met verschillende varianten kunnen voorspellen. Deze modellen waarbij ADE en tijdelijke cross-immuniteit gemodelleerd zijn maar de verschillen in het dynamisch gedrag van verschillende samen voorkomende knokkelziekte serotypes genegeerd worden, hebben goede kwalitatieve overeenkomst tussen empirisch waarnemingen en model voorspellingen laten zien (zie Hoofdstuk 4 en Hoofdstuk 5).

Het vier-varianten model is een 25 dimensionaal systeem in plaats van 9 dimensionaal bij het twee-varianten model. In dit model vormen de verschillende epidemiologische klassen (zoals vatbaar, besmettelijk en genezen) van de vier verschillende varianten, DENV 1, DENV 2, DENV 3 en DENV 4 de SIR waarbij ook nu weer geen epidemiologische asymmetrie tussen de varianten wordt aangenomen. Parameters van een systeem met veel dimensies zijn moeilijk te schatten ondermeer omdat een groot aantal beginwaarden meegeschat moeten worden. Verder zijn waarnemingen over het serotype alleen van recente gevallen beschikbaar en daarmee zijn de waargenomen tijdsreeksen te kort om realistische informatie te verkrijgen over het verschil in biologische parameters zoals infectieviteit en genezingsnelheid van alle varianten. In Hoofdstuk 6 worden bifurcatie diagrammen voor het twee-varianten en het vier-varianten model met elkaar vergeleken waarbij de bijdrage aan de infectieviteit van de tweede infectie kleiner is dan die van de eerste infectie. Knokkelkoorts patiënten met een tweede

besmetting door een andere variant worden vanwege het ADE fenomeen ernstig ziek en opgenomen in het ziekenhuis. Daardoor dragen ze minder bij aan de infectiekracht (dus  $\phi < 1$ ). Daarom zijn de bifurcaties die optreden bij parameterwaarden met  $\phi < 1$  erg interessant en niet alleen voor  $\phi \gg 1$  zoals eerdere modellen suggereerden.

We concluderen dat het twee-varianten model ondanks zijn eenvoud (relatief lage aantal toestandsvariabelen en aantal parameters) een goed model is dat complexe dynamisch gedrag voorspelt en dat de waargenomen empirische waarnemingen kan verklaren. Momenteel wordt dan ook het twee-varianten model gebruikt om, inclusief de beginwaarden, parameters te schatten.





# English summary

Throughout human history, infectious diseases have caused debilitation and premature death to large portions of the human population, leading to serious social-economic concerns. Many factors have contributed to the persistence and increase in the occurrence of infectious disease (such as demographic factors, political, social and economic changes, environmental change, public health care and infrastructure, microbial adaptation, etc.). According to the World Health Organization (WHO), are the second leading cause of death globally after cardiovascular diseases (WHO, 2010). In recent years, mathematical modeling became an important tool for the understanding of infectious disease epidemiology and has led to great advances in conceiving disease control strategies, including vaccination programs.

One of the most important infectious diseases is dengue, a major international public health concern with more than 55% of world population at risk of acquiring the infection. Dengue is a viral mosquito-borne infection, a leading cause of illness and death in the tropics and subtropics. Dengue fever is caused by four antigenically distinct viruses, designated dengue types 1, 2, 3 and 4. Infection by one serotype confers life-long immunity to only that serotype, and temporary cross-immunity to other related serotypes. The temporary cross-immunity period lasts from three to nine months and it is related to antibody levels created during the immune response to a previous dengue infection. It is stated that such high antibody levels would be enough to protect the individual against an immediately new dengue infection caused by a different but related serotype.

Two variants of the disease exist: dengue fever (DF), a non-fatal form of illness, and dengue hemorrhagic fever (DHF), which may evolve toward a severe form known as dengue shock syndrome (DSS). Epidemiological studies support the association of DHF with secondary dengue infection. There is good evidence that sequential infection increases the risk of developing DHF due to a process described as antibody-dependent enhancement (ADE), where the pre-existing antibodies to previous dengue infection cannot neutralize but rather enhance the

new infection.

Treatment of uncomplicated dengue cases is only supportive, and severe dengue cases requires careful attention to fluid management and proactive treatment of hemorrhagic symptoms. A vaccine against dengue is not yet available, since it would have to simulate a protective immune response to all four serotypes, although several candidates of tetravalent vaccines are at various stages of development. So far, prevention of exposure and vector control remain the only alternatives to prevent dengue transmission.

In recent years, mathematical modeling became an interesting tool for the understanding of infectious diseases epidemiology and dynamics. A series of deterministic compartment models such as Susceptible-Infected (SI) and Susceptible-Infected-Recovered (SIR) for example, have been proposed based on the flow patterns between compartments of hosts. The SIR epidemic model divides the population into three classes concerning the disease stages: susceptible ( $S$ ), Infected ( $I$ ) and Recovered ( $R$ ). This model framework can represent infectious diseases where waning immunity can happen. Assuming that the transmission of the disease is contagious from person to person, the susceptibles become infected and infectious, are cured and become recovered. After a waning immunity period, the recovered individual can become susceptible again to reinfection.

Multi-strain dynamics, such as dengue epidemiology, are generally modeled with extended SIR-type models. Dengue fever dynamic is well known to be particularly complex with large fluctuations of disease incidences. To capture differences in primary and secondary dengue infections, a two-strain SIR-type model for the host population has to be considered. Dengue models including multi-strain interactions via ADE, but without temporary cross-immunity, have shown already deterministic chaos when strong infectivity on secondary infection was assumed. The addition of the temporary cross-immunity period in such models brings a new chaotic attractor in wider and unexpected parameter region.

In this thesis we present different extensions of the classical single-strain SIR model motivated by modeling dengue fever epidemiology with its peculiar ADE phenomenology. We focus on a minimalistic model, where the notion of at least two different strains is needed to describe differences between primary and secondary dengue infections. The models divide the host population into susceptible, infected and recovered individuals with subscripts for the respective strains. The individuals can be (1) susceptibles without a previous dengue infection; (2) infected and recovered for the first time; (3) susceptible with an experienced previous dengue infection and (4) infected for the second time with a different strain, more likely to be hospitalized due to the ADE effect leading to severe disease. Our analysis shows a rich dynamic structure, including deterministic chaos in wider and more biologically realistic parameter regions, just by adding temporary cross-immunity to previously existing dengue models.

In Chapter 1 we present the properties of the basic SIR epidemic model applied to infectious diseases. A summary of the analysis of the dynamics identifying the

thresholds and equilibrium points in order to introduce notation and terminology are presented. These results were then generalized to a more advanced models motivated by dengue fever epidemiology. In Chapter 2 the basic two-strain SIR-type model motivated by modeling dengue fever epidemiology is presented. In this chapter we focused on the multi-strain aspect and its effects on the host population. The effects of the vector dynamics or seasonality is taken in account only by the effective parameters of the SIR-type model, but these mechanisms are not modeled explicitly. In Chapter 3 a detailed bifurcation analysis for the basic multi-strain dengue model is presented where the ADE parameter  $\phi$  and the temporary cross-immunity parameter  $\alpha$  are studied.

In Chapter 4 the seasonally forced system with temporary cross-immunity and possible secondary infection is analyzed. This study was motivated by dengue hemorrhagic fever monitoring data. The role of seasonality and import of infected individuals are now considered as biologically relevant effects to determine the dynamical behavior of the system. A comparative study between three different scenarios (non-seasonal, low seasonal and high seasonal with a low import of infected individuals) is presented. The extended models show complex dynamics and qualitatively a good agreement between empirical DHF monitoring data and the obtained model simulation.

At the moment only such minimalistic models have a chance to be qualitatively understood well and eventually tested against existing data. The simplicity of the model (low number of parameters and state variables) offer a promising perspective on parameter values inference from the DHF case notifications. Such a technical parameter estimation is notoriously difficult for chaotic time series due to the long term unpredictability versus short term predictability. Recently, this short term predictability has been used for temporally local approaches in statistical inference on the cost of difficulty in obtaining a final definite best answer to the parameter estimation problem.

Being able to predict future outbreaks of dengue in the absence of human interventions is a major goal if one wants to understand the effects of control measures. Even after a dengue virus vaccine has become accessible or available, this holds true for the implementation of a vaccination program. For example, to perform a vaccine trial in a year where the disease epidemic generate a low number of cases, would make the statistical tests of vaccine efficacy much more difficult compared with the information provided by a vaccine trial performed in a epidemic year with much higher numbers of cases. Thus predictability of the next season's height of the dengue peak, on the basis of deterministic balance of infected and susceptible, would be of major practical use.

Although the fact that disease propagation is an inherently stochastic phenomenon, dengue models are mainly expressed mathematically as a set of deterministic differential equations, which are easier to analyze. The mean field approximation, an approximation of stochastic processes leading to deterministic dynamics, is a good approximation to be used in order to understand better the

behavior of the stochastic systems in certain parameter regions, where the dynamics of the mean quantities are approximated by neglecting correlations. However, it is only stochastic, as opposed to deterministic, models that can capture the fluctuations observed in some of the available time series data. In Chapter 5 the stochastic version of the minimalistic multi-strain model is presented. In this chapter we investigate the interplay between stochasticity, seasonality and imported cases of the disease. The introduction of stochasticity reveal a scenario where noise and complex deterministic skeleton strongly interact. For large enough population size, the stochastic system could be well described by the deterministic skeleton, where the essential dynamics are captured, gaining insight into the relevant parameter values purely on topological information of the dynamics.

The two-strain dengue model is a 9 dimensional system and therefore, future statistical inference can still attempt to estimate all initial conditions as well as the few model parameters. Concerning data availability, long term epidemiological data consist on monthly incidences of hospitalized DHF cases. For such a data scenario, models that are able to generate both primary and secondary infection cases (with a different strain, without the need of considering differences on the dynamics of different co-circulating dengue serotypes), have shown a good qualitative agreement between empirical data and model output (see Chapter 4 and Chapter 5). These results were obtained just by combining the ADE effect, generating difference in transmissibility on primary and secondary infections, with the temporary cross-immunity aspect. Differently from the minimalistic dengue model, the four-strain model is mathematically represented by a system of 26 ODE' s. It becomes a very high dimensional system and obviously very difficult to be used for parameter inference due to the high number of initial conditions. In Chapter 6 we present the multi-strain dengue model for the four existing serotypes. For four different strains, 1, 2, 3 and 4, we now label the SIR classes for the hosts that have seen each one of the possible strains. Again, without epidemiological asymmetry between strains, once the serotype data are recent and very short to give any realistic information concerning difference in biological parameters (such as infection and recovery rates) for a given strain. In this chapter we present the bifurcation diagram comparison for both two-strain and four-strain model. In the relevant parameter region of  $\phi < 1$ , when dengue patients in a secondary infection evolving to severe disease due to the ADE phenomenon contribute less to the force of infection, the bifurcation points appear to happen at similar parameter regions, well below the region of interest  $\phi \approx 1$ .

We conclude that the two-strain model in its simplicity is a good model to be analyzed giving the expected complex behavior to explain the fluctuations observed in empirical data. Statistical inference to estimate the basic parameters of transmission, infectivity, disease severity (ADE parameter) and temporary cross-immunity period using empirical data of incidence of severe disease is needed to identify eventual deviations from the simplest symmetric case investigated here. Further work on the parameter estimation using the minimalistic dengue

model is in progress.

The vector dynamics might also play a role in understanding the final picture when comparing the model output with the available empirical data. Following the investigations described in this thesis, a number of research directions could be addressed, involving the minimalistic dengue model. Future work would be to investigate extensions of the multi-strain model to address the following questions and issues: (1) How much (more or less than first infection) does secondary infection contribute to the force of infection? (2) Does there exist a difference between the forces of infection for the different strains and to what extent can the bifurcation structure explain the viral diversity contribution? (3) Formulate hypotheses using the mechanism of temporary cross-immunity suitable to recurrent infections protection. (4) Model the vaccine trials based on short term predictability of chaotic systems to be applied when tetravalent vaccines will become available. And (5) propose targets for intervention and control design according to the expected impact of the disease. My special interest would be to get the model fully parametrized on data referring to incidence of severe disease and prevalence of infection. With such a model framework we would be able to give an insight into the predictability of upcoming dengue outbreaks. This epidemiological tool would help to understand the effects of control measures and therefore to guide the policies of prevention and control of the dengue virus transmission.



# Chapter 1

## Introduction

Throughout human history, infectious diseases have caused debilitation and premature death to large portions of the human population, leading to serious socio-economic concerns. Many factors have contributed to the persistence and increase in the occurrence of infectious disease (demographic factors, political, social and economic changes, environmental change, public health care and infrastructure, microbial adaptation, etc.), which according to the World Health Organization (WHO), are the second leading cause of death globally after cardiovascular diseases (WHO, 2010).

Research on basic and applied aspects of host, pathogen, and environmental factors that influence disease emergence, transmission and spread have been supported so far, and the development of diagnostics, vaccines, and therapeutics has been greatly increased. In recent years, mathematical modeling became an interesting tool for the understanding of infectious diseases epidemiology and dynamics, leading to great advances in providing tools for identifying possible approaches to control, including vaccination programs, and for assessing the potential impact of different intervention measures.

Epidemiological models are a formal framework to convey ideas about the components of a host-parasite interaction and can act as a tool to predict, understand and develop strategies to control the spread of infectious diseases by helping to understand the behaviour of the system under various conditions. They can also aid data collection and parameter estimation. The purpose of epidemiological models is to take different aspects of the disease as inputs and to make predictions about the numbers of infected and susceptible people over time as output.

In the early 20<sup>th</sup> century, mathematical models were introduced into infectious disease epidemiology, and a series of deterministic compartment models such as Susceptible-Infected (SI), Susceptible-Infected-Susceptible (SIS), Susceptible-Infected-Recovered (SIR), and e.g Susceptible-Exposed-Infected-Recovered (SEIR)



have been proposed based on the flow patterns between compartments of hosts. In our days, most of the models developed try to incorporate other factors focusing on several different aspects of the disease, which can imply rich dynamic behaviour even in the most basic dynamical models. Factors that can go into the models include the duration of disease, the duration of infectivity, the infection rate, the waning immunity, and so forth. In such a way, differential equation models are a simplified representation of reality, which are designed to facilitate prediction and calculation of rates of change as functions of the conditions or the components of the system.

There are two common approaches in modeling, the deterministic and the stochastic one. In the first case, the model is one in which the variable states are uniquely determined by parameters in the model and by sets of previous states of these variables. In mathematics, a deterministic system is a system in which no randomness is involved in the development of future states of the system. In a stochastic model, randomness is present, and variable states are not described by unique values, but rather by probability distributions. Stochastic epidemic models are appropriate stochastic processes that can be used to model disease propagation. Disease propagation is an inherently stochastic phenomenon and there are a number of reasons why one should use stochastic models to capture the transmission process. Real life epidemics, in the absence of intervention from outside, can either go extinct with a limited number of individuals getting ultimately infected, or end up with a significant proportion of the population having contracted the disease in question. It is only stochastic, as opposed to deterministic, models that can capture this behaviour and the probability of each event taking place.

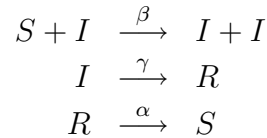
Only few stochastic processes can be solved explicitly. The simplest and most thoroughly studied stochastic model of epidemics are based on the assumption of homogeneous mixing, i.e. individuals interact randomly at a certain rate. The mean field approximation is a good approximation to be used in order to understand better the behaviour of the stochastic systems in certain parameter regions, where the dynamics of the mean quantities are approximated by neglecting correlations, giving closed ordinary differential equations (ODE) systems, hence mathematically deterministic systems which are easier to analyse.

In the following section of this chapter we present the properties of the basic SIR epidemic model for infectious diseases with a summary of the analysis of the dynamics, identifying the thresholds and equilibrium points. The goal is to introduce notation, terminology, and results that will be generalized in later sections on more advanced models motivated by dengue fever epidemiology as an example of multi-strain systems.

## 1.1 The SIR Epidemic Model

The SIR epidemic model divides the population into three classes: susceptible ( $S$ ), Infected ( $I$ ) and Recovered ( $R$ ). It can be applied to infectious diseases where waning immunity can happen, and assuming that the transmission of the disease is contagious from person to person, the susceptibles become infected and infectious, are cured and become recovered. After a waning immunity period, the recovered individual can become susceptible again. This model was for the first time proposed by William Ogilvy Kermack and Anderson Gray McKendrick in 1927 (Weisstein, 2010). The model was brought back to prominence after decades of neglect by Anderson and May (Anderson & May, 1979).

In the simple SIR epidemics without strain structure of the pathogens we have the following reaction scheme for the possible transitions from one to another disease related state, susceptibles  $S$ , infected  $I$  and recovered  $R$ ,



for a host population of  $N$  individuals, with contact and infection rate  $\beta$ , recovery rate  $\gamma$  and waning immunity rate  $\alpha$ . The dynamic model in terms of ordinary differential equations (ODE) reads,

$$\dot{S} = -\frac{\beta}{N}IS + \alpha(N - S - I) \quad (1.1)$$

$$\dot{I} = \frac{\beta}{N}IS - \gamma I \quad , \quad (1.2)$$

where we use the time derivative  $\dot{S} = dS/dt$  with time  $t$  for a constant population size of  $N = S + I + R$  individuals. The solution of  $R(t)$  is given by  $R(t) = N - I(t) - S(t)$  which can be calculated using the solution of the ODEs. The susceptible individuals become infected with infection rate  $\beta$ , recover from the infection with recovery rate  $\gamma$  and become susceptible again after waning immunity rate  $\alpha$ .

In Fig. 1.1 we show the dynamical behaviour of the susceptible, infected and recovered individuals in a given population  $N$ , when solving the above ODE system.

The basic SIR model has only fixed points as possible stationary solutions, that can be calculated setting the rates of change  $\dot{S}$  and  $\dot{I}$  to zero. For the disease free equilibrium state, the solution is given by

$$I_1^* = 0 \quad (1.3)$$

$$S_1^* = N \quad (1.4)$$

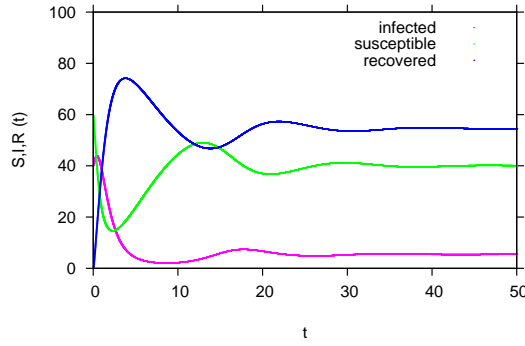


Figure 1.1: Time dependent solution simulation for the SIR epidemic model. With a population  $N = 100$ , and starting values  $I = 40$ ,  $S = 60$  and  $R = 0$ , we fixed  $\beta = 2.5$ ,  $\alpha = 0.1$ , and  $\gamma = 1$ . In green the dynamics for the susceptibles  $S(t)$ , in pink the dynamics for the infected  $I(t)$  and in blue the dynamics of the recovered  $R(t)$ . Note that  $N = 100$  allows for the interpretation for the class abundances in percentages.

and for the disease endemic equilibrium state, the solution is

$$I_2^* = N \left(1 - \frac{\gamma}{\beta}\right) \frac{\alpha}{(\alpha + \gamma)} \quad (1.5)$$

$$S_2^* = N \frac{\gamma}{\beta} . \quad (1.6)$$

The epidemic dynamic as a function of the infection rate parameter  $\beta$  and the recovery rate parameter  $\gamma$  shows the spread of the epidemic when  $\beta > \gamma$  (see Fig. 1.2a)), and its extinction when  $\beta < \gamma$  (see Fig. 1.2b)).

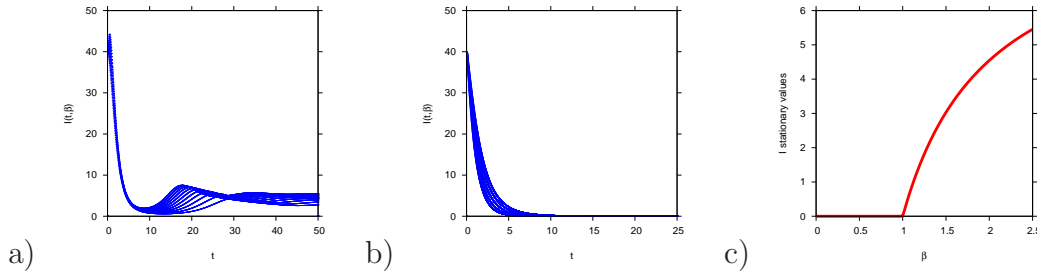


Figure 1.2: Epidemic dynamics as a function of  $\beta$ . With the same initial values as used in Fig. 1.1, we plot time dependent solutions  $I(t)$  for several  $\beta$  values. In a)  $\beta \in [1.5, 2.5]$ , with a resolution  $\Delta\beta = 0.1$  and in b)  $\beta \in [0, 0.9]$  where  $\Delta\beta = 0.2$ . In c) the stable stationary states as function of  $\beta$ .

In order to analyse the stability of the equilibrium states, we look at the Jacobian matrix and its eigenvalues.

Let the dynamics for the state  $\underline{x} := (S, I)$  be  $\underline{f}(\underline{x})$ , hence  $\frac{d}{dt}\underline{x} = \underline{f}(\underline{x})$  which explicitly gives  $\Delta \underline{x} := \underline{x}(t) - \underline{x}^*$  as a small perturbation around the fixed point  $\underline{x}^*$ . We linearize the dynamic  $\frac{d}{dt}\Delta \underline{x} = \frac{d}{dt}(\underline{x}(t) - \underline{x}^*)$  applying Taylor's expansion

$$\underline{f}(\underline{x}^* + \Delta \underline{x}) = \underline{f}(\underline{x}^*) + \left. \frac{d\underline{f}}{d\underline{x}} \right|_{\underline{x}^*} \cdot (\Delta \underline{x}) + \mathcal{O}((\Delta \underline{x})^2) \quad (1.7)$$

with  $\underline{f}(\underline{x}^*) = 0$  for the fixed point and neglecting higher order terms. For our system we have the following linear differential equation system

$$\frac{d}{dt} \begin{pmatrix} S(t) - S^* \\ I(t) - I^* \end{pmatrix} = \left( \begin{array}{cc} \frac{\partial f}{\partial S} & \frac{\partial f}{\partial I} \\ \frac{\partial g}{\partial S} & \frac{\partial g}{\partial I} \end{array} \right) \bigg|_{\begin{pmatrix} S \\ I \end{pmatrix} = \begin{pmatrix} S^* \\ I^* \end{pmatrix}} \cdot \begin{pmatrix} S - S^* \\ I - I^* \end{pmatrix} \quad (1.8)$$

where  $\underline{f} := (f, g)$  and the Jacobian matrix is explicitly given by

$$\begin{pmatrix} -\frac{\beta}{N}I^* - \alpha & -\frac{\beta}{N}S^* - \alpha \\ \frac{\beta}{N}I^* & \frac{\beta}{N}S^* - \gamma \end{pmatrix} =: A \quad (1.9)$$

where we have to insert for  $S^*$  and  $I^*$ , the respective steady states. In order to decouple the linear differential equation system, we diagonalize the matrix  $A$ , (1.9), with the eigenvalue decomposition  $A \underline{u} = \lambda \underline{u}$ ,  $\underline{u}$  is an eigenvector of  $A$ , and  $\lambda$  is an eigenvalue of  $A$  corresponding to the eigenvector  $\underline{u}$ .

The eigenvalues can be calculated setting the determinant of  $[A - \lambda \mathbb{I}]$  equal zero. For the disease free equilibrium state ( $I_1^*$  and  $S_1^*$ ), Eq. (1.3) and Eq. (1.4), the eigenvalues are given by

$$\lambda_1 = \beta - \gamma \quad (1.10)$$

$$\lambda_2 = -\alpha \quad (1.11)$$

and for the disease endemic equilibrium state ( $I_2^*$  and  $S_2^*$ ), Eq. (1.5) and Eq. (1.6), the eigenvalues are giving by

$$\lambda_1 = -\frac{\alpha}{2} \left( 1 + \frac{\beta - \gamma}{\alpha + \gamma} \right) + \sqrt{\left[ \frac{\alpha}{2} \left( 1 + \frac{\beta - \gamma}{\alpha + \gamma} \right) \right]^2 - (\beta - \gamma)\alpha} \quad (1.12)$$

$$\lambda_2 = \underbrace{-\frac{\alpha}{2} \left( 1 + \frac{\beta - \gamma}{\alpha + \gamma} \right)}_{=: a} - \underbrace{\sqrt{\left[ \frac{\alpha}{2} \left( 1 + \frac{\beta - \gamma}{\alpha + \gamma} \right) \right]^2 - (\beta - \gamma)\alpha}}_{=: b} \quad (1.13)$$

Note that if  $b > 0$  the eigenvalues are real numbers, giving the contraction or expansion of the trajectories near to the considered fixed point. If  $b < 0$ , the

eigenvalues become complex, where the real part  $a$  gives the contraction or expansion, and the imaginary part  $i\sqrt{|b|}$  gives the frequency of oscillations of the trajectories spiralling into the fixed point as is shown in Fig. 1.2b).

The fixed point  $I_1^*$  is stable when  $\beta < \gamma$ , where both eigenvalues are negative. For  $\beta > \gamma$  the fixed point  $I_2^*$  is now stable. Here, the real part of the eigenvalues are negative and the imaginary part of the eigenvalues gives the oscillations towards the fixed point. The stability of the system changes when one of the eigenvalues of the system becomes zero. At this critical point,  $I_1^*$  becomes unstable and  $I_2^*$  stable. Figure 1.2c) shows the eigenvalues for the disease free equilibrium state as functions of  $\beta$ . For detailed information on the solution of a linear two dimensional ODE system, see (Mattheij & Molenaar, 1996).

The stochastic SIR epidemic is modelled as a time-continuous Markov process to capture population noise. The dynamics of the probability of integer infected and integer susceptibles, while the recovered follow from this due to constant population size, can be given as a master equation (van Kampen, 1992) in the following form

$$\begin{aligned} \frac{dp(S, I, t)}{dt} = & \frac{\beta}{N}(S+1)(I-1) p(S+1, I-1, t) \\ & + \gamma(I+1) p(S, I+1, t) \\ & + \alpha(N - (S-1) - I) p(S-1, I, t) \\ & - \left( \frac{\beta}{N} + \gamma I + \alpha(N - S - I) \right) p(S, I, t) \quad . \end{aligned} \quad (1.14)$$

This process can be simulated, e.g., by the Gillespie algorithm giving stochastic realizations of infected and susceptibles in time (Gillespie, 1976, 1978).

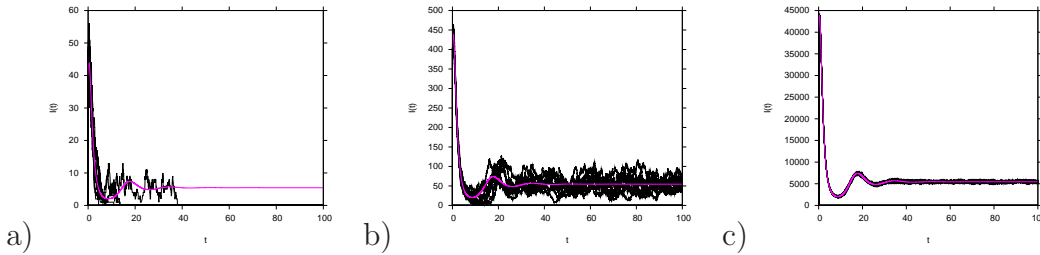


Figure 1.3: Stochastic simulations for the basic SIR epidemic model. Here 10 realizations are plotted. We fixed  $\alpha = 0.1$ ,  $\gamma = 1$  and  $\beta = 2.5$ . The deterministic trajectory is shown (pink line) top of the stochastic realizations for different population size  $N$ . In a)  $N = 100$ , in b)  $N = 1000$  and in c)  $N = 100000$ .

For mean values of infected  $\langle I \rangle$  and susceptibles  $\langle S \rangle$ , defined as e.g.

$$\langle I \rangle(t) := \sum_{S=0}^N \sum_{I=0}^N I p(S, I, t) \quad . \quad (1.15)$$

one can calculate the dynamics by inserting the master equation into the definition of the mean values obtaining

$$\begin{aligned}\frac{d}{dt}\langle S \rangle &= \alpha\langle R \rangle - \frac{\beta}{N}\langle SI \rangle \\ \frac{d}{dt}\langle I \rangle &= \frac{\beta}{N}\langle SI \rangle - \gamma\langle I \rangle\end{aligned}\tag{1.16}$$

with  $\langle R \rangle = N - \langle S \rangle - \langle I \rangle$ . For more details on the calculations see e.g. (Stollenwerk & Jansen, 2011). These equations for the mean dynamics include now due to the non-linear transition rates in the master equation also higher moments  $\langle S \cdot I \rangle$ . The simplest approximation to obtain a closed ODE system is to neglect cross-correlations  $\langle S \cdot I \rangle - \langle S \rangle \cdot \langle I \rangle \approx 0$ , the so-called mean field approximation (originally introduced for spatially extended systems in statistical physics (Stollenwerk et al., 2010)). Hence, the equation system Eq. (1.16), with identifying the higher moment  $\langle S \cdot I \rangle = \langle S \rangle \cdot \langle I \rangle$  by a product of simple moments, gives again the ODE system for SIR system as it was just presented above. For certain parameter regions the mean field approximation describes the system well in terms of its mean dynamics and only small fluctuations around it. Then the previously shown analysis of the system is appropriate. However, noise can stabilize transients, a feature which becomes important in parameter regions where in the deterministic description a fixed point is reached via decreasing oscillations, as we have observed them in the SIR system. The noisy system would show here continued oscillations (Alonso et al., 2006).

In Fig. 1.3 we compare the deterministic and stochastic dynamics and we see that the magnitude of stochastic fluctuations decreases when the population size increases. However, the good approximation (see Fig. 1.3c) is only achieved when the population size is large enough. For small population size, most simulation die out very quickly (see Fig. 1.3a)). Almost all mathematical models of diseases start from the same basic premise, that the population can be subdivided into a set of distinct classes. The most commonly used framework for epidemiological systems, is still the SIR type model, a good and simple model for many infectious diseases. Different extensions of the classical single-strain SIR model show rich dynamic behaviour in measles, e.g. (Stone et al., 2007), or in generalized multi-strain SIR type models to describe the epidemiology of dengue fever, e.g. (Aguiar & Stollenwerk, 2007; Aguiar et al., 2008).

## 1.2 Dengue fever Epidemiology

Dengue is a viral mosquito-borne infection which in recent years has become a major international public health concern. According to the estimates given by (PDVI, 2011), 3.6 billion (55% of world population) are at risk of acquiring

dengue infection (see Fig. 1.4)). It is estimated that every year, there are 70–500 million dengue infections, 36 million cases of dengue fever (DF) and 2.1 million cases of dengue hemorrhagic fever (DHF), with more than 20,000 deaths per year (WHO, 2009; PDVI, 2011; CDC, 2011). In many countries in Asia and South America DF and DHF has become a substantial public health concern leading to serious social-economic costs.

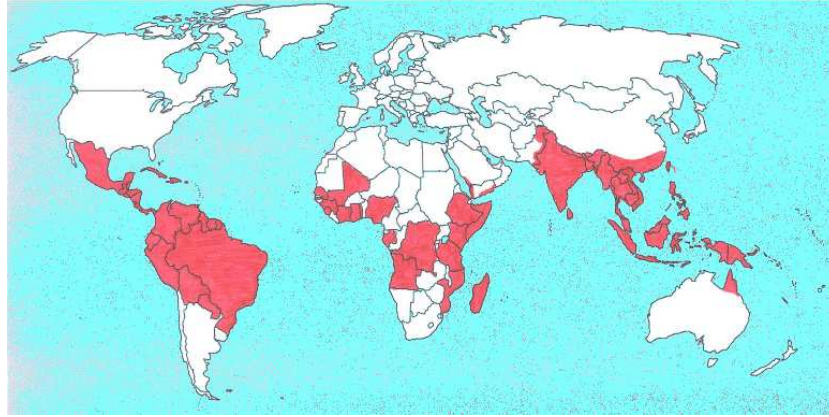


Figure 1.4: Worldwide Dengue distribution 2010. In red Countries and areas where dengue has been reported. Data source: World Health Organization (WHO) & Centers for Disease Control and Prevention (CDC). Adapted from (Gubler, 2002; Mackenzie et al., 2004).

Dengue fever is transmitted by the female domestic mosquito *Aedes aegypti*, although *Ae. albopictus* and *Ae. polynesiensis* can also act as transmission vector (Favier et al., 2005). Virus transmission in its simplest form involves the ingestion of viremic blood by mosquitoes and passage to a second susceptible human host. The mosquito becomes infected when taking a blood meal from a viremic person. After an extrinsic incubation period, the mosquito becomes infective and remains so during its entire life span (Rigau-Pérez et al., 1998). As the blood meal stimulates oviposition, which undergoes at least one, often more, reproductive cycles there is an opportunity of vertical transmission to the eggs, passing the virus to the next generation of mosquitoes (Rosen et al., 1983; Monath, 1994; CDC, 2011).

There are four antigenically distinct dengue viruses, distributed around the world, designated *DEN-1*, *DEN-2*, *DEN-3*, and *DEN-4* (see Fig. 1.5). The co-circulation of all four dengue serotypes and their capacity to produce severe dengue disease was demonstrated as early as 1960 in Bangkok, Thailand (Halstead et al., 1969). DHF occurred first only in Bangkok, but was disseminated to the whole region during the 1970s (Gubler, 2002; Halstead et al., 1969; Chareonsook et al., 1999). Physicians in Thailand are trained to recognize and treat dengue fever and practically all cases of DHF and DSS are hospitalized. A



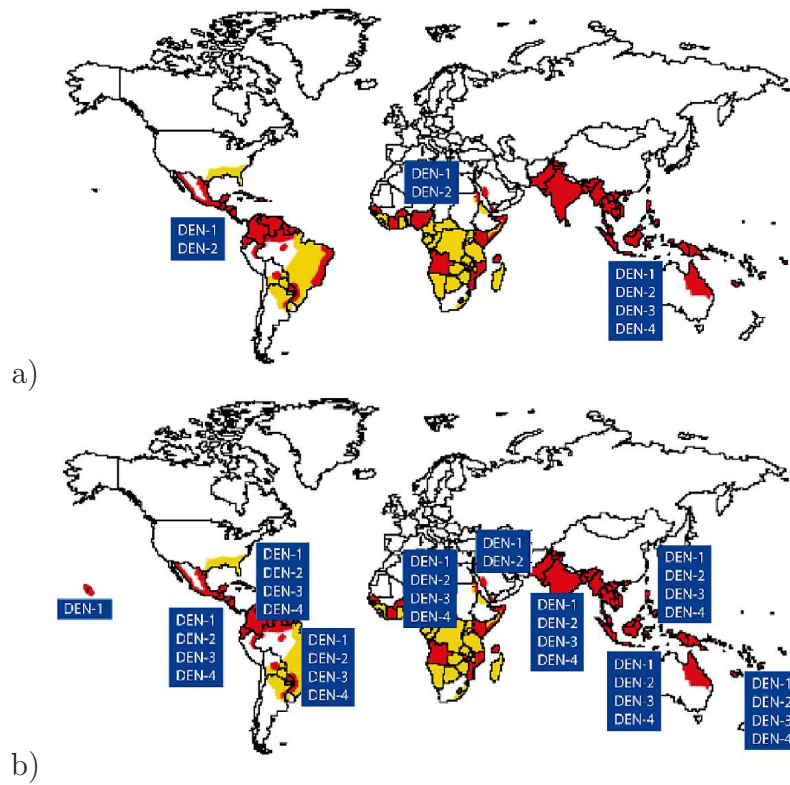


Figure 1.5: Global distribution of dengue virus serotypes. In a) 1970 and in b) 2010. Data source: World Health Organization (WHO) & Centers for Disease Control and Prevention (CDC). Adapted from (Gubler, 2002).



system for reporting communicable diseases including DHF/DSS was considered fully installed in 1974 and the data bank of DHF and DSS is available at the Ministry of Public Health, Bangkok (Chareonsook et al., 1999).

Infection by one serotype confers life-long immunity to only that serotype and temporary cross-immunity to other serotypes exists. It lasts from three to nine months, when the antibody levels created during the response to that infection would be enough to protect against infection by a different but related serotype (Halstead, 1994; Matheus et al., 2005; WHO, 2009; SES, 2010; Dejnirattisai et al., 2010). Two variants of the disease exist: dengue fever (DF), a non-fatal form of illness, and dengue hemorrhagic fever (DHF), which may evolve toward a severe form known as dengue shock syndrome (DSS).

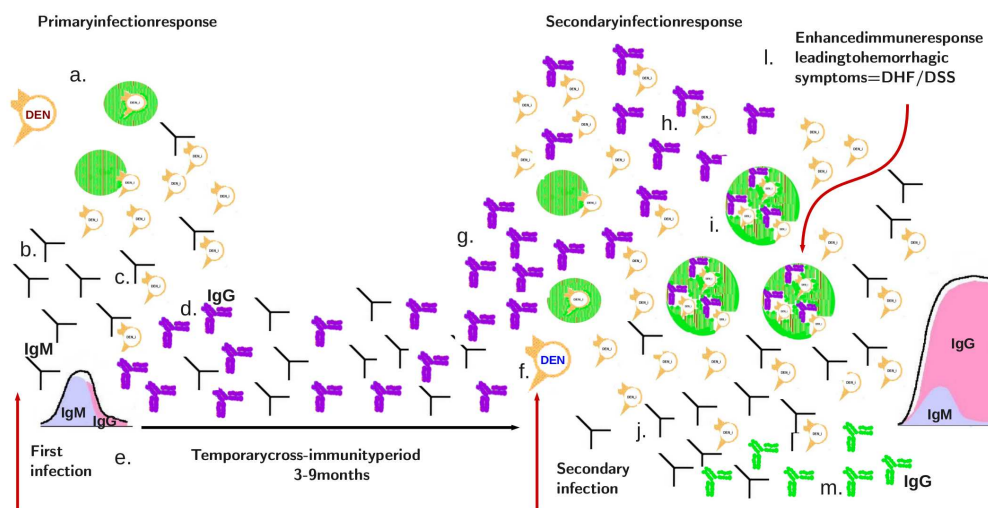


Figure 1.6: Scheme of the immunological response on recurrent dengue infections. In (a.) the first infection with a given dengue virus serotype, in (b.) production of antibodies (Immunoglobulin M (IgM)), in (c.) inactivation of the virus and in (d.) production of antibodies (IgG class, the so called memory antibodies). In (e.) the temporary cross-immunity period, that lasts between 3-9 months. After that period, the individual can get infected again with another dengue virus serotype, different from the first one (f.). In (g.) the IgG from the previous dengue infection binds to the new virus but do not inactivate them. In (h.) the complex antibody-virus enhances the new infection (i.). In (j.) the late production of antibodies (IgM class) which is then able to inactivate the new viruses, leading to (l.), an enhanced immune response, such that hemorrhagic symptoms are observed. In (m.) production of IgG antibodies.

Epidemiological studies support the association of DHF with secondary dengue infection (Halstead, 1982, 2003; Nisalak et al., 2003), and there is good evidence

that sequential infection increases the risk of developing DHF, due to a process described as antibody-dependent enhancement (ADE), where the pre-existing antibodies to previous dengue infection cannot neutralize but rather enhance the new infection.

In the first dengue infection virus particles will be captured and processed by so-called antigen presenting cells. These viruses will be presented to T-cells causing them to become activated. Likewise, B-cells will encounter their antigen free floating and become activated. The B-cells produce antibodies that are used to tag the viruses to encourage their uptake by macrophages and inactivate them. In a second infection, with a different strain, the antibodies from the first infection will attach to the new virus particles but will not inactivate them. The antibody-virus complex suppresses innate immune responses, increasing intracellular infection and generating inflammatory cytokines and chemokines resulting in enhanced disease (Halstead, 1982, 1994; Dejnirattisai et al., 2010; Guzmán et al., 2010). Fig. 1.6 is an scheme to illustrate the immunological response on recurrent dengue infections.

DF is characterized by headache, retro-orbital pain, myalgia, arthralgia, rash, leukopenia, and mild thrombocytopenia. The symptoms resolve after 2 – 7 days. DHF is a potentially deadly complication that is characterized by high fever and hemorrhagic phenomena. DHF develops rapidly, usually over a period of hours, and resolves within 1 – 2 days in patients who receive appropriate fluid resuscitation. Otherwise, it can quickly progress to shock (WHO, 2009; CDC, 2011). Treatment of uncomplicated dengue cases is only supportive, and severe dengue cases requires careful attention to fluid management and proactive treatment of hemorrhagic symptoms (CDC, 2011; WHO, 2009). A vaccine against dengue is not yet available, since it would have to simulate a protective immune response to all four serotypes (Stephenson, 2005), although several candidates of tetravalent vaccines are at various stages of development (WHO, 2011).

Mathematical models describing the transmission of dengue viruses appeared in the literature early as 1970 (Fischer & Halstead, 1970). More recently, mathematical models describing the transmission of dengue viruses have focused on the ADE effect and temporary cross-immunity trying to explain the irregular behaviour of dengue epidemics. Such models ultimately aim to be used as a predictive tool with the objective to guide the policies of prevention and control of the dengue virus transmission, including the implementation of vaccination programs when the candidate dengue fever vaccines will be accessible.

In the literature, multi-strain interaction leading to deterministic chaos via antibody-dependent enhancement effect has been described previously e.g. (Ferguson et al., 1999; Schwartz et al, 2005; Billings et al., 2007) but neglecting temporary cross-immunity. Consideration of temporary cross-immunity is rather complicated and up to now not in detail analysed. Models formulated in e.g. (Wearing & Rohani, 2006; Nagao & Koelle, 2008; Recker et al., 2009; Loureço & Recker, 2010), did not investigate closer the possible dynamical structures. In

(Aguiar et al., 2008, 2009, 2011 a), by including temporary cross-immunity into dengue models with ADE, a rich dynamic structure including deterministic chaos was found in wider and more biologically realistic parameter regions. In the following section of this chapter we present a short review on recent multi-strain models motivated by dengue fever epidemiology.

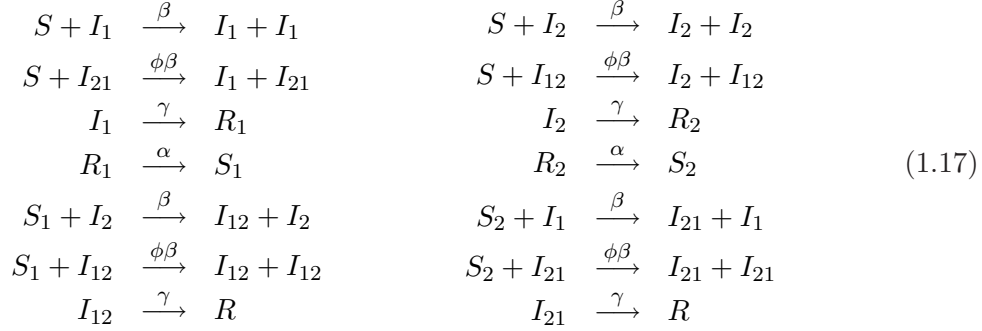
### 1.3 Multi-strain models motivated by dengue fever epidemiology: a review

Multi-strain dynamics are generally modelled with extended SIR-type models and have demonstrated to show critical fluctuations with power law distributions of disease cases, exemplified in meningitis (Stollenwerk & Jansen, 2003 a; Stollenwerk et al., 2004) and in dengue fever (Massad et al., 2008). Dengue models including multi-strain interactions via ADE but without temporary cross-immunity period have shown deterministic chaos when strong infectivity on secondary infection was assumed (Ferguson et al., 1999). The addition of the temporary cross-immunity period in such models brings a new chaotic attractor in an unexpected and more biologically realistic parameter region of reduced infectivity on secondary infection (Aguiar & Stollenwerk, 2007; Aguilar et al., 2008, 2009, 2011 a), i.e. deterministic chaos was found in a wider parameter regions. This indicates that deterministic chaos is much more important in multi-strain models than previously thought, and opens new ways to data analysis of existing dengue time series, as will be shown below. It offers a promising perspective on parameter values inference from dengue cases notifications.

To capture differences in primary infection by one strain and secondary infection by another strain we consider a basic two-strain SIR-type model for the host population, which is only slightly refined as opposed to previously suggested models for dengue fever (Ferguson et al., 1999; Schwartz et al., 2005; Billings et al., 2007). The stochastic version of the multi-strain dengue model is now given in complete analogy to the previously described SIR model, and the mean field ODE system for the multi-strain dengue model can be read from the following reaction scheme (1.17), describing the transitions. It describes for first infection with strain 1 and secondary infection with strain 2, and for the reverse process, where the first infection is caused by strain 2 and the secondary infection is caused by strain 1. The same reaction scheme can be used to describe the transitions by just changing labels.

The basic multi-strain model divides the population into ten classes: susceptible to both strains, 1 and 2 ( $S$ ), primarily infected with strain one ( $I_1$ ) or strain two ( $I_2$ ), recovered from the first infection with strain one ( $R_1$ ) or strain two ( $R_2$ ), susceptible with a previous infection with strain one ( $S_1$ ) or strain two ( $S_2$ ), secondarily infected with strain one when the first infection was caused

by strain two ( $I_{21}$ ) or for second time infected with strain two when the first infection was caused by strain one ( $I_{12}$ ). Notice that infection by one serotype confers life-long immunity to that serotype. Then the individuals recover from the secondary infection ( $R$ ).



The complete system of ordinary differential equations for the two strain epidemiological system is given by system Eq. (1.18) and the dynamics are described as follows. Susceptibles to both strains can get the first infection with strain one or strain two with infection rate  $\beta$  when the infection is acquired via an individual in his first infection or infection rate  $\phi\beta$ , when the infection is acquired via an individual in his second infection. They recover from the first infection with a recovery rate  $\gamma$ , conferring full and life-long immunity against the strain that they were exposed to, and also a short period of temporary cross-immunity  $\alpha$  against the other strain, becoming susceptible to a second infection with a different strain. The susceptible with a previous infection gets the secondary infection, again with two possible infection rates,  $\beta$  or  $\phi\beta$  depending on whom (individual on his primary or secondary infection) is transmitting the infection. Then, with recovery rate  $\gamma$ , the individuals recover and become immune against all strains. No epidemiological asymmetry between strains is assumed, i.e. infections with strain one followed by strain two or vice versa contribute in the same way to the force of infection. Here, the only relevant difference concerning disease transmissibility is that the force of infection varies accordingly to the number of previous infections the hosts have experienced. In a primary infection the individuals transmit the disease with a force of infection  $\frac{\beta I}{N}$  whereas in a secondary infection the transmission is given with a force of infection  $\frac{\phi\beta I}{N}$  where  $\phi$  can be larger or smaller than 1, i.e. increasing or decreasing the transmission rate. The parameter values are given in Table 1.1, if not otherwise explicitly stated. For more information on parametrization of the basic two-strain model, see (Aguiar & Stollenwerk, 2007; Aguiar et al., 2008).

$$\begin{aligned}
\dot{S} &= -\frac{\beta}{N}S(I_1 + \phi I_{21}) - \frac{\beta}{N}S(I_2 + \phi I_{12}) + \mu(N - S) \\
\dot{I}_1 &= \frac{\beta}{N}S(I_1 + \phi I_{21}) - (\gamma + \mu)I_1 \\
\dot{I}_2 &= \frac{\beta}{N}S(I_2 + \phi I_{12}) - (\gamma + \mu)I_2 \\
\dot{R}_1 &= \gamma I_1 - (\alpha + \mu)R_1 \\
\dot{R}_2 &= \gamma I_2 - (\alpha + \mu)R_2 \\
\dot{S}_1 &= -\frac{\beta}{N}S_1(I_2 + \phi I_{12}) + \alpha R_1 - \mu S_1 \\
\dot{S}_2 &= -\frac{\beta}{N}S_2(I_1 + \phi I_{21}) + \alpha R_2 - \mu S_2 \\
\dot{I}_{12} &= \frac{\beta}{N}S_1(I_2 + \phi I_{12}) - (\gamma + \mu)I_{12} \\
\dot{I}_{21} &= \frac{\beta}{N}S_2(I_1 + \phi I_{21}) - (\gamma + \mu)I_{21} \\
\dot{R} &= \gamma(I_{12} + I_{21}) - \mu R \quad ,
\end{aligned} \tag{1.18}$$

Table 1.1: Parameter set, rates given in units per year, ratio without unit

Par.	Description	Values	Ref
$N$	population size	100	(Aguiar et al., 2008)
$\mu$	new born susceptible rate	$1/65y$	(UNWPP, 2011)
$\gamma$	recovery rate	$52y^{-1}$	(WHO, 2009)
$\beta$	infection rate	$2\gamma$	(Ferguson et al., 1999)
$\alpha$	temporary cross-immunity rate	$2y^{-1}$	(Matheus et al., 2005)
$\phi$	ratio of contribution to force of infection	$\in [0, 3]$	(Aguiar et al., 2008)

The time series for  $\phi < 1$  shows that the total number of infected  $I := I_1 + I_2 + I_{12} + I_{21}$  stays quite away from zero, avoiding the chance of extinction in

stochastic systems with reasonable system size (see Fig. 1.7a)). The parameter region previously considered to model ADE effects on dengue epidemiology, i.e.  $\phi > 1$ , leads to rather low troughs for the total number of infected giving unrealistically low numbers of infected (see Fig. 1.7b)). The logarithm of total number of infected goes as low as  $-70$  for  $\phi = 2.7$  in the chaotic region of  $\phi > 1$ , and the population fluctuations would, in this case, drive almost surely the system to extinction.

The state space plots in terms of the variables  $S$  and the logarithm of the total number of infected  $I$  show a rich dynamical behaviour with increasing  $\phi$  from fixed point to limit cycles, till completely irregular behaviour (see Fig. 1.8). Looking for higher values of  $\phi$ , the chaotic attractor becomes unstable, just leaving simple limit cycles as attractors for large parameter regions beyond  $\phi = 1$ . Only for much higher values of  $\phi \gg 1$ , another chaotic attractor appears, the classical chaotic attractor found first by (Ferguson et al., 1999), and then by (Aguiar & Stollenwerk, 2007; Aguiar et al., 2008).

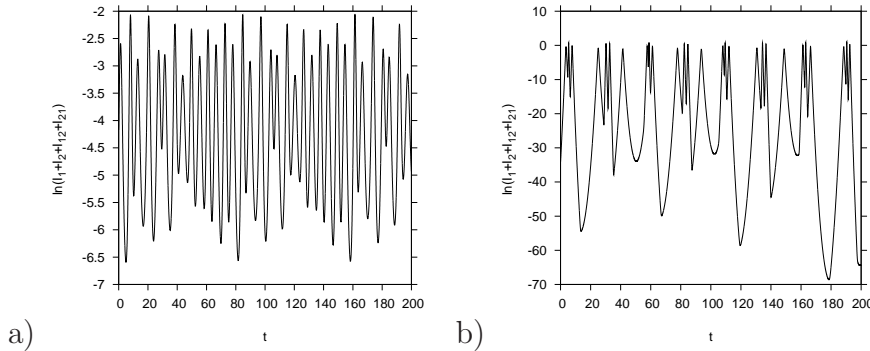


Figure 1.7: Time series of the logarithm of the overall infected ( $\ln(I)$ ) comparison: a) simulation for  $\phi = 2.7$  and b) simulation for  $\phi = 0.6$  for the same time interval.

Bifurcation diagrams (see Fig. 1.9) were obtained plotting the local extrema of the logarithm of total number of infected ( $\ln(I)$ ) over the varying ratio of secondary infection contribution to the force of infection  $\phi$ . Fixed points appear as one dot per parameter value, limit cycles appear as two dots, double-limit cycles as four dots, more complicated limit cycles as more dots, and chaotic attractors as continuously distributed dots for a single  $\phi$  value (Ruelle, 1989). Figure 1.9a) shows two chaotic windows, one for  $\phi < 1$ , where this dynamical behaviour has never been described before, and also another one for  $\phi > 1$  where the minimal values go to very low numbers of infected, already described in previous publications (Ferguson et al., 1999; Schwartz et al, 2005; Billings et al., 2007). When neglecting the temporary cross-immunity period, i.e. by putting  $\alpha \rightarrow \infty$ , the new chaotic window disappears and the complex dynamics is now restricted in a parameter region of  $\phi \gg 1$ , as it is shown in Fig. 1.9b). Here, the recovered individuals can be immediately infected with another strain, and

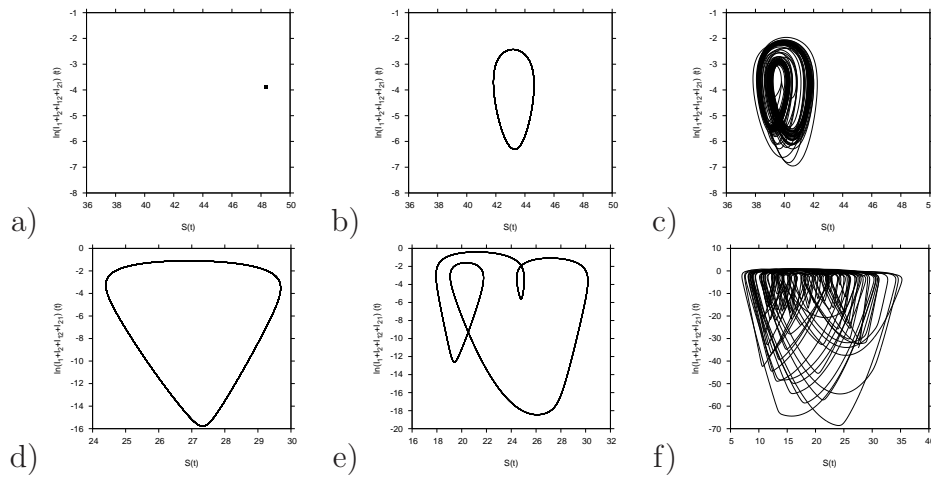


Figure 1.8: Attractors for various values of  $\phi < 1$ : a) fixed point for  $\phi = 0.1$ , in b) limit cycle for  $\phi = 0.4$ , and in c) chaotic attractor for  $\phi = 0.6$ . In d) limit cycle for  $\phi = 1.5$ , in e) a complicated limit cycle for  $\phi = 1.9$  and in f) another chaotic attractor for  $\phi = 2.7$

consideration of temporary cross-immunity brings a new chaotic attractor found first in (Aguiar & Stollenwerk, 2007; Aguiar et al., 2008).

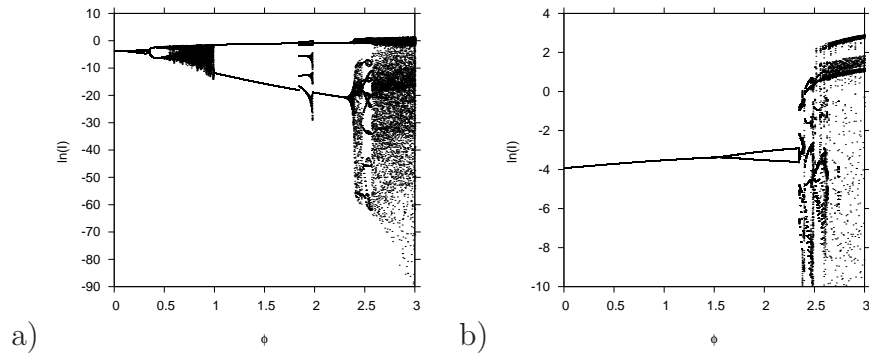


Figure 1.9: Bifurcation diagram for the local extrema of the overall infected with changing parameter  $\phi$ . In a)  $\alpha = 2y^{-1}$  (six month) and in b)  $\alpha = 52y^{-1}$  (one week).

This finding encouraged us to look closer to the parameter region of  $\phi < 1$ , when dengue patients in a secondary infection evolving to severe disease because of the ADE phenomenon contribute less to the force of infection, and not more, as previous models suggested. This assumption is likely to be more realistic for dengue fever since the possible severity of a secondary infection may hospitalize people, not contributing to the force of infections as much as people with first infection.

The attractor structure, fixed point, limit cycle or chaotic attractor can be



quantified by calculating the Lyapunov exponents, (Ruelle, 1989; Ott, 1993), using an iterated technique along a trajectory using the QR decomposition algorithm via Householder matrices (see e.g. (Holzfuss & Lauterborn, 1989; Holzfuss & Parlitz, 1991)). Lyapunov exponents are essentially a generalization of eigenvalues determining stability versus instability along trajectories. A negative largest Lyapunov exponent indicates a stable fixed point as attractor, a zero largest Lyapunov exponent indicates a stable limit cycle and a positive largest Lyapunov exponent indicates a chaotic attractor. The largest four Lyapunov exponents as a function of the parameter  $\phi$ , the ratio of secondary infection contribution to the force of infection, are shown in Fig. 1.10a).

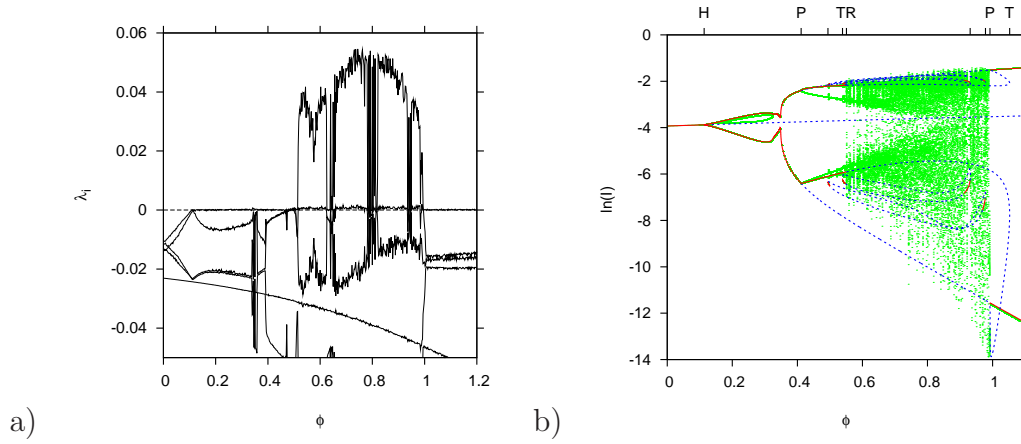


Figure 1.10: In a) spectrum of the four largest Lyapunov exponents with changing the ratio of secondary infection contribution to the force of infection, parameter  $\phi$ , and fixed temporary cross-immunity  $\alpha = 2y^{-1}$ . In b) we show the one-parameter bifurcation diagram with temporary cross-immunity rate of six months ( $\alpha = 2y^{-1}$ ) and varying the ratio of secondary infection contribution to the force of infection  $\phi$ . Solid lines denote stable equilibria or limit cycles, and dashed lines unstable equilibria or limit cycles.

We observe that for small  $\phi$  up to  $\phi = 0.1$  all four Lyapunov exponents are negative, indicating the stable fixed point solution. Then follows a region up to  $\phi = 0.5$  where the largest Lyapunov exponent is zero, characteristic for stable limit cycles. Above  $\phi = 0.5$  a positive Lyapunov exponent, clearly separated from the second largest Lyapunov exponent being zero, indicates deterministic chaos. In the chaotic window between  $\phi = 0.5$  and  $\phi = 1$  also periodic windows appear, giving a zero largest Lyapunov exponent. These findings are in good agreement with the numerical bifurcation diagram shown in Fig. 1.10b). A further analysis of the bifurcation structure, in the region of interest of  $\phi < 1$ , was performed using the numerical software AUTO (AUTO, 2009). Various bifurcations were found: Hopf bifurcation  $H(\phi = 0.11326)$ , pitchfork bifurcations  $P(\phi = 0.41145, 0.99214)$ , torus bifurcation  $TR(\phi = 0.55069)$  and tangent bifur-



cations  $T(\phi = 0.49406, 0.53874, 0.93103, 0.97825, 1.05242)$ . In addition to this main bifurcation pattern we found two isolas, consisting of isolated limit cycles existing between two tangent bifurcations (see Fig. 1.10b). For more information on the isolas see (Aguiar et al., 2009).

Dengue fever epidemiology is characterized as a yearly cycle of incidences (see Fig. 1.11 e.g., the time series of DHF incidence in Thailand), therefore, to reproduce the yearly cycle in dengue incidence, seasonal forcing and a low import of infected had to be included in the models.

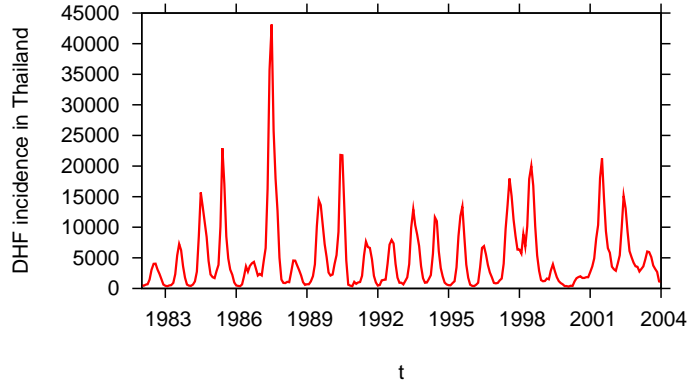


Figure 1.11: Time series of DHF incidence in Thailand.

The previously described non-seasonal model was extended by adding seasonal forcing, mimicking the vectorial dynamics, and also allowing a low import of infected individuals, giving a more realistic pattern of dengue fever epidemics, with irregular, yearly and smooth outbreaks (see Fig. 1.13b)). The seasonal multi-strain model, is represented in Fig. 1.12 by using a state flow diagram where the boxes represent the disease related stages and the arrows indicate the transition rates. Likewise described for the non-seasonal model, the population is divided into ten classes, with constant size  $N = S + I_1 + I_2 + R_1 + R_2 + S_1 + S_2 + I_{12} + I_{21} + R$ . The transition rate  $\mu$  coming out of the class  $R$  represents the death rates of all classes,  $S, I_1, I_2, R_1, R_2, S_1, S_2, I_{12}, I_{21}, R$ , getting into the class  $S$  as a birth rate.

The complete system of ordinary differential equations for the seasonal multi-strain epidemiological model with import of infected can be written as it was shown in system Eq. (1.18), with the difference that now the parameter  $\beta$  takes the seasonal forcing into account as a cosine function given explicitly by

$$\beta(t) = \beta_0 \cdot (1 + \eta \cdot \cos(\omega \cdot t)) \quad , \quad (1.19)$$

where  $\beta_0$  is the infection rate, and  $\eta$  is the degree of seasonality. In the seasonal model with import of infected, the susceptible individual can become infected also by meeting an infected individual from an external population, the so-called imported infection which is realistic in the dynamics of infectious diseases, (hence

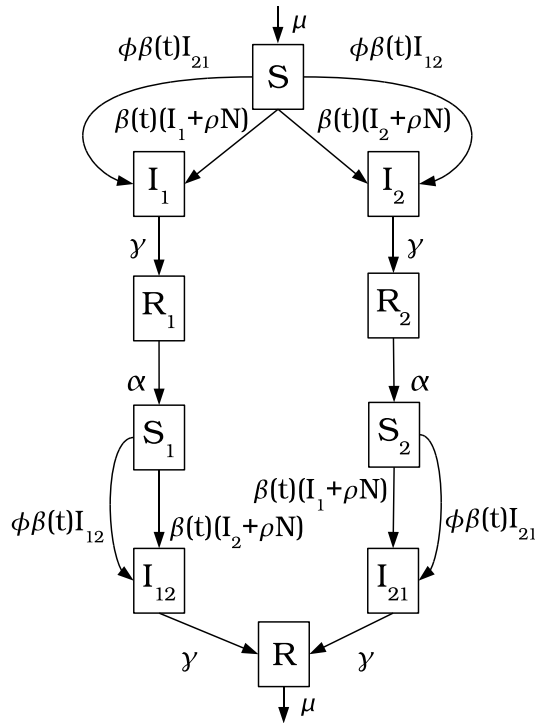


Figure 1.12: The state flow diagram for the seasonal multi-strain model.

$(\beta/N \cdot S \cdot I)$  goes to  $(\beta/N \cdot S \cdot (I + \rho \cdot N))$  contributing to the force of infection with an import parameter  $\rho$ .

The time series simulation for non-seasonal model show an irregular pattern of outbreaks that happens every 5 years, the non-seasonal system and its time series are not able to represent dengue fever epidemiology that is characterized as a yearly cycle of incidences (see Fig. 1.13a)). By adding only low seasonality into this system, the epidemic outbreaks appear every year (see (Aguiar et al., 2011 a)), however, between two large outbreaks there is a very low number of cases in subsequent years, which is also not data alike. The addition of import factor into the seasonal system gives a much more realistic pattern of dengue fever epidemics, with irregular, yearly and smooth outbreaks (see Fig. 1.13b)). The system has a reasonable size, avoiding the chance of extinction in stochastic systems. For detailed analysis on the attractors in state space for the seasonal models, see (Aguiar et al., 2011 a).

For the seasonal model with import AUTO predicted a torus bifurcation  $TR$  at  $\phi = 0.13$ , and at  $\phi = 0.522$  which are also predicted very well when comparing with the results given by the Lyapunov exponent calculation. In the limiting case where the amplitude of the seasonal forcing is zero, the torus bifurcation  $TR$  of the seasonally forced system coincides with the Hopf bifurcation  $H$  of the non-seasonal system. For more information on the bifurcation points comparison, see

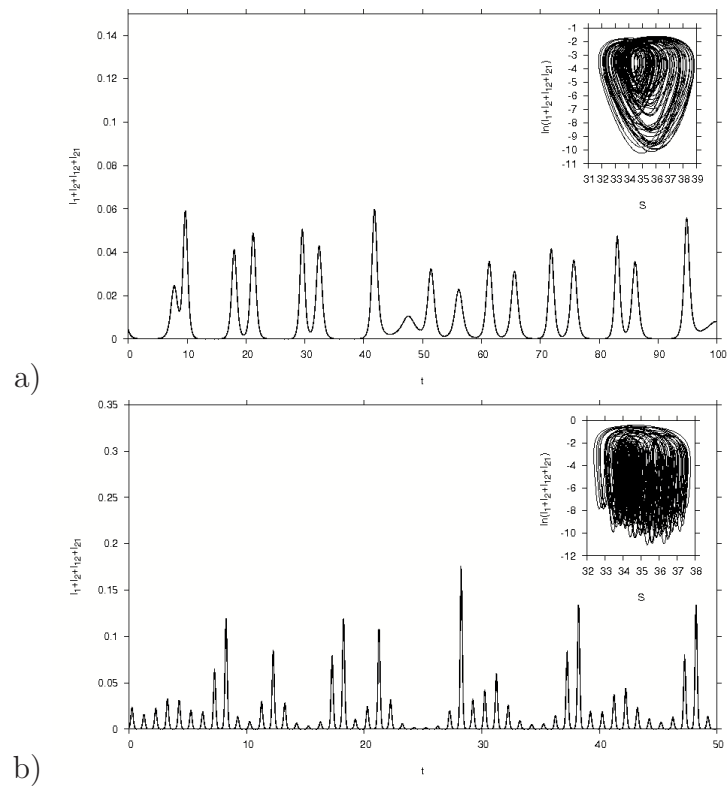


Figure 1.13: Time series simulations. In a) time series simulation for the non-seasonal model ( $\eta = 0$ ). In b) time series simulation for the seasonal model with a low import of infected. Here, the degree of seasonality is  $\eta = 0.35$  and the import factor  $\rho = 10^{-10}$ .

(Aguiar et al., 2011 a).

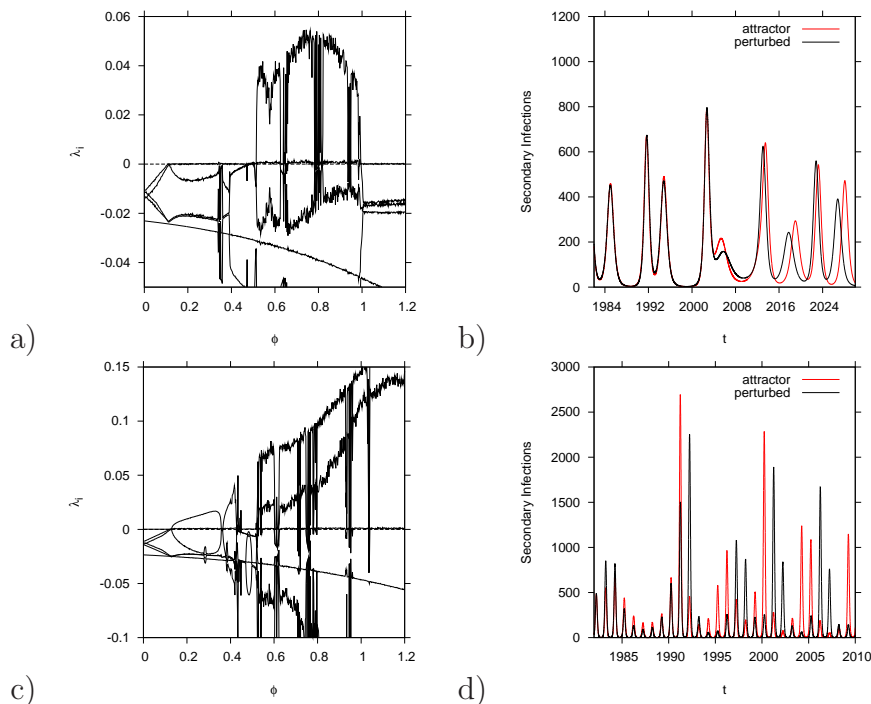


Figure 1.14: Qualitative insight into the predictability in the monthly time series. In a) the Lyapunov spectrum and in b) the time series for the non-seasonal model. In c) the Lyapunov spectrum and in d) the time series for the seasonal model with import.

The Lyapunov spectrum for both non-seasonal model and the seasonal model with import are compared concerning the prediction horizon of the monthly peaks in the multi-strain dengue model time series (see Fig. 1.14).

In order to get a qualitative insight into the predictability in the monthly sampled time series, i.e. to show how the original system behaves under a small perturbation we plot two different trajectories of the same system, where the perturbed system (black line) is compared with the original model simulation (red line). To get the trajectory of the perturbed system, we keep the last point of the transient of the original system and use those values as starting values to compute the new and perturbed trajectory. The perturbation is given by  $S = S + R \cdot \epsilon$  and  $R = R \cdot (1.0 - \epsilon)$ , where  $\epsilon = 0.001$ . For details on the perturbed system see (Aguiar et al., 2011 a).

We take as an example the Dominant Lyapunov Exponent (DLE) for  $\phi = 0.9$  in the region where the system is chaotic (positive DLE). For the non-seasonal system, the  $DLE = 0.04$  giving around 25 years of prediction horizon in the monthly time series (see Fig. 1.14b)), whereas for the seasonal system with import, the  $DLE = 0.118$  giving around 8.5 years of prediction horizon in the monthly time

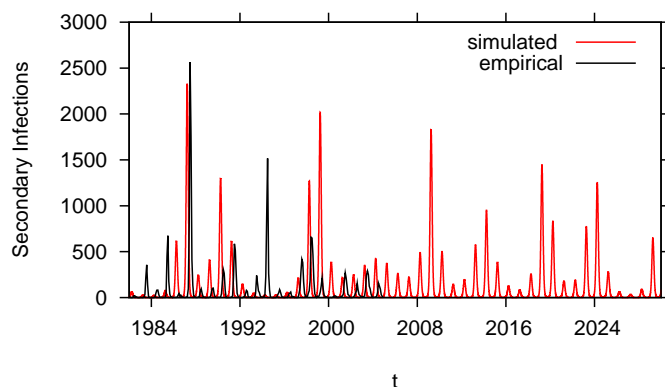


Figure 1.15: Empirical DHF incidence data (in black) matched with the model simulation (in red).

series (see Fig. 1.14d)).

The inspection of the available DHF incidence data in Thailand shows a smooth behaviour with a well defined maximum each year of irregular height for the Northern Provinces. We take the Province of Chiang Mai as a case study where the empirical DHF incidence data and the time series simulation for the seasonal model with import are compared (see Fig. 1.15)). The seasonal model with import shows qualitatively a very good result when comparing empirical DHF and simulations. However, it is important to mention that the extended model would need to be parametrized on data referring to incidence of severe disease.

Although the fact that disease propagation is an inherently stochastic phenomenon and it is only stochastic, as opposed to deterministic, models that can capture the fluctuations observed in some of the available time series data, dengue models are often expressed mathematically as a set of deterministic differential equations which are easier to analyse.

For small population sizes, most simulation die out very quickly (see Fig. 1.3), and since the demographic events often occur at a much slower rate than the infection, the disease has to be necessarily maintained by the import of external infections to avoid the repeated stochastic disease extinction and re-introduction.

For the minimalistic multi-strain dengue model, the individuals can be susceptibles without a previous dengue infection, infected and recovered for the first time, susceptible with an experienced previous infection and infected for the second time, now with a different strain, and more likely been hospitalized due to the ADE effect leading to severe disease. The stochastic realizations of infected in time, shown in Fig. 1.16, were obtained by the Gillespie algorithm (Gillespie, 1976, 1978). The stochastic approach is able to describe both types of the dynamics, the smooth data with a well defined maximum each year of irregular

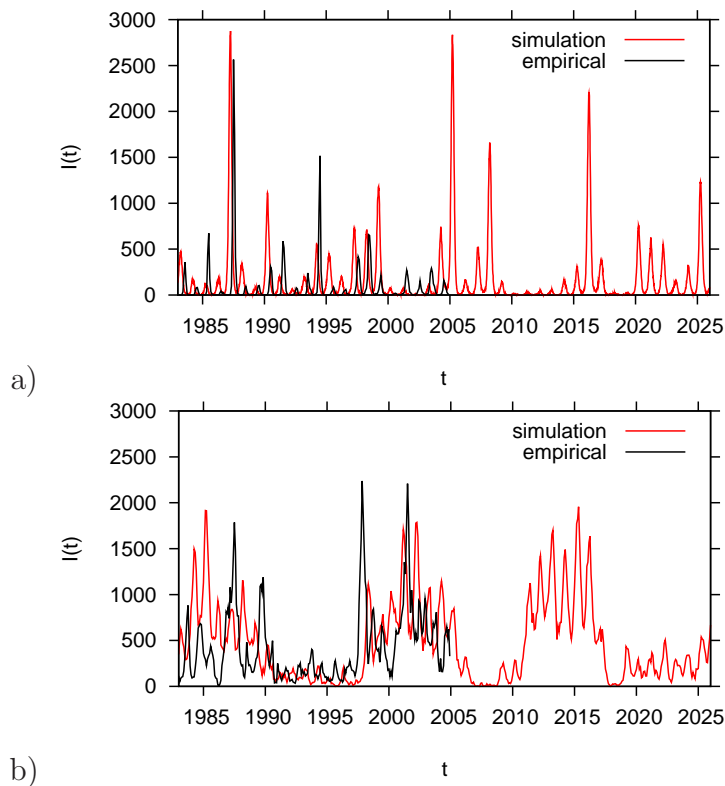


Figure 1.16: Empirical DHF incidence data (in black) matched with one stochastic realization for the seasonal multi-strain dengue model with import (in red). In a) we show the incidences for Chaing Mai. For the stochastic simulation the infection rate is  $\beta_0 = 2\gamma$ , the degree of seasonality  $\eta = 0.2$  and the import factor  $\ln(\rho) = -15.7$ . In b) we show the incidences for Bangkok. For the stochastic simulation the infection rate is  $\beta_0 = 1.1 \cdot \gamma$ , the degree of seasonality  $\eta = 0.06$  and the import factor  $\ln(\rho) = -16.9$ . The other parameter values are listed Table 1.1

height, found in the high endemic regions of Thailand, e.g. in the Chiang Mai Province (see Fig. 1.16a)) and also the noisy data found mainly in low endemic regions of Thailand, e.g. in Bangkok (see Fig. 1.16b)).

Comparison between the deterministic and the stochastic dynamics show that the magnitude of stochastic fluctuations decreases when the population size increases, see Fig. 1.17, and for large enough population size, the stochastic system can be well described by the deterministic skeleton, where the essential dynamics are captured, gaining insight into the relevant parameter values purely on topological information of the dynamics. For more information on the stochastic dengue model see (Aguiar et al., 2011 c).

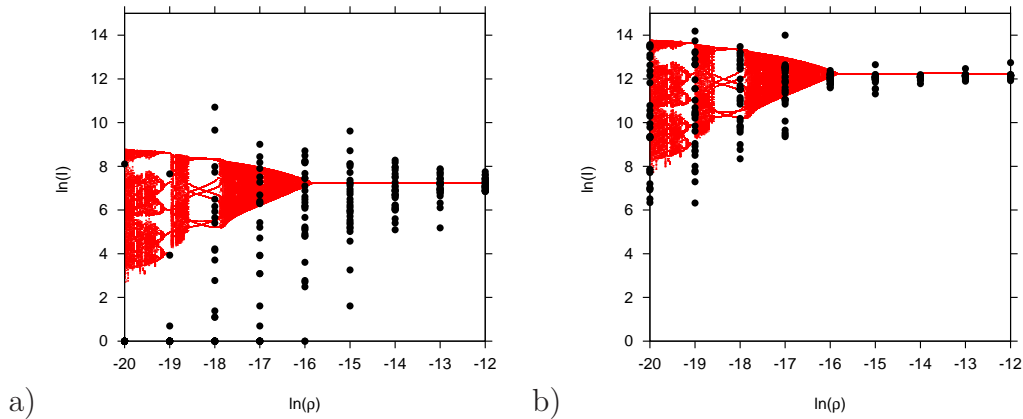


Figure 1.17: Stochastic and deterministic system's interaction. For the same parameter values used in Fig. 1.16, we show the bifurcation diagram for the import parameter for different population sizes  $N$ . In red the deterministic model and in black the stochastic model. In a) the Chiang Mai population size  $N = 1.65 \cdot 10^6$  and in b) a much larger system size, where the population of some countries surrounding Thailand, for instance Burma, Laos, Vietnam and Cambodia, were counted together giving a system where the population size is  $N = 230 \cdot 10^6$ .

The two-strain dengue model is minimalistic in the sense that it can capture the essential differences of primary versus secondary infection but is not too high dimensional, it is a 9 dimensional system, so that future parameter estimation can still attempt to estimate all initial conditions as well as the few model parameters. Concerning data availability, long term epidemiological information come from the Ministry of Public Health in Thailand and consist on monthly incidences of hospitalized DHF cases.

The four-strain model is a 25 dimensional system, dividing the constant population  $N$  into twenty six classes. For four different strains, 1, 2, 3 and 4, we now label the SIR classes, in a similar way to the two-strain model, for the hosts that have seen the individual strains, again without epidemiological

asymmetry between strains, once the serotype data are recent and very short to give any realistic information concerning difference in biological parameters

such as infection and recovery rates for a given strain.

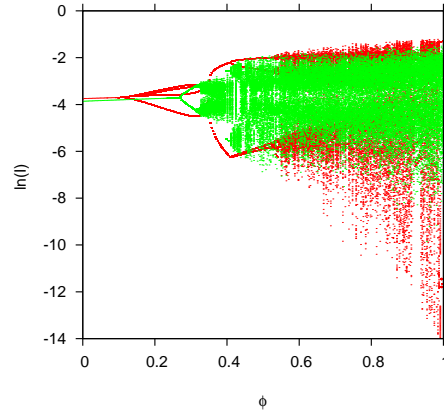


Figure 1.18: Bifurcation diagram comparison between the multi-strain models for the parameter region of  $\phi < 1$ . In red the two-strain model and in green the four-strain model. The local extrema of the overall infected with changing parameter  $\phi$  are plotted.

The bifurcation diagram comparison, for both two-strain and four-strain model, in the relevant parameter region of  $\phi < 1$ , when dengue patients in a secondary infection evolving to severe disease because of the ADE phenomenon contribute less to the force of infection, and not more, as previous models suggested is shown in figure 1.18. Qualitatively, the bifurcation points appear to happen at similar parameter regions, well below the region of interest  $\phi \approx 1$ , and for both models the chaotic dynamics which are able to explain the fluctuations observed in empirical data were found at the same parameter region of interest, when the ratio of secondary infection contribution to the force of infection could be slightly smaller or larger than 1 (see, e.g. (Aguiar et al., 2011 a,d)) and not only when assuming strong infectivity on secondary infection.

The effective dimension of the two-strain model is 9 while of the four-strain model 25. The law of parsimony that recommends selecting the hypothesis that makes the fewest assumptions, implies that the 9 dimensional two-strain model would be the better candidate than the 25 dimensional four strain model to be analyzed, capturing the essential differences of primary versus secondary infection without needing to restrict the ADE effect to one or another region in parameter space. Moreover, for future parameter estimation which is notoriously difficult for chaotic time series, only the two-strain model could attempt to estimate all initial conditions as well as the few model parameters, as opposed of the four-strain model in the near future. For more information on the four-strain dengue model see (Aguiar et al., 2011 d).



## 1.4 Discussion and conclusions

In this chapter we presented the properties of the basic SIR epidemic model for infectious diseases with a summary of the analysis of the dynamics, identifying the thresholds and equilibrium points in order to introduce notation, terminology. These results were generalized to more advanced models motivated by dengue fever epidemiology.

The epidemiology of dengue fever was described presenting the relevant biological features that are taken into the modeling process. Then, multi-strain models previously described in the literature were presented. We focused in a minimal model motivated by dengue fever epidemiology, formulated first by Aguiar et al. (see (Aguiar & Stollenwerk, 2007; Aguiar et al., 2008)), where the notion of at least two different strains is needed to describe differences between primary infections, often asymptomatic, and secondary infection, associated with the severe form of the disease. We discussed the role of seasonal forcing and the import of infected individuals in such systems, the biological relevance and its implications for the analysis of the available dengue data. The extended model (Aguiar et al., 2011 a) shows complex dynamics and qualitatively a good agreement between empirical DHF monitoring data and the model simulation results obtained by trail and error parameter choice, not by a numerical parameter estimation technique. This suggests that the used parameter set can be the starting set for a more detailed parameter estimation procedure. Such a technical parameter estimation is notoriously difficult for chaotic time series but temporally local approaches are possible (Ionides et al., 2006; He et al., 2010). At the moment only such minimalistic models have a chance to be qualitatively understood well and eventually tested against existing data.

The combination of biological aspects such as temporary cross-immunity and ADE have been studied by several authors (Wearing & Rohani, 2006; Nagao & Koelle, 2008; Recker et al., 2009) where four strains are involved, but again limiting the effect of ADE to increase the contribution of secondary cases to the force of infection. Aguiar et al. (2008) have investigated a two-strain dengue model, initially suggested and preliminarily analyzed in (Ferguson et al., 1999), where deterministic chaos was found in a wider parameter regions when including temporary cross-immunity (Aguiar et al., 2008, 2009, 2011 a), not needing to restrict the infectivity on secondary infection to one or another region in parameter space.

The comparison between the two-strain dengue model, which already captures differences between primary and secondary infections, with the four-strain dengue model, that introduces the idea of competition of multiple strains in dengue epidemics, shows that the difference between first and secondary infections and temporary cross-immunity drives the rich dynamics more than the detailed number of strains. Qualitatively, the bifurcation points appear to happen at similar parameter regions, well below the region of interest  $\phi \approx 1$  (Aguiar et al., 2011 d). We therefore conclude that the two-strain model in its simplicity is a

good model to be analysed giving the expected complex behaviour to explain the fluctuations observed in empirical data. For future parameter estimation, the two-strain model can still attempt to estimate all initial conditions as well the few model parameters.

The introduction of stochasticity is needed to explain the fluctuations observed in some of the available data sets, revealing a scenario where noise and complex deterministic skeleton strongly interact (Aguiar et al., 2011 c). Understanding the dynamics of stochastic populations, and how they interact with the deterministic components of epidemiological models have maximum benefit on the practical predictability of the dynamical system by analysing the available epidemiological data via mathematical models, since the classical parameter estimation and its application are generally restricted to fairly simple dynamical scenarios. For more information on parameter estimation, see (Aguiar et al., 2011 b).

Being able to predict future outbreaks of dengue in the absence of human interventions is a major goal if one wants to understand the effects of control measures. Even after a dengue virus vaccine has become accessible, this holds true for the implementation of a vaccination program. For example, to perform a vaccine trial in a year with normally low numbers of cases would make statistical tests of vaccine efficacy much more difficult than when it was performed in a year with naturally high numbers of cases. Thus predictability of the next season's height of the dengue peak on the basis of deterministic balance of infected and susceptible would be of major practical use.



## Chapter 2

# Epidemiology of dengue fever: A model with temporary cross-immunity and possible secondary infection shows bifurcations and chaotic behavior in wide parameter regions

Maíra Aguiar, Bob Kooi and Nico Stollenwerk  
*Math. Model. Nat. Phenom.*, **3**(4): 48-70, 2008.

Basic models suitable to explain the epidemiology of dengue fever have previously shown the possibility of deterministically chaotic attractors, which might explain the observed fluctuations found in empiric outbreak data. However, the region of bifurcations and chaos require strong enhanced infectivity on secondary infection, motivated by experimental findings of antibody-dependent enhancement.

Including temporary cross-immunity in such models, which is common knowledge among field researchers in dengue, we find bifurcations up to chaotic attractors in much wider and also unexpected parameter regions of reduced infectivity on secondary infection, realistically describing more likely hospitalization on secondary infection when the viral load becomes high and the hemorrhagic phenomena is more likely to happen.

The model shows Hopf bifurcations, symmetry breaking bifurcations of limit cycles, coexisting isolas, and two different possible routes to chaos, via the Feigenbaum period doubling and via torus bifurcations.

## 2.1 Introduction

Dengue fever is caused by four antigenically distinct viruses, designated dengue types 1, 2, 3, and 4 (WHO, 2009). Infection by one serotype confers life-long immunity to only that serotype and temporary cross-immunity to other serotypes exists. It lasts from three to nine months, when the antibody levels created during the response to that infection would be enough to protect against infection by a different but related serotype (see (Halstead, 1994; Matheus et al., 2005; WHO, 2009; SES, 2010; Dejnirattisai et al., 2010)). The empiric time of temporary cross-immunity is mainly based on detectable antibody levels, however, the epidemiological period of temporary cross-immunity can be much larger (Welsh & Selin, 2002; SES, 2010).

Among symptomatic cases dengue fever (DF) is often benign. But a severe form known as dengue hemorrhagic fever (DHF), which may evolve towards dengue shock syndrome (DSS), can also occur. Without proper treatment DHF/DSS case fatality rates can exceed 20% (WHO, 2009). There are indeed pre-existing antibodies to previous dengue virus that cannot neutralize but rather enhance infection *in vitro*, a process described as antibody-dependent enhancement (ADE). The ADE theory states that cross-reactive, non-neutralizing antibodies from a previous heterologous dengue virus infection bind to the new infecting serotype and facilitate virus entry via Fc-receptor-bearing cells such as monocytes and macrophages. Increased virus replication and antigen presentation lead to an exaggerated immune response increasing disease manifestation with plasma leakage and hemorrhagic phenomena (Halstead & Rourke, 1977; Kliks et al., 1989; Vaughn et al., 2000). Epidemiological studies support the association of DHF with secondary dengue infection (Halstead, 1982; Guzmán et al., 2000; Halstead, 2003; WHO, 2009). However, there is no animal model of DHF/DSS.

Mathematical models describing the transmission of dengue viruses appeared in the literature as early as 1970 (Fischer & Halstead, 1970). More recently, modeling attention has focused on higher viral load of hosts on secondary infection than on the first infection, due to ADE, hence a higher contribution to the force of infection of each strain, reporting deterministically chaotic attractors (Ferguson et al., 1999) and chaos de-synchronization (Schwartz et al., 2005; Billings et al., 2007) to explain the irregular behavior of dengue epidemics and the co-existence of the known four dengue viral strains. Temporary cross-immunity against all strains after a first infection has been included in mathematical models as well, but again limiting the effect of ADE to increase the contribution of secondary cases to the force of infection (Wearing & Rohani, 2006). To our knowledge, no systematic investigation of the attractor structures of simple multi-strain models with dengue-realistic temporary cross-immunity and decreased contribution of secondary infection to the force of infection, due to severity of infection with a second strain caused by higher viral load and eventual hospitalization, has been

performed so far. Temporary cross-immunity also has to be distinguished from partial cross-immunity as also modeled for dengue (Adams & Boots, 2006, 2007).

We investigate a basic two-strain model, initially suggested and preliminarily analyzed in (Aguiar & Stollenwerk, 2007), to capture primary and secondary infection, with main attention to differences in the force of infection in primary versus secondary infection (parametrized by  $\phi$ ) and the effect of temporary cross-immunity between the first and second infection with distinct strains (parametrized by  $\alpha$ ). Neglecting the effect of temporary cross-immunity or considering a very short period of one week (transition rate  $\alpha = 52y^{-1}$ ) we find the first Hopf bifurcation from a steady state to a limit cycle, hence non-equilibrium dynamic behavior, for a more than one and a half times higher infectivity on secondary infection versus primary (ratio  $\phi > 1.5$ ). Whereas including a realistic value for the temporary cross-immunity of e.g. half a year ( $\alpha = 2y^{-1}$ ), we find the first Hopf bifurcation for the infectivity ratio as low as one tenth ( $\phi = 0.1$ ) and a positive Lyapunov exponent as sign of a deterministically chaotic attractor around  $\phi = 0.5$ .

An extremely rich bifurcation structure is observed for  $\phi < 1$  when taking the temporary cross-immunity in a dengue realistic parameter regime for  $\alpha \in [1, 3]y^{-1}$ . Improving earlier presented results (Aguiar & Stollenwerk, 2007) here we explore and describe in more detail the rich bifurcation structure around such low  $\alpha$  values, especially  $\alpha = 2y^{-1}$  and  $\phi < 1$ . In this parameter region the model shows Hopf bifurcations, symmetry breaking bifurcations of limit cycles, coexisting isolas, and two different possible routes to chaos, via the Feigenbaum period doubling and via torus bifurcations. Whereas previous modeling efforts have concentrated on  $\phi > 1$  we find this rich dynamics when in the secondary infection people are less infectious, i.e. transmitting less the infection, than people in first dengue infection, hence for  $\phi < 1$ . This assumption is likely to be more realistic for dengue fever since the possible severity of a secondary infection may hospitalize people, not contributing to the force of infections as much as people with first infection. Nevertheless, the relatively restrictive assumption of much higher contribution to the force of infection of secondary infectivity previously necessary for complex dynamics can be relaxed significantly when taking the temporary cross-immunity into account.

Hence observed fluctuations in dengue outbreak data could now be understood better considering multi-strain dynamics as significant factor. The more detailed understanding of possible state space scenarios through bifurcation analysis will help in future understanding of dengue epidemiological data and its multi-strain aspects. The basic model structure allows to generalize our findings to other multi-strain epidemiological systems expecting the same complexity.

## 2.2 Basic two-strain epidemic model

The present model is a basic two-strain SIR-type model dividing the host population into susceptible (S), infected (I) and recovered individuals (R). It can be understood as a mean field approximation of a stochastic system. The simple SIR epidemics without strain structure of the pathogens reads

$$\begin{aligned}\dot{S} &= \alpha R - \frac{\beta}{N} \cdot I \cdot S + \mu(N - S) \\ \dot{I} &= \frac{\beta}{N} \cdot I \cdot S - \gamma I - \mu I \\ \dot{R} &= \gamma I - \alpha R - \mu R\end{aligned}\tag{2.1}$$

for a host population of  $N$  individuals, with contact and infection rate  $\beta$ , recovery rate  $\gamma$  and temporary immunity rate  $\alpha$ . Demography is denoted as exits from all classes  $S$ ,  $I$  and  $R$  with rate  $\mu$  to the new born susceptibles. The system has only equilibria steady solutions as attractors. Transients under certain parameter values oscillate into the equilibrium, hence can be already more complex than the final attractor. Stochastic versions of such models with only fixed points possible as attractors but oscillating transients are reported to also show stabilization of the oscillations due to population noise (McKane & Newman, 2005; Alonso et al., 2006).

To capture differences in primary infection by one strain and secondary infection by another strain we consider a basic two-strain SIR-type model for the host population, which is only slightly refined as opposed to previously suggested models for dengue fever (Ferguson et al., 1999; Schwartz et al, 2005). It is capturing the effective dynamics of the human host population for the dengue virus, taking effects of the vector dynamics or seasonality only into account by the effective parameters in the SIR-type model, but not modeling these mechanisms explicitly. Instead we focus on the multi-strain aspect and its effects on the host population. The complete system of ordinary differential equations for the two-strain

epidemiological system is given by

$$\begin{aligned}
\dot{S} &= -\frac{\beta_1}{N}S(I_1 + \phi_1 I_{21}) - \frac{\beta_2}{N}S(I_2 + \phi_2 I_{12}) + \mu(N - S) \\
\dot{I}_1 &= \frac{\beta_1}{N}S(I_1 + \phi_1 I_{21}) - (\gamma + \mu)I_1 \\
\dot{I}_2 &= \frac{\beta_2}{N}S(I_2 + \phi_2 I_{12}) - (\gamma + \mu)I_2 \\
\dot{R}_1 &= \gamma I_1 - (\alpha + \mu)R_1 \\
\dot{R}_2 &= \gamma I_2 - (\alpha + \mu)R_2 \\
\dot{S}_1 &= -\frac{\beta_2}{N}S_1(I_2 + \phi_2 I_{12}) + \alpha R_1 - \mu S_1 \\
\dot{S}_2 &= -\frac{\beta_1}{N}S_2(I_1 + \phi_1 I_{21}) + \alpha R_2 - \mu S_2 \\
\dot{I}_{12} &= \frac{\beta_2}{N}S_1(I_2 + \phi_2 I_{12}) - (\gamma + \mu)I_{12} \\
\dot{I}_{21} &= \frac{\beta_1}{N}S_2(I_1 + \phi_1 I_{21}) - (\gamma + \mu)I_{21} \\
\dot{R} &= \gamma(I_{12} + I_{21}) - \mu R \quad .
\end{aligned} \tag{2.2}$$

For two different strains, 1 and 2, we label the SIR classes for the hosts that have seen the individual strains. Susceptibles to both strains (S) get infected with strain 1 ( $I_1$ ) or strain 2 ( $I_2$ ), with force of infection  $\beta_1$  and  $\beta_2$  respectively. They recover from infection with strain 1 (becoming  $R_1$ ) or from strain 2 (becoming  $R_2$ ), with recovery rate  $\gamma$ . In this recovered class, people have full and life-long immunity against the strain that they were exposed to and infected, and also a short period of temporary cross-immunity against the other strain. After this, with rate  $\alpha$ , they become again susceptible, now with a previous infection ( $S_1$  respectively  $S_2$ ), where the index represents the first infection strain. Now,  $S_1$  can be infected with strain 2 (becoming  $I_{12}$ ), meeting  $I_2$  with infection rate  $\beta_2$  or meeting  $I_{12}$  with infection rate  $\phi_2\beta_2$ . Note that secondary infected individuals contribute differently to the force of infection than primary infected individuals. In the same manner, the  $S_2$  class can be infected with strain 1 (becoming  $I_{21}$ ) meeting  $I_1$  or  $I_{21}$  with infections rates  $\beta_1$  and  $\phi_1\beta_1$  respectively.

The parameter  $\phi$  in our model, as opposed to the previous dengue models, acts decreasing the infectivity of secondary infection, once people with higher



viral load and hemorrhagic symptoms are more likely to be hospitalized because of the severity of the disease (DHF/DSS), and do not contribute to the force of infection as much as people with first infection do. Finally,  $I_{12}$  and  $I_{21}$  become recovered (R), immune against all strains. We include demography of the host population denoting the birth and death rate by  $\mu$ . For constant population size  $N$  we have  $R = N - (S + I_1 + I_2 + R_1 + R_2 + S_1 + S_2 + I_{12} + I_{21})$  and therefore we only need to consider the first 9 equations of system Eq. (2.2). In our numerical studies we take the population size equals  $N = 100$  so that numbers of susceptibles, infected etc., are given in percentage.

To take biological information from experiences in dengue into account we fix the transition rates of the model as far as is known, and only will vary the most unknown parameter  $\phi$ . For simplicity, we consider  $\phi_1 = \phi_2 = \phi$ ,  $\beta_1 = \beta_2 = \beta$ , i.e., no epidemiological asymmetry between strains. The parameter values are given in Table 2.1, if not otherwise explicitly stated.

Table 2.1: Parameter set, rates given in units per year, ratio without unit

Par.	Description	Values	
$N$	population size	100	(Aguiar & Stollenwerk, 2007)
$\mu$	new born susceptible rate	$1/65y$	(UNWPP, 2011)
$\gamma$	recovery rate	$52y^{-1}$	(WHO, 2009)
$\beta_1 = \beta_2 = \beta$	infection rate	$2\gamma$	(Ferguson et al., 1999)
$\alpha$	temporary cross immunity rate	$2y^{-1}$	(Matheus et al., 2005)
$\phi_1 = \phi_2 = \phi$	ratio of contrib. to force of inf.	variable	(Aguiar & Stollenwerk, 2007)

## 2.3 Time series analysis

In this section we investigate time series simulations of the present model, system Eq. (2.2). We performed a detailed analysis of the attractor structure, investigating state space plots for various values of  $\phi$ . Besides the previously analyzed region of  $\phi > 1$  we also observe a rich dynamical behavior from fixed points to bifurcating limit cycles and chaotic attractors for  $\phi < 1$ . Maxima return maps are evaluated from extremely long time series, and Lyapunov exponents are calculated. This rich dynamic structure will be analyzed in the next section in more detail via bifurcation analysis by continuation.

### 2.3.1 Time series simulations

In order to classify the dynamic pattern of the model for various parameters, we discard long transients which would carry information about the initial conditions. In the following simulations we discarded the first 2000 years (see Fig. 2.1). However, also the transients reflect the dynamic behavior of the system under the present parameter values.

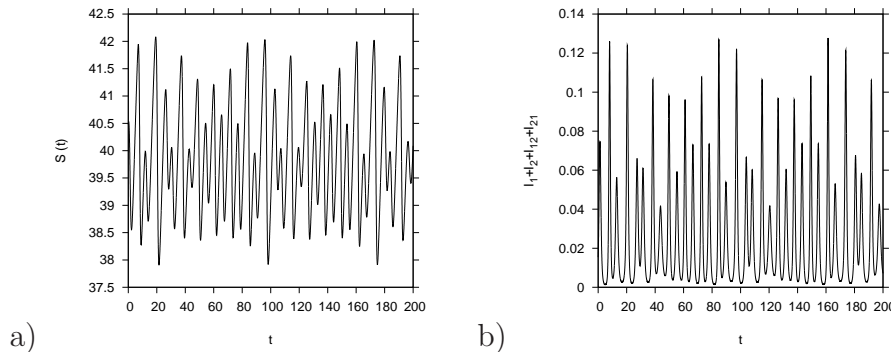


Figure 2.1: For temporary cross-immunity period of six months ( $\alpha = 2y^{-1}$ ) and ratio of secondary infection contribution to the force of infection  $\phi = 0.6$ , we present in a) time series simulations for the susceptibles  $S$ , and in b) time series simulations for the total number of infected  $I$ .

The time series for  $\phi < 1$ , as would be realistic for dengue fever due to more severe disease upon reinfection and larger chance of people being hospitalized, shows that the total number of infected

$$I := I_1 + I_2 + I_{12} + I_{21} \quad (2.3)$$

stays quite away from zero, avoiding the chance of extinction in stochastic systems with reasonable system size (see Fig. 2.1b)).

The parameter region previously considered to model ADE effects on dengue epidemiology, i.e.  $\phi \gg 1$ , leads to rather low troughs for the total number of infected giving unrealistically low numbers of infected. In Fig. 2.2a) the logarithm of total number of infected goes as low as  $-70$  for  $\phi = 2.7$  in the chaotic region of  $\phi > 1$ . Population fluctuations would in this case drive almost surely the system to extinction.

For  $\phi = 0.6$ , hence the chaotic dynamics in the region of  $\phi < 1$ , see Fig. 2.2b), the logarithm of total infected does not pass below  $-7$ . This encourages us to look closer to the parameter region of  $\phi < 1$ , when dengue patients with severe disease because of the ADE phenomenon contribute less to the force of infection due to possible hospitalization, and not more, as previous models suggested.

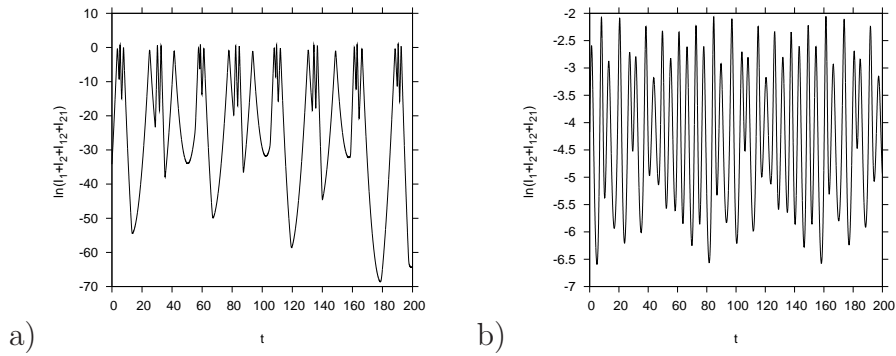


Figure 2.2: Time series of the logarithm of the overall infected ( $\ln(I)$ ) comparison: In a) simulation for ratio of secondary infection contribution to the force of infection  $\phi = 2.7$  and in b) simulation for ratio of secondary infection contribution to the force of infection  $\phi = 0.6$  for the same time interval.

### 2.3.2 State space plots

Next, we investigate the state space plots in terms of the variables  $S$  and the logarithm of the total number of infected  $I$ , since dengue notification data often do not distinguish between the circulating strains, whereas the susceptible class  $S$  is  $N$  minus every host who ever has experienced an infection, an information which eventually can be obtained from serological studies. In eventual data analysis the method of delay coordinates even allows to only work with one time series of  $I$ , and analyzing  $I(t)$ ,  $I(t + \tau)$  etc., with a time delay  $\tau$  obtaining full topological information of the attractor structure (Packard et al., 1980; Farmer & Sidorowich, 1987).

Varying  $\phi$ , the state space plots show a rich dynamical behavior with bifurcations from fixed point to limit cycles, until completely irregular behavior, which is the fingerprint of deterministic chaos (see Fig. 2.3).

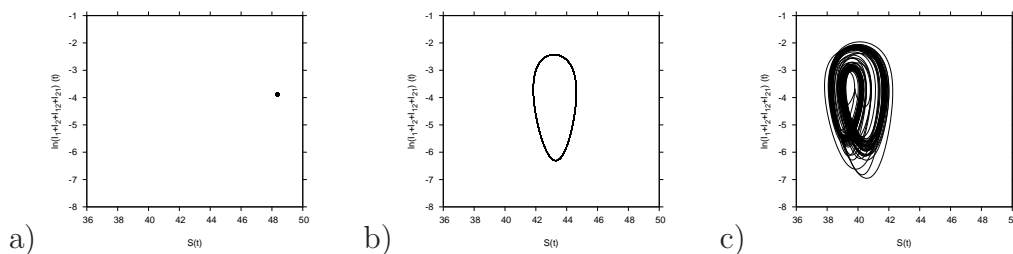


Figure 2.3: Attractors for various values of  $\phi < 1$ : a) fixed point for  $\phi = 0.1$ , and b) limit cycle for  $\phi = 0.4$ , and c) chaotic attractor for  $\phi = 0.6$ .

Looking for higher values of  $\phi$ , the chaotic attractor becomes unstable, just leaving simple limit cycles as attractors for large parameter regions beyond  $\phi = 1$  (Aguiar & Stollenwerk, 2007). Only for much higher values of  $\phi \gg 1$ , another

chaotic attractor appears, the classical ‘‘ADE chaotic attractor’’ (Ferguson et al., 1999; Schwartz et al, 2005; Aguiar & Stollenwerk, 2007).

### 2.3.3 Maxima return map of $I$ from state space plot

We investigate maxima return maps in order to classify the dynamics for various parameter values from extremely long time series. For the time  $t_{max}$ , at which the total number of infected  $I(t)$  has a local maximum, we plot the logarithm of the number of infected at that time  $\ln(I(t_{max}))$  and at the next local maximum  $\ln(I(t_{returnmax}))$  (see Fig. 2.4).

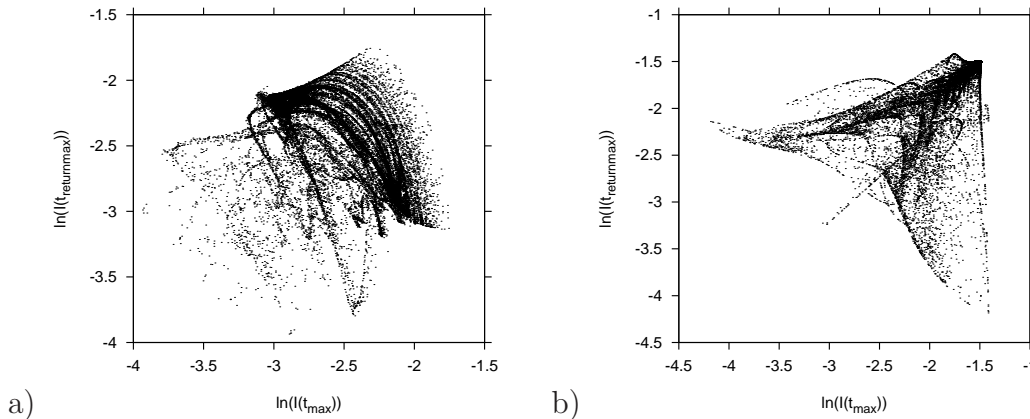


Figure 2.4: Maxima return maps for  $\alpha = 2y^{-1}$  and 200000 years of transient discarded. Deterministically chaotic attractors for a)  $\phi = 0.6$  and b)  $\phi = 0.99$  are observed.

We discarded long transients and plotted 200000 years of simulation. A deterministically chaotic attractor was obtained from our basic two-strain model with temporary cross-immunity in the region of  $\phi < 1$ , where the secondary infection contributes less than the first infection to the overall force of infection. We observed that even after 400000 years, the dots never come back to the same point, so the fingerprint of chaotic attractors is clearly visible now.

### 2.3.4 Numerical bifurcation diagram

The bifurcation diagram was obtained plotting the local extrema of  $\ln(I)$  over the varying parameter  $\phi$  (see Fig. 2.5). Fixed points appear as one dot per parameter value, limit cycles appear as two dots, double-limit cycles as four dots, more complicated limit cycles as more dots, and chaotic attractors as continuously distributed dots for a single  $\phi$  value (Ruelle, 1989).

We observe a chaotic window for  $\phi < 1$  where this dynamical behaviour has never been described before, and also another chaotic window for  $\phi > 1$ , where the minimal values go to very low numbers of infected, the classical ‘‘ADE chaotic

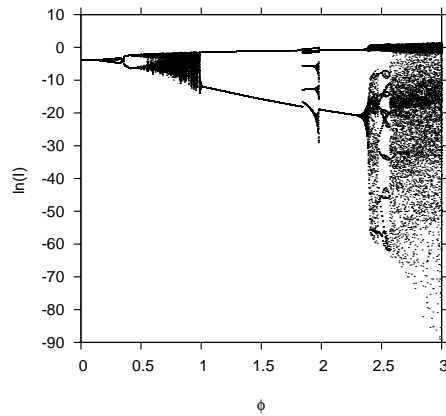


Figure 2.5: Bifurcation diagram for the local extrema of the logarithm of overall infected ( $\ln(I)$ ) with changing parameter  $\phi$  and fixed  $\alpha = 2y^{-1}$ . Here, 2000 years of transients were discarded.

region”, which already has been described in previous publications (Ferguson et al., 1999; Schwartz et al, 2005; Billings et al., 2007).

However, to be sure that this unexpected behavior for  $\phi < 1$  not just appears because of this specific  $\alpha$  value, i.e. assuming temporary cross-immunity period of 6 months, we look at the robustness of the findings by varying the temporary cross-immunity parameter values. For  $\alpha = 1y^{-1}$  e.g (temporary cross-immunity of 12 months, which is also acceptable for dengue when we realize that because of seasonality of the disease, people generally do not get sick more than once per year), both chaotic windows appear, and surprisingly in the region of  $\phi < 1$  this window is even larger (see Fig. 2.6a)). The bifurcation diagram appears to be quite robust against changes of parameters around the region under investigation, in the sense that it shows chaotic windows for  $\phi < 1$  and for  $\phi > 1$ .

For very large values of  $\alpha \rightarrow \infty$ , we get close to the models found in the literature, where temporary cross-immunity becomes shorter or unimportant due to the low resident times in the classes  $R_1$  and  $R_2$ . In this case the chaotic window for  $\phi < 1$  disappears, and then ADE as increasing infectivity on a secondary infection condition seems to be the only mechanism to observe deterministic chaos (see Fig. 2.6b)). We observed again that for  $\phi > 1$  the number of infected goes to very low troughs, whereas in the chaotic region for  $\phi < 1$  and  $\alpha = 2y^{-1}$ , the overall number of infected stays always sustainably high, i.e. never goes lower than  $-15$  in logarithmic scale (see Fig. 2.5).

In Fig. 2.6 it becomes clear that for larger  $\alpha$  (for vanishing temporary cross-immunity), there is no other dynamics in the region for  $\phi < 1$ , than equilibria or limit cycles, the reason why chaos for  $\phi < 1$  has not been observed before.

This observation is further confirmed by a two-parameter bifurcation diagram where  $\phi$  and  $\alpha$  are the free parameters, see Fig. 2.7. The Hopf bifurcation line in the  $\phi - \alpha$  plane only shows Hopf bifurcation to limit cycles in the region of  $\phi < 1$

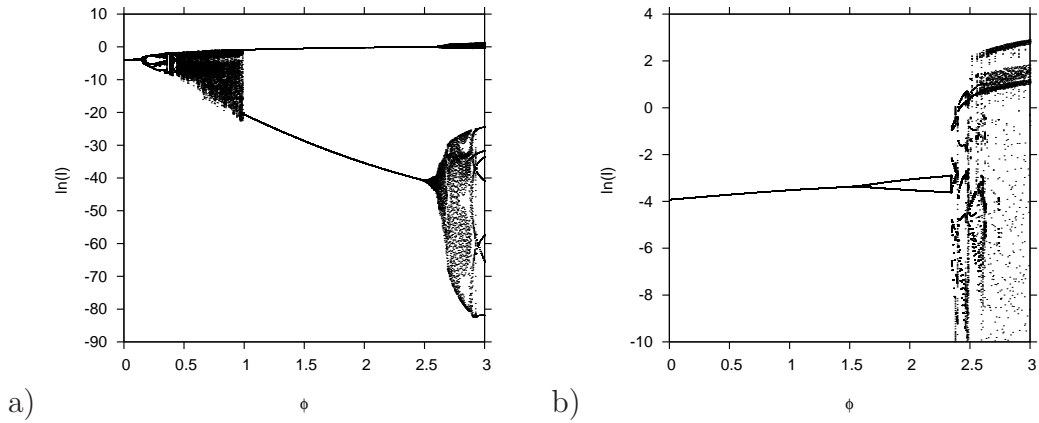


Figure 2.6: Bifurcation diagram for the local extrema of the logarithm of overall infected ( $\ln(I)$ ) with changing parameter  $\phi$ . In a)  $\alpha = 1y^{-1}$  (temporary cross-immunity period of 1 year) and in b)  $\alpha = 52y^{-1}$  (temporary cross-immunity period of 1 week) . Only the upper part of the bifurcation diagram is shown. The minima in  $\ln(I)$  go down as low as -400 in logarithmic scale.

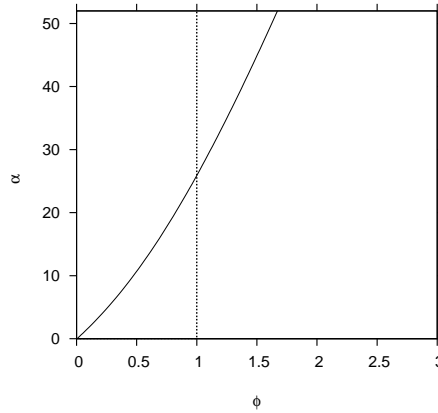


Figure 2.7: Line of the Hopf bifurcation from stable fixed point to limit cycle in the  $\phi - \alpha$  plane. Here we clearly see that in the region of  $\phi < 1$  the Hopf bifurcation happens when the temporary cross-immunity is considerable ( $\alpha < 20y^{-1}$  or  $\approx 2.5$  weeks). When the temporary cross-immunity is less significant ( $\alpha > 30y^{-1}$  or  $\approx 1.5$  weeks), the Hopf bifurcation point appears only in the region of  $\phi > 1$ .

until  $\alpha \approx 20y^{-1}$ , i.e.  $\approx 2.5$  weeks, where the temporary cross-immunity period is still considerable. For  $\alpha > 20y^{-1}$ , i.e. less significant temporary cross-immunity period, the Hopf bifurcation exists only in the  $\phi > 1$  region which was described in the literature before. There is also a sharp bend of the Hopf bifurcation line for very small  $\alpha$  values close to the origin and the bifurcation curve continues close to the horizontal axis for increasing  $\phi$ . However this region is of no biological importance since here the parameter  $\alpha$  is even smaller than the birth and death rate  $\mu$ .

### 2.3.5 Quantifying unpredictability: Lyapunov exponents

We now quantify the attractor structure, fixed point, limit cycle or chaotic attractor etc., by calculating Lyapunov exponents (Ruelle, 1989; Ott, 1993). A negative largest Lyapunov exponent indicates a stable fixed point as attractor, a zero largest Lyapunov exponent indicates a stable limit cycle and a positive largest Lyapunov exponent indicates a chaotic attractor.

As short hand notation for system Eq. (2.2), let the dynamics for the state

$$\underline{x} := (S, I_1, I_2, \dots, R) \quad (2.4)$$

be  $\underline{f}(\underline{x})$ , hence

$$\frac{d}{dt}\underline{x} = \underline{f}(\underline{x}) \quad (2.5)$$

which explicitly gives the dynamics as written down above. Then we analyze the stability in all 9 directions of the state space of this ODE system by calculating deviations  $\Delta\underline{x}$  along a numerically integrated solution of Eq. (2.5) in the attractor with attractor trajectory  $\underline{x}^*(t)$ , hence

$$\frac{d}{dt}\Delta\underline{x} = \left. \frac{df}{d\underline{x}} \right|_{\underline{x}^*(t)} \cdot \Delta\underline{x} \quad (2.6)$$

Here, any attractor is notified by  $\underline{x}^*(t)$ , be it a fixed point, periodic orbit or chaotic attractor. In this ODE system the linearized dynamics is given with the Jacobian matrix  $\left. \frac{df}{d\underline{x}} \right|_{\underline{x}^*(t)}$  of the ODE system Eq. (2.5) evaluated at the trajectory points  $\underline{x}^*(t)$  given in notation of  $\left. \frac{df}{d\underline{x}} \right|_{\underline{x}^*(t)}$ .

The Lyapunov exponents then are the logarithms of the eigenvalues of the integrated Eq. (2.6) in the limit of large integration times. Besides for very simple iterated maps no analytic expressions for chaotic systems can be given for the Lyapunov exponents. For the calculation of the iterated Jacobian matrix and its eigenvalues, we use the QR decomposition algorithm (Farmer & Sidorowich, 1986; Parlitz, 1992) With the matrix  $A(\underline{x}^*(t)) := \mathbb{I} + \Delta t \left. \frac{df}{d\underline{x}} \right|_{\underline{x}^*(t)} = Q(\underline{x}^*(t)) \cdot R(\underline{x}^*(t))$ ,

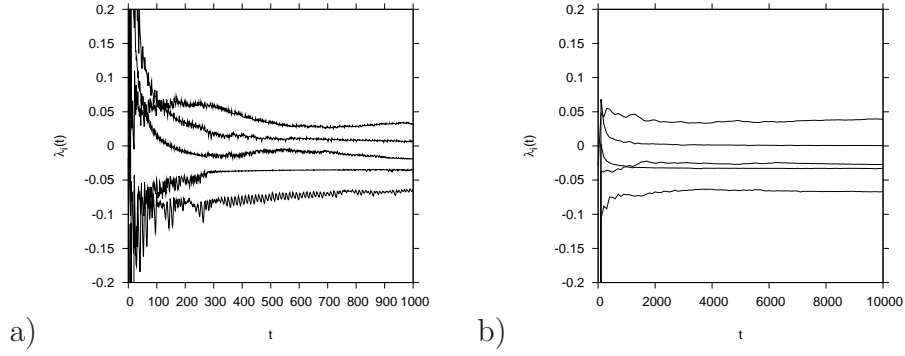


Figure 2.8: Lyapunov exponents measuring chaoticity of the attractor a) along short trajectory fast converging to qualitatively right behavior, b) along longer trajectory for higher numerical precision. The five largest Lyapunov exponents are shown. Parameters are temporary cross-immunity rate  $\alpha = 2y^{-1}$  and ratio of secondary infection contribution to the force of infection  $\phi = 0.6$ .

where  $\mathbb{I}$  is the unit  $(9 \times 9)$ -matrix, we have

$$\begin{aligned} \Delta \underline{x}(t_0 + (n+1)\Delta t) &= A_n \cdot A_{n-1} \cdot \dots \cdot A_0 \cdot \Delta \underline{x}(t_0) \\ &= Q_n \cdot R_n \cdot R_{n-1} \cdot \dots \cdot R_0 \cdot \Delta \underline{x}(t_0) \end{aligned} \quad (2.7)$$

for  $A_n = A(\underline{x}(t_0 + n \Delta t))$ . From  $R_n \cdot R_{n-1} \cdot \dots \cdot R_0 = \prod_{\nu=0}^n R_\nu$  with the diagonal elements  $r_{ii}(\nu)$  of the right diagonal matrix  $R_\nu$  the Lyapunov exponents are given for large  $t = n\Delta t$  by

$$\lambda_i(t) = \frac{1}{n \cdot \Delta t} \ln \left( \prod_{\nu=0}^n |r_{ii}(\nu)| \right) . \quad (2.8)$$

Plots with  $\lambda_i$  as function of time  $t = n\Delta t$  are given in Fig. 2.8. For small integration times, see Fig. 2.8a), the Lyapunov exponents change a lot along the attractor, but soon settle towards their final size, still showing small oscillations. For long integration times, see Fig. 2.8b), these oscillations also disappear, giving reliable values for the infinity time limit of the Lyapunov exponents  $\lambda_i = \lim_{t \rightarrow \infty} \lambda_i(t)$ .

Fig. 2.9 shows the largest four Lyapunov exponents as a function of  $\phi$ . We observe that for small  $\phi$  up to 0.1 all four Lyapunov exponents are negative, indicating the stable fixed point solution. Then follows a region up to  $\phi = 0.5$  where the largest Lyapunov exponent is zero, characteristic for stable limit cycles. Above  $\phi = 0.5$  a positive Lyapunov exponent, clearly separated from the second largest Lyapunov exponent being zero, indicates deterministically chaotic attractors. In the chaotic window between  $\phi = 0.5$  and  $\phi = 1$  also periodic windows appear, giving a zero largest Lyapunov exponent. These findings are in



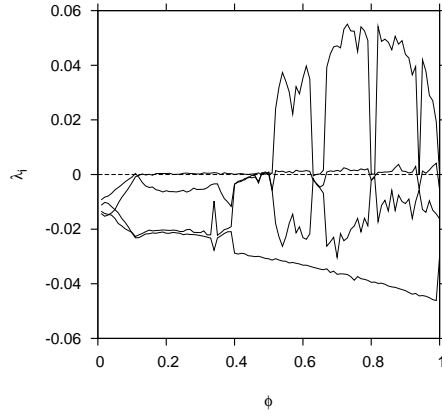


Figure 2.9: Spectrum of the four largest Lyapunov exponents with changing parameter  $\phi$  and fixed  $\alpha = 2y^{-1}$ .

good agreement with the numerical bifurcation diagram, and we will now further investigate this bifurcation structure in the next section.

## 2.4 Bifurcation analysis by continuation

In this section we give the analytic solution for the equilibria and describe the further analysis of the bifurcation structure, using numerical software like AUTO (AUTO, 2009). In this case the bifurcation analysis is done by continuation techniques, i.e. starting from the equilibrium solution for small  $\phi$  by following the solution for increasing  $\phi$  and simultaneously the eigenvalue spectrum, until the eigenvalues show a loss of stability. At this point a Hopf bifurcation gives rise to a stable limit cycle, which subsequently is followed in parameter space, until it becomes unstable at the next bifurcation point etc. up to bifurcations which do not give limit cycles any more, like a torus bifurcation. Also accumulated period doubling bifurcations become increasingly difficult to follow. But first we can give an analytical solution for the equilibria which also serves as a cross check for the numerical programs.

### 2.4.1 Stationary states for the symmetric case

The stationary states can be calculated analytically by setting the time derivatives in system Eq. (2.2) to zero. For the symmetric case, i.e.,  $\beta_1 = \beta_2 = \beta$  and  $\phi_1 = \phi_2 = \phi$  the stationary states are given by

$$S^* = \frac{\mu N - (\gamma + \mu)(I_1^* + I_2^*)}{\mu}$$

$$\begin{aligned}
I_{21}^* &= \frac{1}{\phi_1} \left( \frac{N}{\beta_1 S^*} (\gamma + \mu) - 1 \right) I_1^* \\
I_{12}^* &= \frac{1}{\phi_2} \left( \frac{N}{\beta_2 S^*} (\gamma + \mu) - 1 \right) I_2^* \\
S_1^* &= \frac{(\gamma + \mu) I_{12}^* N}{(I_2^* + \phi_2 I_{12}^*) \beta_2} \\
S_2^* &= \frac{(\gamma + \mu) I_{21}^* N}{(I_1^* + \phi_1 I_{21}^*) \beta_1} \\
R_1^* &= \frac{\gamma}{\alpha + \mu} I_1^* \\
R_2^* &= \frac{\gamma}{\alpha + \mu} I_2^* \quad ,
\end{aligned} \tag{2.9}$$

where still the stationary values of  $I_1^*$  and  $I_2^*$  have to be determined.

The solution of coexistence of both strains for  $I_1 = I_2 = I^*$  is given by the following expression

$$\begin{aligned}
I_1^* = I_2^* &= - \left[ \frac{\frac{\alpha\gamma}{(\alpha+\mu)(\gamma+\mu)}\phi + \left( \frac{(\gamma+\mu)}{\beta} - 3 \right)}{4 \frac{(\gamma+\mu)}{\mu} \left( 1 - \frac{\alpha\gamma}{(\alpha+\mu)(\gamma+\mu)}\phi \right)} \right] N \\
&\quad - \sqrt{ \frac{N^2}{4} \left[ \frac{\frac{\alpha\gamma}{(\alpha+\mu)(\gamma+\mu)}\phi + \left( \frac{(\gamma+\mu)}{\beta} - 3 \right)}{2 \frac{(\gamma+\mu)}{\mu} \left( 1 - \frac{\alpha\gamma}{(\alpha+\mu)(\gamma+\mu)}\phi \right)} \right]^2 + \left[ \frac{N^2 \mu \left( \frac{(\gamma+\mu)}{\beta} - 1 \right)}{2 \frac{(\gamma+\mu)^2}{\mu} \left( 1 - \frac{\alpha\gamma}{(\alpha+\mu)(\gamma+\mu)}\phi \right)} \right] } ,
\end{aligned} \tag{2.10}$$

and the solution of the extinction of one of the strains is as follows

$$\begin{aligned}
I_1^* &= \frac{\mu N (\beta - (\gamma + \mu))}{(\gamma + \mu) \beta} \\
I_2^* &= 0 \quad .
\end{aligned} \tag{2.11}$$

Finally, the stationary value of  $R^*$ , when host have been recovered from both strains, is given by the balance equation for the total population size  $N$ , explicitly

$$R^* = N - (S^* + I_1^* + I_2^* + R_1^* + R_2^* + S_1^* + S_2^* + I_{12}^* + I_{21}^*) \quad . \tag{2.12}$$

These analytic results agree well with the numerical results from the time series analysis for small  $\phi$  values, where the fixed point solution is stable. We will now continue with the bifurcation analysis beyond this fixed point solution using the continuation method.

## 2.4.2 Bifurcations analysis beyond equilibria

We investigate in detail the region of interest of  $\phi < 1$  for  $\alpha = 2y^{-1}$ . All other parameter values are fixed and given in Table 2.1. In Figure 2.10a) the bifurcation diagram by continuation, obtained with the numerical software AUTO (AUTO, 2009), is shown for the interval of  $0 \leq \phi \leq 1.1$  for the logarithm of the total number of infected  $I$ . As opposed to the previous bifurcation diagrams (Figs. 2.5 and 2.6), where all local extrema where shown, AUTO only gives the global extrema for the limit cycles.

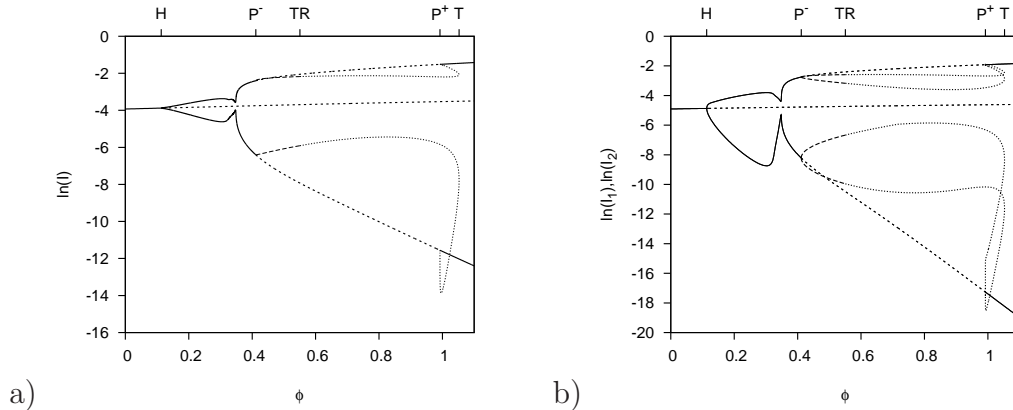


Figure 2.10: a) Equilibria or maximum and minimum values for limit cycles of the logarithm for the total number of infected ( $\ln(I)$ ). We find a Hopf bifurcation  $H$  at  $\phi = 0.1133$ , pitchfork (multiplier 1) bifurcations  $P^-$  at  $\phi = 0.4114$  and  $P^+$  at  $\phi = 0.9921$ , torus bifurcation  $TR$  at  $\phi = 0.5507$  and tangent bifurcation  $T$  at  $\phi = 1.0524$ . b) Equilibria or maximum and minimum values for limit cycles for  $I_1$  and  $I_2$ . On the primary branch we have  $\tilde{I}_1(t) = \tilde{I}_2(t)$ ,  $\tilde{R}_1(t) = \tilde{R}_2(t)$ ,  $\tilde{S}_1(t) = \tilde{S}_2(t)$  and  $\tilde{I}_{12}(t) = \tilde{I}_{21}(t)$ , for times  $t$  up to the period length of the limit cycle. On the secondary branch two stable limit cycles coexist because of the symmetry.

In Fig. 2.10a) we see that the fixed equilibrium becomes unstable at a supercritical Hopf bifurcation  $H$  where a stable fixed limit cycle originates. The Hopf bifurcation appears at  $\phi = 0.1133$ . This stable limit cycle becomes unstable at a pitchfork bifurcation point  $P^-$  for a limit cycle at  $\phi = 0.4114$ . Solid lines denote stable equilibria or limit cycles, dashed lines unstable equilibria or periodic-one limit cycles. Thin lines are the secondary limit cycles: long-dashed stable and dotted unstable.

This point marks the origin of a pair of  $\mathbf{S}$ -conjugate stable limit cycles besides the now unstable fixed limit cycle in the following sense: The system Eq. (2.2) in the symmetric case, hence for  $\beta_1 = \beta_2 = \beta$  and  $\phi_1 = \phi_2 = \phi$  is  $\mathbb{Z}^2$ -symmetric

(Kuznetsov, 2004). With a symmetry transformation matrix  $\mathbf{S}$

$$S := \begin{pmatrix} 1 & 0 & 0 & 0 & 0 & 0 & 0 & 0 & 0 & 0 \\ 0 & 0 & 1 & 0 & 0 & 0 & 0 & 0 & 0 & 0 \\ 0 & 1 & 0 & 0 & 0 & 0 & 0 & 0 & 0 & 0 \\ 0 & 0 & 0 & 0 & 1 & 0 & 0 & 0 & 0 & 0 \\ 0 & 0 & 0 & 1 & 0 & 0 & 0 & 0 & 0 & 0 \\ 0 & 0 & 0 & 0 & 0 & 0 & 1 & 0 & 0 & 0 \\ 0 & 0 & 0 & 0 & 0 & 1 & 0 & 0 & 0 & 0 \\ 0 & 0 & 0 & 0 & 0 & 0 & 0 & 0 & 1 & 0 \\ 0 & 0 & 0 & 0 & 0 & 0 & 0 & 1 & 0 & 0 \\ 0 & 0 & 0 & 0 & 0 & 0 & 0 & 0 & 0 & 1 \end{pmatrix} \quad (2.13)$$

for an equilibrium point  $\mathbf{S}\underline{x}^* = \underline{x}^*$  holds, the state being defined by Eq. (2.4). Then this equilibrium is called *fixed* (see (Kuznetsov, 2004)). For limit cycles a similar terminology holds. A periodic solution is called *fixed* (see (Kuznetsov, 2004)) when  $\mathbf{S}\tilde{\underline{x}}(t) = \tilde{\underline{x}}(t)$  and the associated limit cycles are also called *fixed*. There is another type of periodic solution that is not fixed but called *symmetric* when

$$\mathbf{S}\tilde{\underline{x}}(t) = \tilde{\underline{x}}\left(t + \frac{T}{2}\right) \quad (2.14)$$

where  $T$  is the period, hence the limit cycle is shifted by half a period length. Again the associated limit cycles are also called *symmetric*. Both type of limit cycles  $L$  are  $\mathbf{S}$ -invariant as curves :  $\mathbf{S}L = L$ . An  $\mathbf{S}$ -invariant cycle is either fixed or symmetric. Two non-invariant limit cycles ( $\mathbf{S}L \neq L$ ) are called  $\mathbf{S}$ -conjugate if their corresponding periodic solutions satisfy  $\tilde{\underline{y}}(t) = \mathbf{S}\tilde{\underline{x}}(t)$  for all times  $t$ .

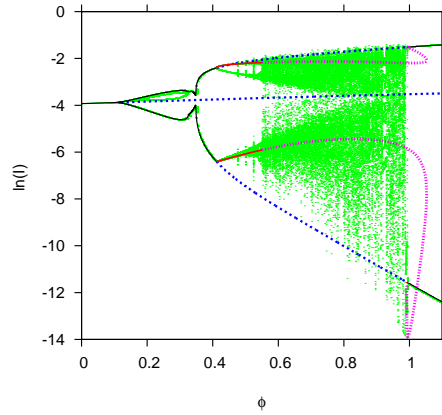


Figure 2.11: Comparison between bifurcation analysis by continuation from Fig. 2.10a) (colored lines) and the numerical bifurcation diagram (green dots) as part for  $\phi < 1.1$  from Fig. 2.5. The overall bifurcation structure agrees well between both methods.

Table 2.2: List of bifurcations.

Bifurcation	Description
$H$	Hopf bifurcation equilibrium becomes unstable origin of stable limit cycle
$T$	Tangent bifurcation bifurcation of limit cycle one multiplier = 1 collision of two limit cycles
$P$	Pitchfork bifurcation bifurcation of limit cycle one Floquet multiplier = 1 origin of two secondary stable limit cycle branches
$F$	Flip bifurcation or period doubling bifurcation bifurcation of limit cycle one Floquet multiplier = -1 origin of a limit cycle with double period length
$TR$	Torus bifurcation bifurcation of limit cycle pair of complex conjugate multipliers with magnitude 1 origin of an invariant torus

Figure 2.10b) gives the results for the infected with a single strain  $I_1$  and  $I_2$ . Because these two variables are interchangeable this can also be interpreted as the stable limit cycles for the single variable say  $I_1$ . The fixed stable equilibrium below the Hopf bifurcation, where we have  $I_1^* = I_2^*$ ,  $R_1^* = R_2^*$ ,  $S_1^* = S_2^*$  and  $I_{12}^* = I_{21}^*$ , is a fixed equilibrium. At the Hopf bifurcation  $H$  the stable fixed equilibrium point becomes an unstable fixed equilibrium point. The originating stable limit cycle in the parameter interval between the Hopf bifurcation and the pitchfork bifurcation is symmetric.

In the parameter interval between the two pitchfork bifurcations, two stable limit cycles coexist and these limit cycles are  $\mathbf{S}$ -conjugate. At the pitchfork bifurcation points the fixed limit cycle becomes unstable and remains fixed, and two stable  $\mathbf{S}$ -conjugate limit cycles originate (see (Kuznetsov, 2004, Theorem 7.7)).

The invariant plane  $I_1 = I_2, R_1 = R_2, S_1 = S_2, I_{12} = I_{21}$  forms the separatrix between the pair of stable  $\mathbf{S}$ -conjugate limit cycles  $\tilde{\mathbf{x}}(t)$  and  $\mathbf{S}\tilde{\mathbf{x}}(t)$  for all times  $t$ . The initial values of the two state variables  $S(0)$  and  $R(0)$  together with the point on the invariant plane, determine to which limit cycle the system converges.

Continuation of the two stable  $\mathbf{S}$ -conjugate limit cycles gives a torus bifur-

cation or Neimark-Sacker bifurcation at the parameter point denoted by  $TR$  at  $\phi = 0.5507$ . At this point the limit cycles become unstable because a pair of complex-conjugate Floquet multipliers crosses the unit circle. Floquet multipliers replace in the stability analysis of limit cycles (Floquet theory) often the eigenvalues used to analyze fixed point stability (Kuznetsov, 2004). In (Albers & Sprott, 2006) a sequence of Neimark-Sacker bifurcations into chaos is mentioned as one possible route to chaos.

Increasing the bifurcation parameter  $\phi$  along the now unstable pair of  $S$ -conjugate limit cycles leads to a tangent bifurcation  $T$  where a pair of two unstable limit cycles collide. This branch terminates at the second pitchfork bifurcation point denoted by  $P^+$  at  $\phi = 0.9921$ . Because the first fold point gave rise to a stable limit cycle and this fold point to an unstable limit cycle we call the first pitchfork bifurcation super-critical and the latter pitchfork bifurcation subcritical.

These results agree very well with the simulation results shown in the bifurcation diagram for the maxima and minima of the overall infected in Figure 2.11. Notice that AUTO calculates only the global extrema during a cycle, not the local extrema.

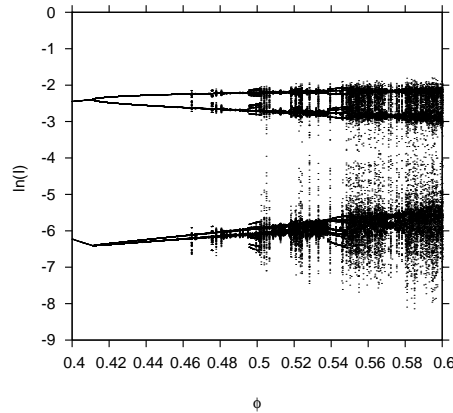


Figure 2.12: Detailed bifurcation diagram with high resolution in integration, transients and bifurcation parameter  $\phi$ , here for  $\alpha = 2y^{-1}$  and for  $\phi$  between 0.4 and 0.6. Besides chaotic attractors respectively long chaotic transients also complicated limit cycles appear already for  $\phi$  values around 0.50, long before the torus bifurcation for  $\phi$  around 0.55.

The previous results have been obtained by continuation starting from the fixed point solutions, system Eq. (2.9), tracking after the first Hopf bifurcation the limit cycles and their bifurcations, until new dynamical structures like toruses appear. The main bifurcation structures can be understood in comparison between the numerical bifurcation diagram and the present results in Figure 2.11. However, with the time series analysis shown in the previous section, more is observed, especially positive Lyapunov exponents appear around or even before the torus bifurcation.

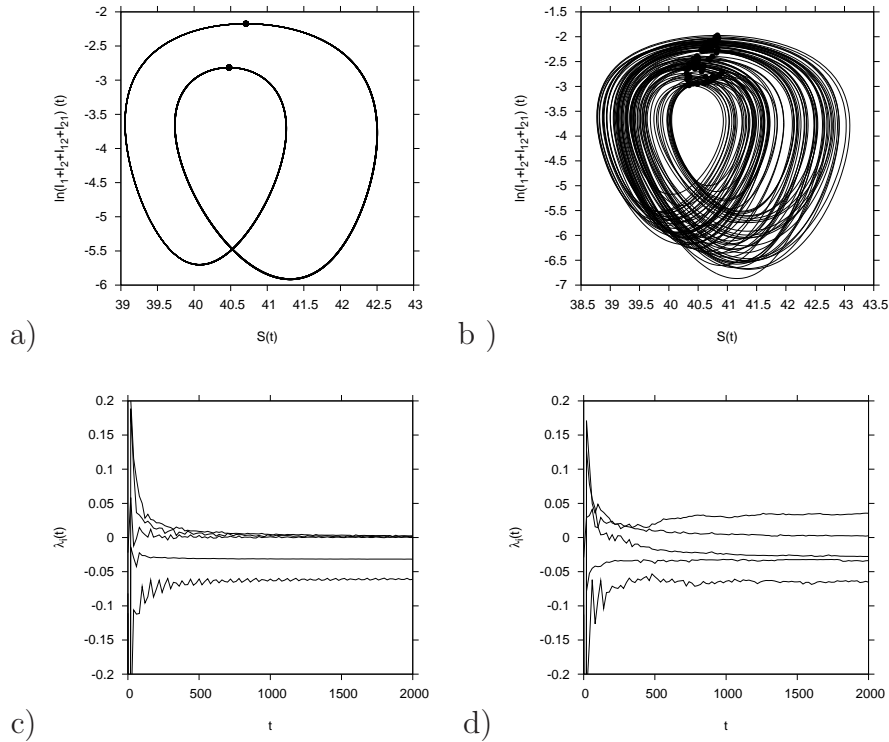


Figure 2.13: a) State space plot for  $\phi = 0.5504$ , in the region of previously unexplained co-existences of limit cycles, torus bifurcations and attractors with positive Lyapunov exponents. Special initial conditions were taken, to obtain the simple limit cycle found in numeric bifurcation analysis. b) Same parameter values, but arbitrarily different initial conditions. The attractor looks chaotic. c) Calculation of Lyapunov exponent along the limit cycle shown in a). The largest Lyapunov goes to zero, as do the next two due to closeness to a bifurcation. d) Same as in c), but with arbitrary initial conditions. The largest Lyapunov exponent converges to a value significantly larger than zero, the second towards zero. Hence the attractor in b) is chaotic.

We investigate in detail a region for temporary cross-immunity rate  $\alpha = 2y^{-1}$  and ratio of secondary infection contribution to the force of infection  $\phi$  around 0.55 where AUTO found limit cycles and torus bifurcations via continuation methods from earlier detected limit cycles, but where also more complicated attractors appear as a more detailed bifurcation diagram with arbitrary initial conditions reveals in Fig. 2.12.

We then search for the respective state space structures, see Fig. 2.13. In Fig. 2.13a) the state space plot for  $\phi = 0.5504$  shows a limit cycle, as predicted by the continuation method. This is the region where the bifurcation diagram by continuation initially gives different results, limit cycles and torus bifurcation, from the bifurcation analysis by time series methods and the analysis of Lyapunov exponents, where already a positive Lyapunov exponent appears. For the limit cycle in Fig. 2.13a) and c) special initial conditions were taken, as obtained from the analysis with AUTO. For this limit cycle given in Fig. 2.13a) we find a zero largest Lyapunov exponent, see Fig. 2.13c). The next two Lyapunov exponents also around zero indicate that we are close to a bifurcation point of this limit cycle, the soon coming torus bifurcation.

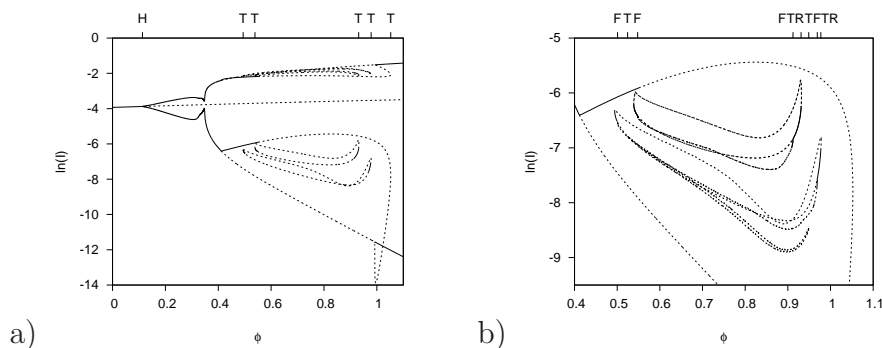


Figure 2.14: a) Equilibria or maximum and minimum values for limit cycles for the logarithm of the total infected ( $\ln(I)$ ), now including the new isolas between tangent bifurcations  $T$  at  $\phi = 0.4941, 0.5387, 0.9310, 0.9783$  and  $1.0524$ . These new isolas are found starting at  $\phi$  values smaller than the torus bifurcation. b) Isola bifurcations in more detail: tangent bifurcations  $T$  at  $\phi = 0.5245$  and  $0.9491$ , torus bifurcations  $TR$  at  $\phi = 0.9310$  and  $0.9773$  and flip bifurcations  $F$  at  $\phi = 0.5009, 0.5479, 0.9120$  and  $0.9691$ . Some of the tangent bifurcations are not indicated in the plot (namely  $T$  at  $\phi = 0.4941, 0.5387, 0.9310, 0.9783, 1.0524$ ).

However, when taking arbitrarily different initial conditions we find for the same parameter values of the model as used in Fig. 2.13a), especially the same  $\phi$  value, the attractor shown in 2.13b). This attractor shows a largest Lyapunov exponent significantly larger than zero, see Fig. 2.13d). The second largest Lyapunov exponent converges to zero, as expected for a non-equilibrium attractor.

For values of  $\phi$  slightly smaller than 0.5504, the same analysis shows co-



existing limit cycles (from which the attractor in Fig. 2.13b) originates). Tracing such a limit cycle by AUTO finally gives new isola solutions in the analysis performed by AUTO, which previously have been missed by continuation starting at the equilibria and via the first Hopf-bifurcation. An isola is an isolated solution branch of limit cycles (Golubitsky & Schaeffer, 1985). These isola cycles  $L$  are not  $\mathbf{S}$ -invariant, that is  $\mathbf{S}L \neq L$ . The new isolas are shown relatively to the previously obtained bifurcation diagram by continuation in Fig. 2.14a).

In Fig. 2.14b) we investigate in more detail these isolas, obtaining flip or period doubling bifurcations and further torus bifurcations. These period doubling bifurcation sequences indicate another route to chaos than the previously found torus bifurcation. These results suggest that for these isolas two classical routes to chaos exist, namely via the torus or Neimark-Sacker bifurcation where the dynamics on the originating torus is chaotic, and the cascade of period doubling route to chaos. Two windows with period solutions within the chaotic windows, see Fig. 2.11, are filled by the two stable limit cycles of the isola's shown in Fig. 2.14. The study of the two windows with zero largest Lyapunov exponent shown in Fig. 2.9 is beyond the scope of this paper.

In order to obtain further insight into the possible bifurcation structures for the model under investigation we also looked at other parameter values in the symmetric, and also briefly, the asymmetric case. For other values of temporary cross-immunity rate ( $\alpha \in [1, 3]y^{-1}$ ) we found a period doubling route to chaos as well as the torus bifurcation already mentioned for  $\alpha = 2y^{-1}$ .

The bifurcation analysis presented here was only possible in close comparison between the bifurcation analysis by continuation, giving accurate bifurcation points and classifications due to the analysis of the stability changes via Floquet multipliers, and direct numerical bifurcation plots, revealing co-existing dynamic structures which continuation easily misses, and Lyapunov exponent calculations. The analysis even for the symmetric case with  $\alpha = 2y^{-1}$  is not exhaustive, more co-existing structures might appear when zooming further into the parameter space. But we obtained a good agreement between the different methods for the overall sketch of the dynamic complexity in the region of interest of  $\phi < 1$  in the symmetric case.

We also looked at numerical bifurcation diagrams for some asymmetric cases  $\phi_1 \neq \phi_2$  and  $\beta_1 \neq \beta_2$ , which already indicated similarly if not more complicated bifurcation structures (not shown here). Future work on the relevant parameters for dengue epidemiology will be needed to identify eventual deviations from the simplest symmetric case investigated here.

## 2.5 Conclusion

Our analysis showed deterministically chaotic attractors for a multi-strain model in an unexpected parameter region just by adding temporary cross-immunity to

previously existing dengue models.

Our model is a basic two-strain SIR-type model for the host population and was motivated by modeling dengue fever epidemiology with its peculiar ADE phenomenology. The simple structure of the model allows to generalize our findings to other multi-strain epidemiological systems, capturing the effective dynamics of the human host population. We could find deterministic chaos in a very basic model with only two strains and one reinfection possible, not needing the strong ADE mechanism, but rather stating that upon second infection hosts spread a disease less likely, since it might be more harmful, leading to hospitalization.

In this work, we focused on the multi-strain aspect and its effects on the host population, taking effects of the vector dynamics or seasonality only in account by the effective parameters in the SIR-type model, but not modeling these mechanisms explicitly. Since seasonally forced SIR systems can show already deterministic chaos (Stone et al., 2007), we expect that rather more complex dynamics will appear.

For such scenarios new tools of non-linear data analysis like Takens' embedding are available (Packard et al., 1980; Takens, 1980), and allow to obtain topological information (fixed points, periodic orbits and the nature of chaotic attractors) about the whole multi-strain epidemiological system from time series of overall infecteds only, not needing any single strain data sets.

This indicates that deterministic chaos is much more important in multi-strain models than previously thought, and opens new ways to data analysis of existing dengue time series.



# Chapter 3

## Torus bifurcations, isolas and chaotic attractors in a simple dengue fever model with ADE and temporary cross-immunity

Maíra Aguiar, Nico Stollenwerk and Bob W. Kooi

*International Journal of Computer Mathematics*, **86**(10-11):1867-1877, 2009.

We analyze an epidemiological model of competing strains of pathogens and hence differences in transmission for first versus secondary infection due to interaction of the strains with previously acquired immunities, as has been described for dengue fever, known as antibody-dependent enhancement (ADE). These models show a rich variety of dynamics through bifurcations up to deterministic chaos. Including temporary cross-immunity even enlarges the parameter range of such chaotic attractors, and also gives rise to various coexisting attractors, which are difficult to identify by standard numerical bifurcation programs using continuation methods. A combination of techniques, including classical bifurcation plots and Lyapunov exponent spectra has to be applied in comparison to get further insight into such dynamical structures. Here we present for the first time multi-parameter studies in a range of biologically plausible values for dengue. The multi-strain interaction with the immune system is expected to also have implications for the epidemiology of other diseases.

### 3.1 Introduction

Epidemic models are classically phrased in ordinary differential equation (ODE) systems for the host population divided in classes of susceptible individuals and

infected ones (SIS system), or in addition, a class of recovered individuals due to immunity after an infection to the respective pathogen (SIR epidemics). The infection term includes a product of two variables, hence a non-linearity which in extended systems can cause complicated dynamics. Though these simple SIS and SIR models only show equilibria as stationary solutions, they already show non-trivial equilibria arising from bifurcations, and in stochastic versions of the system critical fluctuations at the critical point. Further refinements of the SIR model in terms of external forcing or distinction of infections with different strains of a pathogen, hence classes of infected with one or another strain recovered from one or another strain, infected with more than one strain etc., can induce more complicated dynamical attractors including equilibria, limit cycles, tori and chaotic attractors.

Classical examples of chaos in epidemiological models are childhood diseases with extremely high infection rates, so that a moderate seasonal forcing can generate Feigenbaum sequences of period doubling bifurcations into chaos. The success in analyzing childhood diseases in terms of modeling and data comparison lies in the fact that they are just childhood diseases with such high infectivity. Otherwise host populations cannot sustain the respective pathogens. In other infectious diseases much lower forces of infection have to be considered leading to further conceptual problems with noise affecting the system more than the deterministic part. This shows even critical fluctuations with power law behavior, when considering evolutionary processes of harmless strains of pathogens versus occasional accidents of pathogenic mutants (Stollenwerk & Jansen, 2003 b). In these circumstances only explicitly stochastic models, of which the classical ODE models are mean field versions, can capture the fluctuations observed in time series data (Stollenwerk et al., 2004).

The situation is again different in multi-strain models, which have attracted attention recently. It has been demonstrated that the interaction of various strains on the infection of the host with eventual cross-immunities or other interactions between host immune system and multiple strains can generate complicated dynamic attractors. A prime example is dengue fever. A first infection is often mild or even asymptomatic and leads to life long immunity against this strain. However, a subsequent infection with another strain of the virus often causes clinical complications up to life threatening conditions and hospitalization, due to antibody-dependent enhancement effect (ADE). More on the biology of dengue and its consequences for the detailed epidemiological model structure can be found in Aguiar & Stollenwerk (Aguiar & Stollenwerk, 2007; Aguiar et al., 2008) including literature on previous modeling attempts. For additional literature on dengue models see also (Massad et al., 2008). On the biological evidence for ADE see e.g. (Halstead, 2003). Besides the difference in the force of infection between primary and secondary infection, parametrized by a so called ADE parameter  $\phi$  or ratio of secondary infection contribution to the force of infection, which has been demonstrated to show chaotic attractors in a certain parameter

region, another effect, the temporary cross-immunity after a first infection against all dengue virus strains, parametrized by the temporary cross-immunity rate  $\alpha$ , shows bifurcations up to chaotic attractors in a much wider and biologically more realistic parameter region.

The model presented in Appendix 3.A has been described in detail in (Aguiar & Stollenwerk, 2007) and has recently been analyzed for a parameter value of  $\alpha = 2y^{-1}$  corresponding to on average half a year of temporary cross-immunity which is biologically plausible (Aguiar et al., 2008). At low ratio of secondary infection contribution to the force of infection (ADE parameter  $\phi$ ) there is a stable equilibrium. Increasing  $\phi$  this equilibrium bifurcates via a Hopf bifurcation into a stable limit cycle and then after further continuation the limit cycle becomes unstable in a torus bifurcation. This torus bifurcation can be located using numerical bifurcation software based on continuation methods tracking known equilibria or limit cycles up to bifurcation points (AUTO, 2009). The continuation techniques and the theory behind it are described e.g. in (Kuznetsov, 2004). Complementary methods like Lyapunov exponent spectra can also characterize chaotic attractors (Ruelle, 1989; Ott, 1993), and led ultimately to the detection of coexisting attractors to the main limit cycles and tori originated from the analytically accessible equilibrium for small  $\phi$ . Such coexisting structures are often missed in bifurcation analysis of higher dimensional dynamical systems but are demonstrated to be crucial at times in understanding qualitatively the real world data, as for example demonstrated previously in a childhood disease study (Drepper et al., 1994). In such a study first the understanding of the deterministic system's attractor structure is needed, and then eventually the interplay between attractors mediated by population noise in the stochastic version of the system gives the full understanding of the data.

Here we present for the first time extended results of the bifurcation structure for various parameter values of the temporary cross-immunity  $\alpha$  in the region of biological relevance and multi-parameter bifurcation analysis. This reveals besides the torus bifurcation route to chaos also the classical Feigenbaum period doubling sequence and the origin of so called isola solutions. The symmetry of the different strains leads to symmetry breaking bifurcations of limit cycles, which are rarely described in the epidemiological literature but well known in the biochemical literature, e.g. for coupled identical cells. The interplay between different numerical procedures and basic analytic insight in terms of symmetries help to understand the attractor structure of multi-strain interactions in the present case of dengue fever, and will contribute to the final understanding of dengue epidemiology including the observed fluctuations in real world data. In the literature the multi-strain interaction leading to deterministic chaos via ADE has been described previously, e.g. (Ferguson et al., 1999; Schwartz et al., 2005; Billings et al., 2007) but neglecting temporary cross-immunity and hence getting stuck in rather biologically unrealistic parameter regions, whereas more recently the first considerations of temporary cross-immunity in rather complicated and

up to now not in detail analyzed models including all kinds of interactions have appeared (Wearing & Rohani, 2006; Nagao & Koelle, 2008), in this case failing to investigate the possible dynamical structures in more detail.

## 3.2 Dynamical system

The multistrain model under investigation can be given as an ODE system

$$\frac{d}{dt} \underline{x} = \underline{f}(\underline{x}, \underline{a}) \quad (3.1)$$

for the state vector of the epidemiological host classes  $\underline{x} := (S, I_1, I_2, \dots, R)^{tr}$  and besides other fixed parameters which are biologically undisputed the parameter vector of varied parameters  $\underline{a} = (\alpha, \phi)^{tr}$ , with  $tr$  for transposed of a vector or matrix. For a detailed description of the biological content of state variables and parameters see (Aguiar & Stollenwerk, 2007; Aguiar et al., 2008). The ODE equations and fixed parameter values are given in the appendix 3.A. The equilibrium values  $\underline{x}^*$  are given by the equilibrium condition  $\underline{f}(\underline{x}^*, \underline{a}) = 0$ , respectively for limit cycles  $\underline{x}^*(t + T) = \underline{x}^*(t)$  with period  $T$ . For chaotic attractors the trajectory of the dynamical system reaches in the time limit of infinity the attractor trajectory  $\underline{x}^*(t)$ , equally for tori with irrational winding ratios. In all cases the stability can be analyzed considering small perturbations  $\Delta \underline{x}(t)$  around the attractor trajectories

$$\frac{d}{dt} \Delta \underline{x} = \left. \frac{d\underline{f}}{d\underline{x}} \right|_{\underline{x}^*(t)} \cdot \Delta \underline{x} \quad (3.2)$$

Here, any attractor is notified by  $\underline{x}^*(t)$ , be it an equilibrium, periodic orbit or chaotic attractor. In this ODE system the linearized dynamics is given with the Jacobian matrix  $(d\underline{f}/d\underline{x})$  of the ODE system Eq. (3.1) evaluated at the trajectory points  $\underline{x}^*(t)$  given in notation of  $(d\underline{f}/d\underline{x})|_{\underline{x}^*(t)}$ . The Jacobian matrix is analyzed for equilibria in terms of eigenvalues to determine stability and the loss of it at bifurcation points, where a negative real part indicate stability. For the stability and loss of it for limit cycles, Floquet multipliers are more common (essentially the exponentials of eigenvalues), multipliers inside the unit circle indicating stability, and where they leave eventually the unit circle determining the type of limit cycle bifurcations. And for chaotic systems, Lyapunov exponents are determined from the Jacobian around the trajectory, where positive largest exponents show deterministic chaos, zero largest exponent shows limit cycles, including tori (at least 2 zero largest exponents), and largest smaller zero indicate fixed points.

### 3.2.1 Symmetries

To investigate the bifurcation structure of the system under investigation we first observe the symmetries due to the multi-strain structure of the model. This be-

comes important for the time being for equilibria<sup>1</sup> and limit cycles. We introduce the following notation: With a symmetry transformation matrix  $\mathbf{S}$

$$\mathbf{S} := \begin{pmatrix} 1 & 0 & 0 & 0 & 0 & 0 & 0 & 0 & 0 & 0 \\ 0 & 0 & 1 & 0 & 0 & 0 & 0 & 0 & 0 & 0 \\ 0 & 1 & 0 & 0 & 0 & 0 & 0 & 0 & 0 & 0 \\ 0 & 0 & 0 & 0 & 1 & 0 & 0 & 0 & 0 & 0 \\ 0 & 0 & 0 & 1 & 0 & 0 & 0 & 0 & 0 & 0 \\ 0 & 0 & 0 & 0 & 0 & 0 & 1 & 0 & 0 & 0 \\ 0 & 0 & 0 & 0 & 0 & 1 & 0 & 0 & 0 & 0 \\ 0 & 0 & 0 & 0 & 0 & 0 & 0 & 0 & 1 & 0 \\ 0 & 0 & 0 & 0 & 0 & 0 & 0 & 1 & 0 & 0 \\ 0 & 0 & 0 & 0 & 0 & 0 & 0 & 0 & 0 & 1 \end{pmatrix} \quad (3.3)$$

we have the following symmetry:

If

$$\underline{x}^* = (S^*, I_1^*, I_2^*, R_1^*, R_2^*, S_1^*, S_2^*, I_{12}^*, I_{21}^*, R^*)^{tr} \quad (3.4)$$

is equilibrium or limit cycle, then also

$$\mathbf{S} \underline{x}^* = (S^*, I_2^*, I_1^*, R_2^*, R_1^*, S_2^*, S_1^*, I_{21}^*, I_{12}^*, R^*)^{tr} \quad (3.5)$$

with  $\underline{x}^*$  equilibrium values or  $\underline{x}^* = \underline{x}^*(t)$  limit cycle for all times  $t \in [0, T]$ . For the right hand side  $\underline{f}$  of the ODE system Eq. (3.1) the kind of symmetry found above is called  $\mathbb{Z}_2$ -symmetry when the following equivariance condition holds

$$\underline{f}(\mathbf{S}\underline{x}, \underline{a}) = \mathbf{S}\underline{f}(\underline{x}, \underline{a}) \quad (3.6)$$

with  $\mathbf{S}$  a matrix that obeys  $\mathbf{S} \neq \mathbf{I}$  and  $\mathbf{S}^2 = \mathbf{I}$ , where  $\mathbf{I}$  is the unit matrix. Observe that besides  $\mathbf{S}$  also  $\mathbf{I}$  satisfies Eq. (3.6). The symmetry transformation matrix  $\mathbf{S}$  in Eq. (3.3) fulfills these requirements. It is easy to verify that the  $\mathbb{Z}_2$ -equivariance conditions (Eq. (3.6)) and the properties of  $\mathbf{S}$  are satisfied for our ODE system. In Seydel (Seydel, 1994) a simplified version of the famous Brusselator that shows this type of symmetry is discussed. There, an equilibrium and also a limit cycle show a pitchfork bifurcation with symmetry breaking.

An equilibrium  $\underline{x}^*$  is called *fixed* when  $\mathbf{S}\underline{x}^* = \underline{x}^*$  (see (Kuznetsov, 2004)). Two equilibria  $\underline{x}^*, \underline{y}^*$  where  $\mathbf{S}\underline{x}^* \neq \underline{x}^*$ , are called *S-conjugate* if their corresponding solutions satisfy

$\underline{y}^* = \mathbf{S}\underline{x}^*$  (and because  $\mathbf{S}^2 = \mathbf{I}$  also  $\underline{x}^* = \mathbf{S}\underline{y}^*$ ). For limit cycles a similar terminology is introduced. A periodic solution is called *fixed* when  $\mathbf{S}\underline{x}^*(t) = \underline{x}^*(t)$  and the associated limit cycles are also called *fixed* (Kuznetsov, 2004). There is another type of periodic solution that is not fixed but called *symmetric* when

$$\mathbf{S}\underline{x}^*(t) = \underline{x}^* \left( t + \frac{T}{2} \right) \quad (3.7)$$

---

<sup>1</sup>Equilibria are often called fixed points in dynamical systems theory, here we try to avoid this term, since in symmetry the term *fixed* is used in a more specific way, see below.



where  $T$  is the period. Again the associated limit cycles are also called *symmetric*. Both types of limit cycles  $L$  are  $\mathbf{S}$ -invariant as curves :  $\mathbf{S}L = L$ . That is, in the phase-plane where time parametrizes the orbit, the cycle and the transformed cycle are equal. A  $\mathbf{S}$ -invariant cycle is either fixed or symmetric. Two non-invariant limit cycles ( $\mathbf{S}L \neq L$ ) are called  $\mathbf{S}$ -conjugate if their corresponding periodic solutions satisfy  $\underline{y}^*(t) = \mathbf{S}\underline{x}^*(t)$ ,  $\forall t \in \mathbb{R}$ . The properties of the symmetric systems and the introduced terminology are used below with the interpretation of the numerical bifurcation analysis results. We refer to (Kuznetsov, 2004) for an overview of the possible bifurcations of equilibria and limit cycles of  $\mathbb{Z}_2$ -equivariant systems.

### 3.3 Bifurcation diagrams for various $\alpha$ values

We show the results of the bifurcation analysis in bifurcation diagrams for several  $\alpha$  values, varying  $\phi$  continuously. Besides the previously investigated case of  $\alpha = 2y^{-1}$ , we show also a case of smaller and a case of larger  $\alpha$  value, obtaining more information on the bifurcations possible in the model as a whole. The above mentioned symmetries help in understanding the present bifurcation structure.

#### 3.3.1 Bifurcation diagram for $\alpha = 3y^{-1}$

For  $\alpha = 3y^{-1}$  the one-parameter bifurcation diagram is shown in Fig. 3.1a). Starting with  $\phi = 0$  there is a stable fixed equilibrium, fixed in the above mentioned notion for symmetric systems. This equilibrium becomes unstable at a Hopf bifurcation  $H$  at  $\phi = 0.16445$ . A stable symmetric limit cycle originates at this Hopf bifurcation. This limit cycle shows a super-critical pitch-fork bifurcation  $P^-$ , i.e. a bifurcation of a limit cycle with Floquet multiplier 1, splitting the original limit cycle into two new ones. Besides the now unstable branch two new branches originate for the pair of conjugated limit cycles. The branches merge again at another supercritical pitch-fork bifurcation  $P^-$ , after which the limit cycle is stable again for higher  $\phi$ -values. The pair of  $\mathbf{S}$ -conjugate limit cycles become unstable at a torus bifurcation  $TR$  at  $\phi = 0.89539$ .

Besides this main bifurcation pattern we found two isolas, that is an isolated solution branch of limit cycles (Golubitsky & Schaeffer, 1985). These isola cycles  $L$  are not  $\mathbf{S}$ -invariant, that is  $\mathbf{S}L \neq L$ . Isolae consisting of isolated limit cycles exist between two tangent bifurcations. One isola consists of a stable and an unstable branch. The other shows more complex bifurcation patterns. There is no full stable branch. For  $\phi = 0.60809$  at the tangent bifurcation  $T$  a stable and an unstable limit cycle collide. The stable branch becomes unstable via a flip bifurcation or periodic doubling bifurcation  $F$ , with Floquet multiplier  $(-1)$ , at  $\phi = 0.61918$  which is also pitchfork bifurcation for the period-two limit cycles. At the other end of that branch at the tangent bifurcation  $T$  at  $\phi = 0.89768$  both

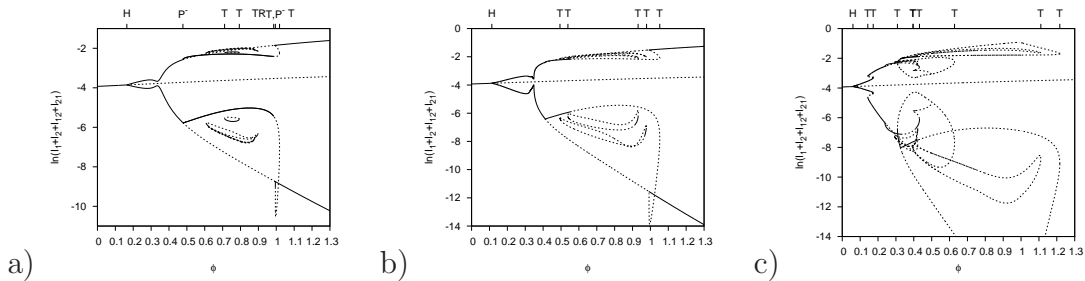


Figure 3.1: a)  $\alpha = 3y^{-1}$ : Equilibria or extremum values for limit cycles for logarithm of total infected ( $\ln(I_1 + I_2 + I_{12} + I_{21})$ ). Solid lines denote stable equilibria or limit cycles, dashed lines unstable equilibria or periodic-one limit cycles. Hopf bifurcation  $H$  around  $\phi = 0.16$  two pitchfork bifurcations  $P^-$  and a torus bifurcation  $TR$ . Besides this main bifurcation structure we found coexisting tangent bifurcations  $T$  between which some of the isolas live, see especially the one between  $\phi = 0.71$  and  $\phi = 0.79$ . Additionally found flip bifurcations are not marked here, see text. b)  $\alpha = 2y^{-1}$ : In this case we have a Hopf bifurcation  $H$  at  $\phi = 0.11$ , and besides the similar structure as found in a) also more separated tangent bifurcations  $T$  at  $\phi = 0.494, 0.539, 0.931, 0.978$  and  $1.052$  c)  $\alpha = 1y^{-1}$ : Here we have the Hopf bifurcation at  $\phi = 0.0598$  and thereafter many tangent bifurcations  $T$ , again with coexisting limit cycles.

colliding limit cycles are unstable. Close to this point at one branch there is a torus bifurcation  $TR$ , also called Neimark-Sacker bifurcation, at  $\phi = 0.89539$  and a flip bifurcation  $F$  at  $\phi = 0.87897$  which is again a pitchfork bifurcation  $P$  for the period-two limit cycles. Continuation of the stable branch originating for the flip bifurcation  $F$  at  $\phi = 0.61918$  gives another flip bifurcation  $F$  at  $\phi = 0.62070$  and one closed to the other end at  $\phi = 0.87897$ , namely at  $\phi = 0.87734$ . These results suggest that for this isola two classical routes to chaos can exist, namely via the torus or Neimark-Sacker bifurcation where the dynamics on the originating torus is chaotic, and the cascade of period doubling route to chaos.

### 3.3.2 Bifurcation diagram for $\alpha = 2y^{-1}$

For  $\alpha = 2y^{-1}$  the one-parameter bifurcation diagram is shown in Fig. 3.1b). The stable fixed equilibrium becomes unstable at a super-critical Hopf bifurcation  $H$  at  $\phi = 0.11329$  where a stable fixed limit cycle originates. This stable limit cycle becomes unstable at a super-critical pitchfork bifurcation point  $P^-$  at  $\phi = 0.41145$  for a limit cycle. This point marks the origin of a pair of  $\mathbf{S}$ -conjugate stable limit cycles besides the now unstable fixed limit cycle. Here one has to consider the two infected subpopulations  $I_1$  and  $I_2$  to distinguish the conjugate limit cycles. Because the two variables  $I_1$  and  $I_2$  are interchangeable this can also be interpreted as the stable limit cycles for the single variable say  $I_1$ . The

fixed stable equilibrium below the Hopf bifurcation where we have  $I_1^* = I_2^*$ ,  $R_1^* = R_2^*$ ,  $S_1^* = S_2^*$  and  $I_{12}^* = I_{21}^*$  is a fixed equilibrium. At the Hopf bifurcation  $H$  the stable fixed equilibrium point becomes an unstable fixed equilibrium point. The originating stable limit cycle in the parameter interval between the Hopf bifurcation and the pitchfork bifurcation is symmetric. In the parameter interval between the two pitchfork bifurcations  $P^-$  at  $\phi = 0.41145$  and subcritical  $P^+$  at  $\phi = 0.99214$ , two stable limit cycles coexist and these limit cycles are  $\mathbf{S}$ -conjugate. At the pitchfork bifurcation points the fixed limit cycle becomes unstable and remains fixed, and two stable  $\mathbf{S}$ -conjugate limit cycles originate (see (Kuznetsov, 2004, Theorem 7.7)). The invariant plane  $I_1 = I_2, R_1 = R_2, S_1 = S_2, I_{12} = I_{21}$  forms the separatrix between the pair of stable  $\mathbf{S}$ -conjugate limit cycles  $x^*(t)$  and  $\mathbf{S}x^*(t)$ ,  $\forall t \in \mathbb{R}$ . The initial values of the two state variables  $S(t_0)$  and  $R(t_0)$  together with the point on the invariant plane, determine to which limit cycle the system converges. Continuation of the stable symmetric limit cycle gives a torus or Neimark-Sacker bifurcation at point denoted by  $TR$  at  $\phi = 0.55069$ . At this point the limit cycles become unstable because a pair of complex-conjugate multipliers crosses the unit circle. Observe that at this point in the bifurcation diagram plot (Aguiar & Stollenwerk, 2007, there Fig. 12) and (Aguiar et al., 2008, there Fig. 5) the chaotic region starts. In (Albers & Sprott, 2006) the following route to chaos, namely the sequence of Neimark-Sacker bifurcations into chaos, is mentioned. Increasing the bifurcation parameter  $\phi$  along the now unstable pair of  $\mathbf{S}$ -conjugate limit cycles leads to a tangent bifurcation  $T$  at  $\phi = 1.0524$  where a pair of two unstable limit cycles collide. This branch terminates at the second pitchfork bifurcation point denoted by  $P^+$  at  $\phi = 0.99214$ . Because the first fold point gave rise to a stable limit cycle and this fold point to an unstable limit cycle we call the first pitchfork bifurcation super-critical and the latter pitchfork bifurcation subcritical. These results agree very well with the simulation results shown in the bifurcation diagram for the maxima and minima of the overall infected (Aguiar & Stollenwerk, 2007, there Fig. 15) and (Aguiar et al., 2008, there Fig. 5). Notice that AUTO (AUTO, 2009) calculates only the global extrema during a cycle, not the local extrema. Fig. 3.1b) shows also two isolas similar to those for  $\alpha = 3y^{-1}$  in Fig. 3.1 a).

### 3.3.3 Bifurcation diagram for $\alpha = 1y^{-1}$

For  $\alpha = 1y^{-1}$  the bifurcation diagram is shown in Fig 3.1c). In the lower  $\phi$  parameter range there is bistability of two limit cycles in an interval bounded by two tangent bifurcations  $T$ . The stable manifold of the intermediate saddle limit cycle acts as a separatrix. Increasing  $\phi$  the stable limit cycles become unstable at the pitchfork bifurcation  $P$  at  $\phi = 0.23907$ . Following the unstable primary branch, for larger values of  $\phi$  we observe an open loop bounded by two tangent bifurcations  $T$ . The extreme value for  $\phi$  is at  $\phi = 0.62790$ . Then lowering  $\phi$  there is a pitchfork bifurcation  $P$  at  $\phi = 0.50161$ . Later we will return to

the description of this point. Lowering  $\phi$  further the limit cycle becomes stable again at the tangent bifurcations  $T$  at  $\phi = 0.30863$ . Increasing  $\phi$  this limit cycle becomes unstable again at the pitchfork bifurcation  $P$  at  $\phi = 0.32532$ .

Continuation of the secondary branch of the two  $\mathbf{S}$ -conjugated limit cycles from this point reveals that the stable limit cycle becomes unstable at a torus bifurcation  $TR$  at  $\phi = 0.42573$ . The simulation results depicted in (Aguiar & Stollenwerk, 2007, Fig. 13) and (Aguiar et al., 2008, there Fig. 6a)) show that there is chaos beyond this point. The secondary pair of  $\mathbf{S}$ -conjugate limit cycles that originate from pitchfork bifurcation  $P$  at  $\phi = 0.23907$  becomes unstable at a flip bifurcation  $F$ . Increasing  $\phi$  further it becomes stable again at a flip bifurcation  $F$ . Below we return to the interval between these two flip bifurcations. The stable part becomes unstable at a tangent bifurcation  $T$ , then continuing, after a tangent bifurcation  $T$  and a Neimark-Sacker bifurcation  $TR$ . This bifurcation can lead to a sequence of Neimark-Sacker bifurcations into chaos. The unstable limit cycles terminates via a tangent bifurcation  $F$  where the primary limit cycle possesses a pitchfork bifurcation  $P$  at  $\phi = 0.50161$ . At the flip bifurcation  $F$  the cycle becomes unstable and a new stable limit cycle with double period emanates. The stable branch becomes unstable at a flip bifurcation again. We conclude that there is a cascade of period doubling route to chaos. Similarly this happens in reversed order ending at the flip bifurcation where the secondary branch becomes stable again.

Fig. 3.2a) gives the results for the interval  $0.28 \leq \phi \leq 0.44$  where only the minima are show. In this plot also a “period three” limit cycle is shown. In a small region it is stable and coexists together with the “period one” limit cycle. The cycles are shown in Fig. 3.2b) and c) for  $\phi = 0.294$ . The one in c) looks like a period-3 limit cycle. In Fig. 3.2 continuation of the limit cycle gives a closed graph bounded at the two ends by tangent bifurcations  $T$  where a stable and an unstable limit cycle collide. The intervals where the limit cycle is stable, are on the other end bounded by flip bifurcations  $F$ . One unstable part intersects the higher period cycles that originate via the cascade of period doubling between the period-1 limit cycle flip bifurcations  $F$  at  $\phi = 0.32816$  and  $\phi = 0.41126$ . This suggest that the period-3 limit cycle is associated with a “period-3 window” of the chaotic attractor. We conjecture that this interval is bounded by two homoclinic bifurcations for a period-3 limit cycle (see (Boer et al., 1999, 2001; Kooi & Boer, 2002; Kooi et al., 2004)). The bifurcation diagrams shown in (Aguiar & Stollenwerk, 2007, there Fig. 13) and in (Aguiar et al., 2008, there Fig. 6a)) show the point where the chaotic attractor disappears abruptly, possible at one of the two homoclinic bifurcations. In that region the two conjugated limit cycles that originate at the pitchfork bifurcation  $P$  at  $\phi = 0.32532$  are the attractors. These results suggest that there are chaotic attractors associated with the period-1 limit cycle, one occurs via a cascade of flip bifurcations originating from the two ends at  $\phi = 0.32816$  and  $\phi = 0.41126$  and one via a Neimark-Sacker bifurcation  $TR$  at  $\phi = 0.42573$ .

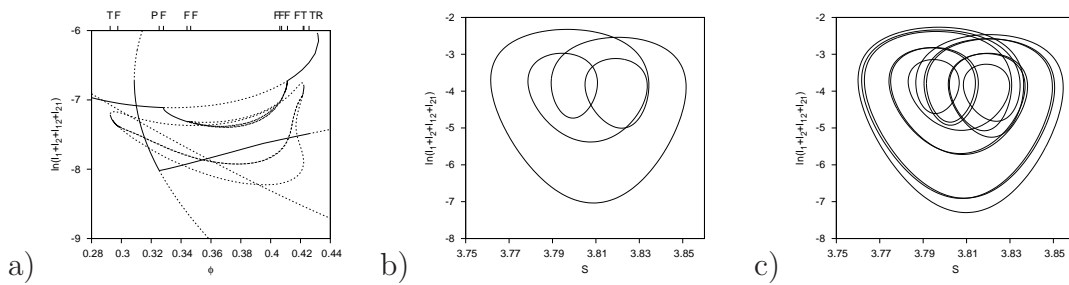


Figure 3.2: a) Detail of Fig. 3.1 c),  $\alpha = 1y^{-1}$ . We find pitchfork bifurcations  $P$  at  $\phi = 0.239$  and  $0.325$ , flip bifurcations  $F$  at  $\phi = 0.298, 0.328, 0.344, 0.346, 0.406, 0.407, 0.411$  and  $0.422$ , further tangent bifurcations  $T$  at  $\phi = 0.292, 0.346$  and  $0.422$ . Four almost coexisting bifurcations, namely  $F$ 's at  $\phi = 0.4112590$ . b) and c) state-space plots of susceptibles ( $S$ ) and logarithm of total infected ( $\ln(I_1 + I_2 + I_{12} + I_{21})$ ) for  $\alpha = 1y^{-1}$  and  $\phi = 0.294$  where two coexisting stable limit cycles appear.

### 3.4 Two-parameter diagram

We will now link the three studies of the different  $\alpha$  values by investigating a two-parameter diagram for  $\phi$  and  $\alpha$ , concentrating especially on the creation of isolated limit cycles, which sometimes lead to further bifurcations inside the isola region. Fig. 3.3 gives a two-parameter bifurcation diagram where  $\phi$  and  $\alpha$  are the free parameters. For low  $\phi$ -values there is the Hopf bifurcation  $H$  and all other curves are tangent bifurcation curves.

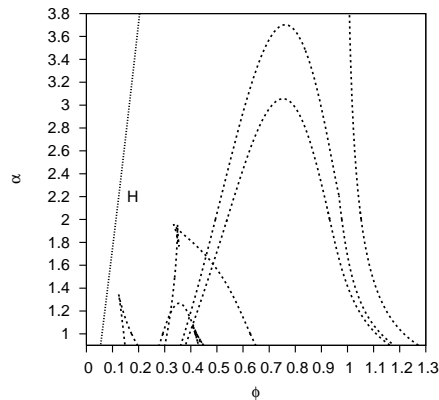


Figure 3.3: Two-dimensional parameter bifurcation diagram with  $\phi$  and  $\alpha$  as parameters. Only one Hopf bifurcation (dotted line) and many tangent bifurcation curves for limit cycles (dashed lines) are shown in the range  $\alpha \in [1, 3.8]y^{-1}$ . The isolated limit cycles originate above  $\alpha = 3y^{-1}$ . For lower values of  $\alpha$  periodic doubling routes to chaos originate.

Isolas appear or disappears upon crossing an isola variety. At an elliptic isola

point an isolated solution branch is born, while at a hyperbolic isola point an isolated solution branch vanishes by coalescence with another branch (Golubitsky & Schaeffer, 1985). From Fig. 3.3 we see that at two values of  $\alpha > 3y^{-1}$  isolas are born. Furthermore, period doubling bifurcations appear for lower  $\alpha$  values, indicating the Feigenbaum route to chaos. However, only the calculation of Lyapunov exponents, which are discussed in the next section, can clearly indicate chaos.

### 3.5 Lyapunov spectra for various $\alpha$ values

The Lyapunov exponents are the logarithms of the eigenvalues of the Jacobian matrix along the integrated trajectories, Eq. (dynamicsdeltaf), in the limit of large integration times. Besides for very simple iterated maps no analytic expressions for chaotic systems can be given for the Lyapunov exponents. For the calculation of the iterated Jacobian matrix and its eigenvalues, we use the QR decomposition algorithm (Farmer & Sidorowich, 1986; Parlitz, 1992).

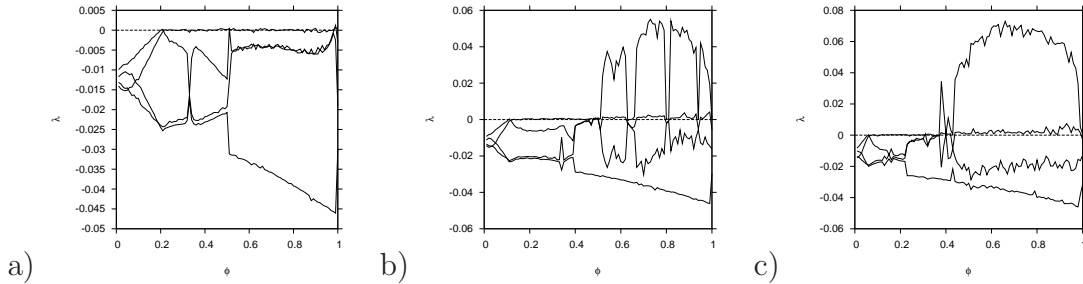


Figure 3.4: Spectrum of the four largest Lyapunov exponents with changing parameter  $\phi$  and (a) fixed  $\alpha = 4y^{-1}$ , (b)  $\alpha = 2y^{-1}$  and (c)  $\alpha = 1y^{-1}$ .

In Fig. 3.4 we show, for various  $\alpha$  values, the four largest Lyapunov exponents in the  $\phi$  range between zero and one. For  $\alpha = 4y^{-1}$  in Fig. 3.4a) we see for small  $\phi$  values fixed point behavior indicated by a negative largest Lyapunov exponent up to around  $\phi = 0.2$ . There, at the Hopf bifurcation point, the largest Lyapunov exponent becomes zero, indicating limit cycle behavior for the whole range of  $\phi$ , apart from the final bit before  $\phi = 1$ , where a small spike with positive Lyapunov exponent might be present, but difficult to distinguish from the noisy numerical background.

For  $\alpha = 2y^{-1}$  in Fig. 3.4b) however, we see a large window with positive largest Lyapunov exponent, well separated from the second largest being zero. This is a clear sign of deterministically chaotic attractors present for this  $\phi$  range. Just a few windows with periodic attractors, indicated by the zero largest Lyapunov exponent are visible in the region of  $0.5 < \phi < 1$ . For smaller  $\phi$  values we observe qualitatively the same behavior as already seen for  $\alpha = 4y^{-1}$ . For the

smaller value of  $\alpha = 1y^{-1}$ , in Fig. 3.4c), the chaotic window is even larger than for  $\alpha = 2y^{-1}$ . Hence deterministic chaos is present for temporary cross-immunity in the range around  $\alpha = 2y^{-1}$  in the range of  $\phi$  between zero and one.

## 3.6 Conclusions

We have presented a detailed bifurcation analysis for a multi-strain dengue fever model in terms of the different ratios of secondary infections contribution to the force of infection (ADE parameter  $\phi$ ), in the previously not well investigated region between zero and one, and for the temporary cross-immunity parameter  $\alpha$ . The symmetries implied by the strain structure, are taken into account in the analysis. Many of the possible bifurcations of equilibria and limit cycles of  $\mathbb{Z}_2$ -equivariant systems can be distinguished. Using AUTO (AUTO, 2009) the different dynamical structures were calculated. Future time series analysis of epidemiological data has good chances to give insight into the relevant parameter values purely on topological information of the dynamics, rather than classical parameter estimation of which application is in general restricted to fairly simple dynamical scenarios.

## 3.A Epidemic model equations

The complete system of ordinary differential equations for a two-strain epidemiological system allowing for differences in primary versus secondary infection and temporary cross-immunity is given by system Eq. (3.8). For two different strains, named 1 and 2, we label the SIR classes for the hosts that have seen the individual strains. Susceptibles to both strains ( $S$ ) get infected with strain 1 ( $I_1$ ) or strain 2 ( $I_2$ ), with infection rate  $\beta$ . They recover from infection with strain 1 (becoming  $R_1$ ) or from strain 2 (becoming  $R_2$ ), with recovery rate  $\gamma$ , and so on.

With temporary cross-immunity rate  $\alpha$ , the  $R_1$  and  $R_2$  become again susceptible with a previous infection ( $S_1$  being immune against strain 1 but susceptible to 2, respectively  $S_2$ ), where the index represents the first infection strain. Now,  $S_1$  can be reinfected, now with strain 2 (becoming  $I_{12}$ ), meeting  $I_2$  with infection rate  $\beta$  or meeting  $I_{12}$  with infection rate  $\phi\beta$ , secondary infected contributing differently to the force of infection than primary infected, and so on.

We include demography of the host population denoting the birth and death rate by  $\mu$ . For constant population size  $N$  we have for the immune to all strains  $R = N - (S + I_1 + I_2 + R_1 + R_2 + S_1 + S_2 + I_{12} + I_{21})$  and therefore we only need to consider the first 9 equations of system Eq. (3.8), giving 9 Lyapunov exponents.

In our numerical studies we take the population size equal to  $N = 100$  so that mean proportions of susceptibles, infected etc. are given in percentage. As fixed parameter values we take  $\mu = 1/65y$ ,  $\gamma = 52y^{-1}$ ,  $\beta = 2 \cdot \gamma$ . The parameters



$\phi$  and  $\alpha$  are varied. For more information on the parametrization of the basic two-strain model, see (Aguiar & Stollenwerk, 2007; Aguiar et al., 2008).

$$\begin{aligned}
\frac{d}{dt}S &= -\frac{\beta}{N}S(I_1 + \phi I_{21}) - \frac{\beta}{N}S(I_2 + \phi I_{12}) + \mu(N - S) \\
\frac{d}{dt}I_1 &= \frac{\beta}{N}S(I_1 + \phi I_{21}) - (\gamma + \mu)I_1 \\
\frac{d}{dt}I_2 &= \frac{\beta}{N}S(I_2 + \phi I_{12}) - (\gamma + \mu)I_2 \\
\frac{d}{dt}R_1 &= \gamma I_1 - (\alpha + \mu)R_1 \\
\frac{d}{dt}R_2 &= \gamma I_2 - (\alpha + \mu)R_2 \\
\frac{d}{dt}S_1 &= -\frac{\beta}{N}S_1(I_2 + \phi I_{12}) + \alpha R_1 - \mu S_1 \\
\frac{d}{dt}S_2 &= -\frac{\beta}{N}S_2(I_1 + \phi I_{21}) + \alpha R_2 - \mu S_2 \\
\frac{d}{dt}I_{12} &= \frac{\beta}{N}S_1(I_2 + \phi I_{12}) - (\gamma + \mu)I_{12} \\
\frac{d}{dt}I_{21} &= \frac{\beta}{N}S_2(I_1 + \phi I_{21}) - (\gamma + \mu)I_{21} \\
\frac{d}{dt}R &= \gamma(I_{12} + I_{21}) - \mu R \quad .
\end{aligned} \tag{3.8}$$





## Chapter 4

# The role of seasonality and import in a minimalistic multi-strain dengue model capturing differences between primary and secondary infections: complex dynamics and its implications for data analysis

Maíra Aguiar, Sebastien Ballesteros, Bob W. Kooi and Nico Stollenwerk  
*Journal of Theoretical Biology*, **289**:181-196, 2011.

In many countries in Asia and South-America dengue fever (DF) and dengue hemorrhagic fever (DHF) has become a substantial public health concern leading to serious social-economic costs. Mathematical models describing the transmission of dengue viruses have focused on the so called antibody-dependent enhancement (ADE) effect and temporary cross-immunity trying to explain the irregular behavior of dengue epidemics by analyzing available data. However, no systematic investigation of the possible dynamical structures has been performed so far. Our study focuses on a seasonally forced (non-autonomous) model with temporary cross-immunity and possible secondary infection, motivated by dengue fever epidemiology. The notion of at least two different strains is needed in a minimalistic model to describe differences between primary infections, often asymptomatic, and secondary infection, associated with the severe form of the disease. We extend the previously studied non-seasonal (autonomous) model by

adding seasonal forcing, mimicking the vectorial dynamics, and a low import of infected individuals, which is realistic in the dynamics of dengue fever epidemics. A comparative study between three different scenarios (non-seasonal, low seasonal and high seasonal with a low import of infected individuals) is performed. The extended models show complex dynamics and qualitatively a good agreement between empirical DHF monitoring data and the obtained model simulation. We discuss the role of seasonal forcing and the import of infected individuals in such systems, the biological relevance and its implications for the analysis of the available dengue data. At the moment only such minimalistic models have a chance to be qualitatively understood well and eventually tested against existing data. The simplicity of the model (low number of parameters and state variables) offer a promising perspective on parameter values inference from the DHF case notifications.

## 4.1 Introduction

Dengue is a viral mosquito-borne infection which in recent years has become a major international public health concern, a leading cause of illness and death in the tropics and subtropics. It is estimated that every year, there are 70 – 500 million dengue infections, 36 million cases of dengue fever (DF) and 2.1 million cases of dengue hemorrhagic fever (DHF), with more than 20.000 deaths per year (WHO, 2009; PDVI, 2011). Dengue is caused by four antigenically distinct but closely related viruses, designated by dengue types 1,2,3, and 4, where infection by one serotype confers life-long immunity to only that serotype and a short period of temporary cross-immunity to other serotypes (WHO, 2009; Alcon et al., 2002; Matheus et al., 2005; SES, 2010; Wearing & Rohani, 2006; Halstead, 2004; Dejnirattisai et al., 2010). Two variants of the disease exist: dengue fever (DF), a non-fatal form of illness, and dengue hemorrhagic fever (DHF), which may evolve towards a severe form known as dengue shock syndrome (DSS). Epidemiological studies support the association of DHF with secondary dengue infection (Guzmán et al., 2000; Vaughn et al., 2000; Halstead, 1982, 2003; Nisalak et al., 2003), and there is good evidence that sequential infection increases the risk of developing DHF, due to a process described as antibody-dependent enhancement (ADE) (WHO, 2009; Halstead, 2004; Dejnirattisai et al., 2010). The risk for DHF with a third or fourth dengue infection relative to a first or second exposure is not known. An analysis of a database of admitted cases to the Queen Sirikit National Institute of Child Health and Kamphaeng Phet Provincial Hospital with suspected dengue illness revealed that the number of dengue admissions caused by a third or fourth dengue virus infection was extremely low and once admitted, the risk for DHF relative to DF was not different for those experiencing third or fourth dengue virus infections over those experiencing a second dengue virus infection (Endy et al., 2002; Gibbons et al., 2007; Halstead, 2008). It is

suggested that the majority of secondary dengue infections occur at a spacing of more than 6 months (SES, 2010), and from cohort studies and prospective seroepidemiological studies of defined populations, the hospitalization rates for individuals experiencing secondary dengue infections are in the range of 2–3% of all infected individuals (Halstead, 2003; Rothman et al., 2004). There is no specific treatment for dengue, and a vaccine is not yet available. So far, prevention of exposure and vector control remain the only alternatives to prevent dengue transmission.

Mathematical models describing the transmission of dengue viruses appeared in the literature as early as 1970 (Fischer & Halstead, 1970). More recently, mathematical models describing the transmission of dengue viruses have focused on the ADE effect and temporary cross-immunity trying to explain the irregular behavior of dengue epidemics. In the literature the multi-strain interaction leading to deterministic chaos via ADE has been described previously, e.g. (Ferguson et al., 1999; Schwartz et al., 2005; Billings et al., 2007) but neglecting temporary cross-immunity. Consideration of temporary cross immunity is rather complicated and up to now not in detail analyzed. Models formulated in (Wearing & Rohani, 2006; Nagao & Koelle, 2008; Recker et al., 2009; Loureço & Recker, 2010), did not investigate closer the possible dynamical structures. In (Aguiar & Stollenwerk, 2007; Aguiar et al., 2008, 2009) by including temporary cross-immunity into dengue models with ADE, a rich dynamic structure including deterministic chaos was found in wider and more biologically realistic parameter regions. However, in order to be able to reproduce the yearly cycle in dengue incidence seasonal forcing and a low import of infected have to be included in the models.

In addition to *ab-initio* simulation techniques to solve the mathematical model numerically, we use bifurcation analysis to study the dependence of the dynamics on parameter values. This separates the parameter space in regions with qualitatively different long-term dynamics: steady-state solution (equilibrium), periodic solution (limit cycle) and non-periodic solution (aperiodic or chaotic attractors). For non-periodic solutions the dynamics is classified further based on Lyapunov exponents. In the case of sinusoidal forcing the non-autonomous system is, for analysis purposes, replaced by an equivalent autonomous system whereby the original model is augmented with the so called Hopf oscillator producing the sinusoidal forcing.

In this paper, we investigate the extended multi-strain model with temporary cross-immunity and possible secondary infection, motivated by dengue fever epidemiology presented first in (Aguiar & Stollenwerk, 2007; Aguiar et al., 2008) and (Aguiar et al., 2009). We add seasonal forcing into the previous multi-strain dengue model, mimicking the vectorial dynamics, and a low import of infected individuals, which is realistic in the dynamics of dengue fever epidemics. The complete analysis of the extended models shows complex dynamics and qualitatively a very good result when comparing empirical DHF data and model simulation. The effects of the vector dynamics are only taken into account by

the force of infection parameters in the SIR-type model, but not modeling this mechanisms explicitly ( see also (Wearing & Rohani, 2006)). Since vector models without multi-strain aspects only shows stationary dynamics (Esteva & Vargas, 1998, 2000) and seasonally forced SIR systems can show already deterministic chaos (Stone et al., 2007), the presented model is minimalistic in the sense that it can capture the essential differences of primary versus secondary infection under periodic forcing but is not too high dimensional so that future parameter estimation can still attempt to estimate all initial conditions as well as the few model parameters.

## 4.2 The seasonal multi-strain epidemic model

The seasonal multi-strain model is represented in Fig. 4.1 by using a state flow diagram, dividing the population into ten classes: susceptible to both strains, 1 and 2 ( $S$ ), primarily infected with strain one ( $I_1$ ) or strain two ( $I_2$ ), recovered from the first infection with strain one ( $R_1$ ) or strain two ( $R_2$ ), susceptible with a previous infection with strain one ( $S_1$ ) or strain two ( $S_2$ ), secondarily infected with strain one when the first infection was caused by strain two ( $I_{21}$ ) or for second time infected with strain two when the first infection was caused by strain one ( $I_{12}$ ). Notice that infection by one serotype confers life-long immunity to that serotype. Then the recovered individuals from the secondary infection ( $R$ ). To give more reality to the dynamics of the disease, we also add a low import factor of infected individuals into the system.

The complete system of ordinary differential equations for the seasonal multi-strain epidemiological model is shown in system Eq. (4.1), and the dynamics are described as follows. Susceptibles to both strains can get the first infection with strain one or strain two with force of infection  $\frac{\beta I}{N}$  when the infection is acquired via an individual in his first infection or  $\frac{\phi \beta I}{N}$  when the infection is acquired via an individual in his second infection (for more information on the parametrization of ADE and secondary dengue infection by  $\phi$ , see (Ferguson et al., 1999; Aguiar et al., 2008)). They recover from the first infection with a recovery rate  $\gamma$ , conferring full and life-long immunity against the strain that they were exposed to, and also a short period of temporary cross-immunity  $\alpha$  against the other strain, becoming susceptible to a second infection with a different strain. The susceptible with a previous infection gets the secondary infection with force of infection  $\frac{\beta I}{N}$  or  $\frac{\phi \beta I}{N}$  depending on whom (individual on his primary or secondary infection) is transmitting the infection. Then, with recovery rate  $\gamma$ , the individuals recover and become immune against all strains.

We assume no epidemiological asymmetry between strains ( $\beta_1 = \beta_2 = \beta$ ,  $\phi_1 = \phi_2 = \phi$ ), i.e. infections with strain one or strain two contribute in the same way to the force of infection. Here, the only relevant difference concerning disease transmissibility is that the force of infection varies accordingly to the

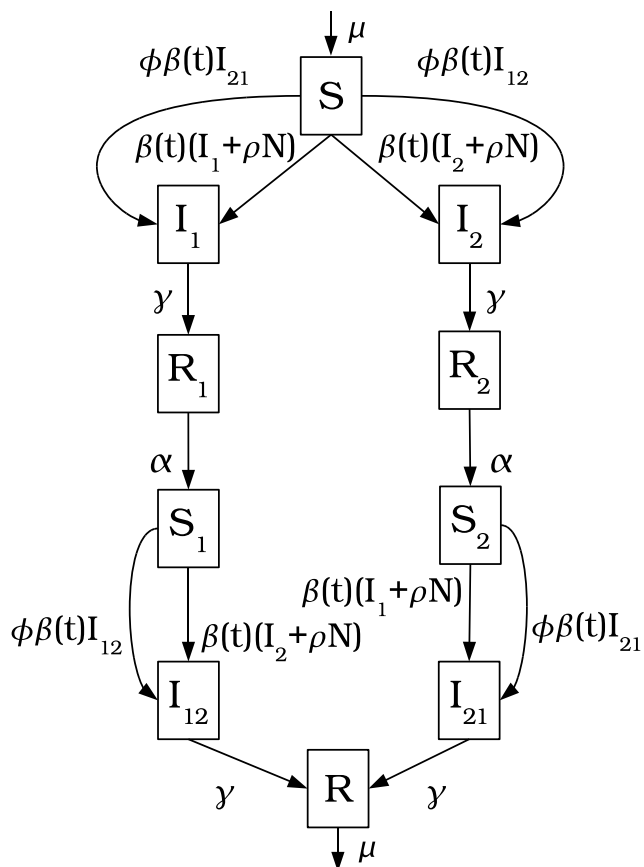


Figure 4.1: The state flow diagram for the seasonal two-strain model. The boxes represent the disease related stages and the arrows indicate the transition rates. The transition rate  $\mu$  coming out of the class  $R$  represents the death rates of all classes,  $S, I_1, I_2, R_1, R_2, S_1, S_2, I_{12}, I_{21}, R$ , getting into the class  $S$  as a birth rate.

number of previous infections the hosts have experienced. In a primary infection the individuals transmit the disease with a force of infection  $\frac{\beta I}{N}$  whereas in a secondary infection the transmission is given with a force of infection  $\frac{\phi \beta I}{N}$  where  $\phi$  can be larger or smaller than unit, i.e. increasing or decreasing the transmission rate.

$$\begin{aligned}
\dot{S} &= -\frac{\beta(t)}{N}S(I_1 + \rho \cdot N + \phi I_{21}) \\
&\quad -\frac{\beta(t)}{N}S(I_2 + \rho \cdot N + \phi I_{12}) \\
&\quad +\mu(N - S) \\
\dot{I}_1 &= \frac{\beta(t)}{N}S(I_1 + \rho \cdot N + \phi I_{21}) - (\gamma + \mu)I_1 \\
\dot{I}_2 &= \frac{\beta(t)}{N}S(I_2 + \rho \cdot N + \phi I_{12}) - (\gamma + \mu)I_2 \\
\dot{R}_1 &= \gamma I_1 - (\alpha + \mu)R_1 \\
\dot{R}_2 &= \gamma I_2 - (\alpha + \mu)R_2 \tag{4.1} \\
\dot{S}_1 &= -\frac{\beta(t)}{N}S_1(I_2 + \rho \cdot N + \phi I_{12}) + \alpha R_1 - \mu S_1 \\
\dot{S}_2 &= -\frac{\beta(t)}{N}S_2(I_1 + \rho \cdot N + \phi I_{21}) + \alpha R_2 - \mu S_2 \\
\dot{I}_{12} &= \frac{\beta(t)}{N}S_1(I_2 + \rho \cdot N + \phi I_{12}) - (\gamma + \mu)I_{12} \\
\dot{I}_{21} &= \frac{\beta(t)}{N}S_2(I_1 + \rho \cdot N + \phi I_{21}) - (\gamma + \mu)I_{21} \\
\dot{R} &= \gamma(I_{12} + I_{21}) - \mu R
\end{aligned}$$

The parameter  $\beta$  takes the seasonal forcing into account as a cosine function and is given explicitly by

$$\beta(t) = \beta_0 \cdot (1 + \eta \cdot \cos(\omega \cdot (t + \varphi))) \tag{4.2}$$

where  $\beta_0$  is the infection rate,  $\eta$  is the degree of seasonality and  $\varphi$  the phase which becomes important only when considering empirical time series.

Table 4.1: Parameter set, rates given in units per year, ratio without unit

Par.	Description	Values	Ref
$N$	population size	100	—
$\mu$	birth and death rate	$1/65y$	(UNWPP, 2011)
$\gamma$	recovery rate	$52y^{-1}$	(WHO, 2009)
$\beta_0$	infection rate	$2 \cdot \gamma$	(Ferguson et al., 1999)
$\eta$	degree of seasonality	0.1 to 0.35	(Nagao & Koelle, 2008)
$\varphi$	phase	0	—
$\rho$	import parameter	0 to $10^{-10}$	(Nagao & Koelle, 2008)
$\alpha$	temporary cross-immunity rate	$2y^{-1}$	(Matheus et al., 2005)
$\phi$	ratio of secondary infections contributing to force of infection	variable ( $< 1$ )	(Halstead, 2004)

In this model, a susceptible individual can become infected also by meeting an infected individual from an external population (hence  $(\beta/N \cdot S \cdot I)$  goes to  $(\beta/N \cdot S \cdot (I + \rho \cdot N))$ ) contributing to the force of infection with an import parameter  $\rho$ . The parameter  $\phi$  in our model, is the ratio of secondary infection contribution to the force of infection. For instance, we study the region of the parameter  $\phi < 1$ , which acts as decreasing the infectivity of secondary dengue infection, where the hospitalization is more likely due to the ADE effect associated with the severity of the disease. The secondary infected individuals do not contribute to the force of infection as much as people with first infection do.

The deterministic model formulation is based on the large number assumption. As a consequence the number of individuals can be used to scale all state variables of the model. The constant population  $N = 100$  is used for clarity so that all epidemiological proportions (susceptibles, infected and recovered) are given in percentage. The demography rate is denoted by  $\mu$  and the parameter values are given in Table 4.1.

### 4.3 Analysis techniques

The previous analysis of the non-seasonal multi-strain dengue model has shown a rich variety of dynamics through bifurcations up to deterministically chaotic attractors in an unexpected parameter region of  $\phi < 1$ , where secondary infected individual (due to the likely hospitalization) contribute less to overall force of infection than an individual that is for the first time infected, just by adding



temporary cross-immunity to a previously existing dengue model. In (Aguiar et al., 2008) a time series analysis (simulations and calculation of Lyapunov exponents) and a numerical bifurcation analysis were performed. In this manuscript, we extend the analysis of the non-seasonal model with a two-parameter bifurcation analysis where both, the ratio of secondary infection contribution to the force of infection (parameter  $\phi$ ) and temporary cross-immunity rate (parameter  $\alpha$ ) vary simultaneously (see Fig. 4.2c). Two scenarios of seasonally forced systems are also analyzed. We used the software AUTO (AUTO, 2009) to calculate the bifurcation curves presented, and the Lyapunov exponents were calculated using an iterated technique using the QR decomposition algorithm via Householder matrices (see (Aguiar et al., 2008; Ruelle, 1986; Holzfuss & Lauterborn, 1989; Holzfuss & Parlitz, 1991)).

The equilibrium values of the state variables are calculated by solving the non-linear system Eq. (4.1) equal to zero. Often multiple equilibria coexist. The stability of each equilibrium is found by linearization, that is calculating the eigenvalues of the Jacobian matrix evaluated at that point. When all eigenvalues have negative real parts the equilibrium is stable, otherwise it is unstable.

A bifurcation point is defined as a parameter value where the long-term dynamics of the system changes qualitatively at points where one eigenvalue is zero (or its real part). One important bifurcation is the Hopf bifurcation point where the real parts of a pair of conjugated eigenvalues are zero. At that point the equilibrium loses stability and the system starts to oscillate, that is, where a periodic solution or limit cycle originates when a parameter is varied crossing that point.

A limit cycle can be found numerically by solving a boundary value problem, whereby the boundary conditions are cyclic. Observe that the period of this solution is an additional parameter calculated along with the solution. The stability of limit cycles is determined by so-called Floquet multipliers. A limit cycle is stable when all multiplier are inside the unit circle of the complex plane, and unstable when at least one is outside. At a bifurcation point, the bifurcation parameter value is such that one multiplier lies on the unit circle of the complex plane. When this multiplier equals 1, it is a tangent bifurcation while when this multiplier equals  $-1$ , a period-doubling (or flip) bifurcation occurs. Changing a parameter can give a cascade of period-doubling bifurcation leading to chaotic dynamics.

Another important bifurcation point is the torus or Neimark-Sacker bifurcation of the limit cycle where two complex conjugate multipliers are on the unit circle. At such a point, limit cycles or quasi-periodic dynamics on the torus or chaotic dynamics originate when the bifurcation parameter is varied. For an introduction into bifurcation analysis we refer the reader to (Guckenheimer & Holmes, 1985; Kuznetsov, 2004), and for applications in eco-epidemiological models (Malchow et al., 2008; Stiefs et al., 2009; Kooi et al., 2011).

The Lyapunov exponent is a generalization of both an eigenvalue and a Flo-

quet multiplier. While for a fixed point the contraction and expansion rates are given by the eigenvalues and for a limit cycle by Floquet multipliers, for more complex geometrical objects (torus, chaotic attractors) the contraction and expansion rates are given by the Lyapunov exponents (Ott, 1993). For instance, the dynamics on or beyond a torus is classified as periodic, when one Lyapunov exponent zero, aperiodic when two Lyapunov exponents zero, and chaotic when one Lyapunov exponent zero and at least one positive. Lyapunov exponents can be calculated along the trajectory as

$$\lambda_i(n) = \frac{1}{n \cdot \Delta t} \ln \left( \prod_{\nu=1}^n |r_{ii}(\nu)| \right) \quad (4.3)$$

where  $\Delta t$  is the time-step,  $n$  the (large) number of time steps and  $r_{ii}$  are the diagonal elements of the upper triangular matrix  $R$  of the  $\nu$ -th QR-decomposition at the  $\nu$ -th time-step.

Just as with the eigenvalues of the Jacobian matrix, the number of Lyapunov exponents equals the dimension of the system (9 for system Eq. (4.1) and 11 for the augmented system described in Appendix 4.A). The so called Dominant Lyapunov Exponent (DLE) is the exponent with the largest magnitude. The set of Lyapunov exponents is called the Lyapunov spectrum which can be calculated for all parameter values. The situation when all Lyapunov exponents are negative gives a stable equilibrium, one dominant zero Lyapunov exponent indicates a stable limit cycle, two dominant zero Lyapunov exponents quasi-periodicity (for instance on a torus), a positive Lyapunov exponent chaotic behavior and multiple positive Lyapunov exponent hyperchaos.

Both the bifurcation analysis (for equilibria and limit cycles) and the Lyapunov spectrum calculation (for chaotic dynamics), can be done for autonomous and non-autonomous (e.g. seasonally forced) systems. With sinusoidal forcing, the non-autonomous system (system Eq. (4.1)) can be coupled with the Hopf oscillator (a set of two ODE'S), to get an equivalent autonomous system of dimension 11. Notice that the period of the forcing is fixed: equal to 1, and that a steady-state solution does not exist. The basal dynamics is now a periodic solution with period equal to the forcing period, which is a limit cycle of the equivalent autonomous system. Hence the dynamics can be analyzed in the same way as described above and shown in Appendix 4.A.

## 4.4 Bifurcation analysis

In this section we start with a bifurcation analysis of the non-seasonal model and then continue with two scenarios of seasonally forced systems, namely the low seasonal model and the high seasonal model with a low import of infected individuals.

### 4.4.1 Bifurcation analysis of the non-seasonal model

In this section we show briefly the results for the non-seasonal system published in (Aguiar et al., 2008, 2009) on which the further results of the present article are based. First we show in Fig. 4.2a) the Lyapunov exponents in the parameter range  $\phi \in [0, 0.2]$ . The DLE is negative below and becomes zero at  $\phi = 0.108$ , the Hopf bifurcation point which is also predicted by AUTO (AUTO, 2009).

Secondly, we show the one-parameter bifurcation diagram for  $\phi \in [0, 1.3]$  (see Fig. 4.2b)). At fine grid in this parameter range, system Eq. (4.1) was solved numerically. We discarded 2000 years of transients and plot the varying ratio of the secondary infection contribution to the force of infection ( $\phi$ ) over the steady state or local maxima of logarithm of total number of infected ( $\ln(I)$ , where  $I := I_1 + I_2 + I_{12} + I_{21}$ ), obtaining the one-parameter bifurcation diagram.

The one-parameter diagram is shown in Fig. 4.2b). Here the logarithm of total number of infected are shown, where solid lines denote stable equilibria or limit cycles, and dashed lines unstable equilibria or limit cycles. Various bifurcations are: Hopf bifurcation  $H(\phi = 0.11326)$ , pitchfork bifurcations  $P(\phi = 0.41145, 0.99214)$ , torus bifurcation  $TR(\phi = 0.55069)$  and tangent bifurcations  $T(\phi = 0.4.9406, 0.53874, 0.93103, 0.97825, 1.05242)$ .

In addition to this main bifurcation pattern we found two isolas, consisting of isolated limit cycles existing between two tangent bifurcations (for more information on the isolas see (Aguiar et al., 2009)). At the Hopf bifurcation  $H$  ( $\phi = 0.1133$ ) the stable fixed equilibrium becomes an unstable fixed equilibrium and in the parameter interval between the Hopf bifurcation and the pitchfork bifurcation  $P$  ( $\phi = 0.4114$ ) there is a symmetric stable limit cycle (for more information on the bifurcation analysis by continuation for the non-seasonal multi-strain model see (Aguiar et al., 2008, 2009), however, in these articles it is wrongly stated that it is a fixed limit cycle instead of the symmetric limit cycle). At a pitchfork bifurcation point, the symmetric limit cycle becomes unstable and remains symmetric, while two stable S-conjugate limit cycles originate (see (Kuznetsov, 2004), Theorem 7.7). These S-conjugate limit cycles become unstable at a torus bifurcation  $TR$  ( $\phi = 0.5507$ ). At this torus or Neimark-Sacker bifurcation the dynamics becomes chaotic (positive Lyapunov exponent). Increasing the ratio of secondary infection contribution to the force of infection ( $\phi$ ) further, this chaotic behavior disappears at a second pitchfork bifurcation  $P$  ( $\phi = 0.9921$ ). At this pitchfork bifurcation the branch of limit cycles, that was originated at the first pitchfork bifurcation, terminates after going through a region where two limit cycles coexist and disappear at a tangent bifurcation. In the small  $\phi$  interval between the pitchfork bifurcation and the tangent bifurcation  $T$  ( $\phi = 0.931$ ) two stable limit cycles coexist. This means that the stable manifold of the unstable intermediate limit cycle forms the separatrix for the two basins of attraction in the state space. We remark that the sudden disappearance of the chaotic attractor at the pitchfork bifurcation is similar to the classical intermittency route to

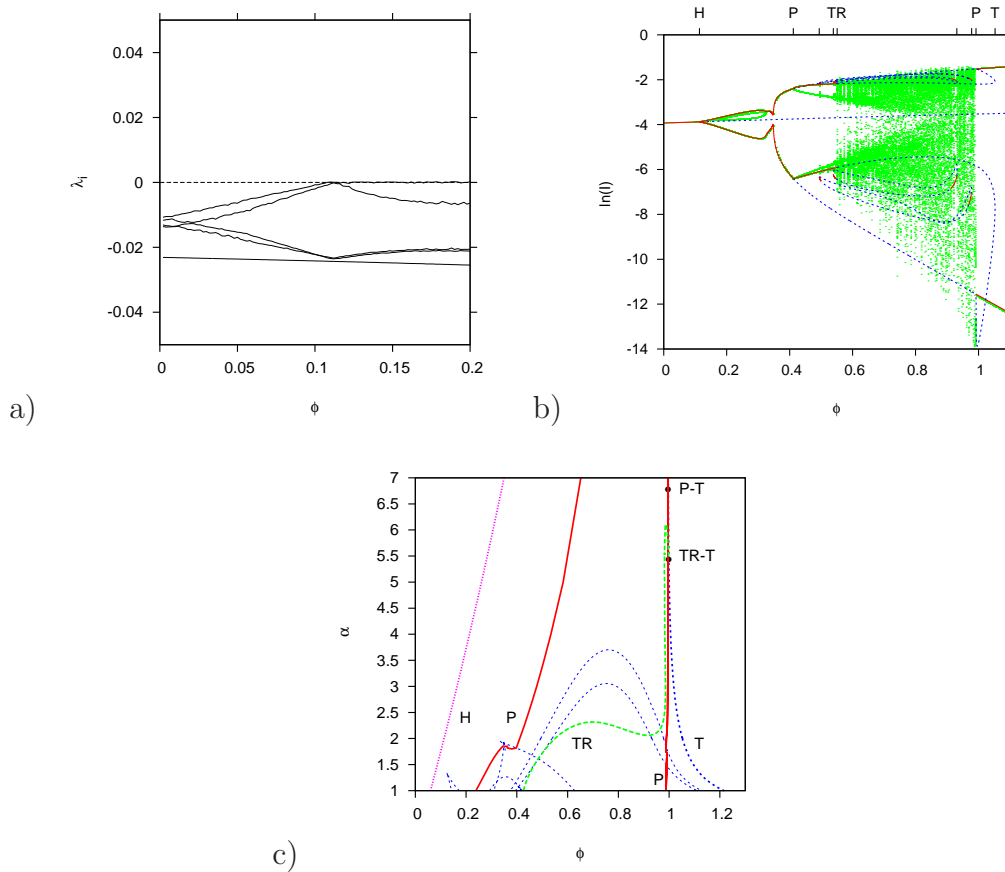


Figure 4.2: Bifurcation diagram of the non-seasonal model. With temporary cross-immunity rate  $\alpha = 2y^{-1}$  and varying the ratio of secondary infection contribution to the force of infection  $\phi$ , in a) we show the Lyapunov spectrum in the parameter range of  $\phi \in [0, 0.2]$ . In b) we show the one-parameter bifurcation diagram calculated using AUTO, where solid lines denote stable equilibria or limit cycles, and dashed lines unstable equilibria or limit cycles, on top of the numerical bifurcation diagram (in green). In c) we show the two-dimensional parameter bifurcation diagram with temporary cross-immunity rate  $\alpha$  and the ratio of secondary infection contribution to the force of infection  $\phi$  varying simultaneously in the range  $\phi \in [0, 1.3]$  and  $\alpha \in [1, 7]y^{-1}$ , calculated using AUTO. In addition to the Hopf bifurcation  $H$  (dotted lines) and many tangent bifurcation  $T$  curves (dashed lines), the torus  $TR$  and pitchfork  $P$  bifurcations are shown. At the codim-two points  $P - T$  the pitchfork and tangent bifurcations for limit cycles meet and at point  $TR - T$  the pitchfork and torus bifurcations.

chaos occurring at for instance a tangent bifurcation.

Fig. 4.2c) gives the most important bifurcation curves where both  $\phi$  and  $\alpha$  vary simultaneously: for an equilibrium the Hopf bifurcation  $H$ , and for limit cycles the torus-bifurcation  $TR$  and the pitchfork bifurcation  $P$  and a tangent bifurcation  $T$ . At the two codim-two points,  $P - T$  and  $TR - T$ , the tangent bifurcation for a limit cycle splits off a pitchfork and a torus bifurcation. This diagram shows for which  $\phi$  and  $\alpha$  parameter values chaotic behavior can occur, namely below the torus-bifurcation  $TR$  and on the left hand side of the pitchfork bifurcation  $P$  that originates from the  $P - T$  point. However, within this region there are periodic windows such as shown in Fig. 4.2b). We found isolas coexisting with the attractors of this main bifurcation structure. A stable limit cycle was calculated by simulation starting from initial values in the state space obviously outside the basin of attraction of the attractors of the main bifurcation structure. Continuation starting from this limit cycle gave rise to bifurcations into chaos. For a detailed analysis of the attractors in state space for the non-seasonal model, see also Appendix 4.B.1 and (Aguiar et al., 2008, 2009).

Note that by adding a low import factor into the non-seasonal model the classical ADE chaotic region for  $\phi > 1$  found in (Ferguson et al., 1999; Aguiar et al., 2008) disappears (see Appendix 4.C, Fig. 4.15)

#### 4.4.2 Bifurcation analysis of the seasonal models

In this section we relate and compare the results for the seasonally forced systems to that of the non-seasonal system discussed in the previous section. First we compare the bifurcation diagrams obtained for the non-seasonal and seasonal models. In the special case where  $\eta = 0$ , the seasonal system is decoupled in the original non-seasonal system studied in (Aguiar et al., 2008, 2009) with  $\beta = \beta_0$  and the augmented oscillator described in Appendix 4.A, by system Eq. (4.4). It is easy to show that the augmented system with system Eq. (4.4) is  $\mathbb{Z}_2$ -symmetric just as the original seasonal model (system Eq. (4.1)). This has consequences for the type of bifurcations to be expected. If the non-seasonal system possesses a Hopf bifurcation, the seasonally forced system has a torus bifurcation.

The bifurcation diagrams for the seasonal models are shown in Fig. 4.3a) and Fig. 4.3b). In Fig. 4.3a) the bifurcation diagram for the system with low seasonality ( $\eta = 0.1$ ) is not very informative since we have many local extrema, even for the most simple case of the torus. When increasing the ratio of secondary infection contribution to the force of infection ( $\phi$  values), the troughs become very low, with the logarithm of total infected going as low as  $-160$ . By adding a low import of infected ( $\rho = 10^{-10}$ ) into the seasonal model, the logarithm of total infected does not pass below  $-16$  (see Fig. 4.3b)), avoiding the chance of extinction in stochastic systems with reasonable system size.

In order to get more insight about the disappearance of the chaotic behavior we study a two-parameter diagram (see Fig. 4.4) for each one of the models,

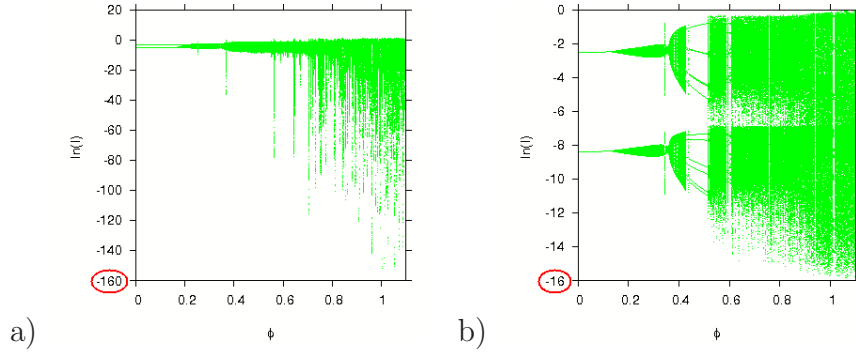


Figure 4.3: Bifurcation diagram comparison between seasonal models. We plot the varying ratio of the secondary infection contribution to the force of infection ( $\phi$ ) over the steady state or local maxima of logarithm of total number of infected ( $\ln(I)$ ). In a) bifurcation diagram for the low seasonal model without import of infected, where the degree of seasonality  $\eta = 0.1$  and in b) bifurcation diagram for the high seasonal model with a low import of infected. Here, the degree of seasonality  $\eta = 0.35$  and the import factor  $\rho = 10^{-10}$ . These bifurcation diagrams can be compared with Fig. 4.2b) for the non-seasonal model ( $\eta = 0$ ). The other parameter values are listed in Table 4.1. Notice that for low seasonality without import factor, the infected go to very low numbers, unrealistically low for any empirical epidemiological system.

(non-seasonal, low seasonal and high seasonal with import of infected), where the ratio of the secondary infection contribution to the force of infection  $\phi$  and the temporary cross-immunity rate  $\alpha$  are varied simultaneously. The time series simulations (section 4.5) and state space plots (Appendix 4.B) are also analyzed and the results are compared for the different case scenarios.

### Bifurcation analysis of the low seasonal model

For the non-seasonal system, with 6 months of temporary cross-immunity ( $\alpha = 2y^{-1}$ ), there is a stable equilibrium that becomes unstable at a super-critical Hopf bifurcation  $H$  at ( $\phi = 0.1133$ ) leading to a stable limit cycle for higher  $\phi$  values (see Fig. 4.4a)). By adding low seasonal forcing ( $\eta = 0.1$ ) into the system, a torus bifurcation  $TR$  appears at  $\phi = 0.1145$ , slightly above the Hopf bifurcation of the non-seasonal system (see Fig. 4.4b)). When a low import factor ( $\rho = 10^{-10}$ ) of infected is included into the high seasonal system ( $\eta = 0.35$ ), the torus bifurcation  $TR$  is predicted by AUTO at  $\phi = 0.13$  (see Fig. 4.4b)).

These results show that on the right-hand side of the torus bifurcation  $TR$  possibly chaotic dynamics can occur. Therefore we continue our analysis with the calculation of the Lyapunov exponent spectrum in Fig. 4.5.

Figure 4.5a) shows the Lyapunov spectrum in the parameter range  $\phi \in [0, 1.2]$  for the low seasonal model where  $\eta = 0.1$ . The DLE in the chaotic area goes

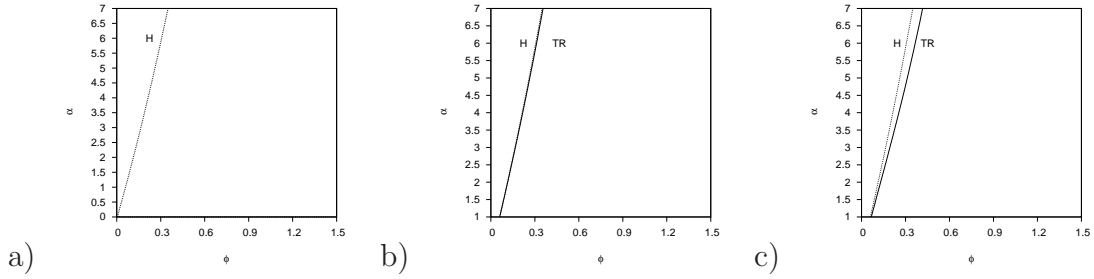


Figure 4.4: Two-dimensional parameter bifurcation diagram with the ratio of secondary infection contribution to the force of infection  $\phi$  and temporary cross-immunity rate  $\alpha$  as bifurcation parameters. In a) the Hopf bifurcation line for the non-seasonal model, i.e.  $\eta = 0$ , in b) the torus bifurcation line for the low seasonal model, i.e.  $\eta = 0.1$ , is close to the Hopf bifurcation line for the non-seasonal model ( $\eta = 0$ ) and in c) the torus bifurcation line for the high seasonal model with low import factor, i.e.  $\eta = 0.35$  and  $\rho = 10^{-10}$ , in comparison with the Hopf bifurcation line for the non-seasonal model ( $\eta = 0$ ). The other parameter values are listed in Table 4.1

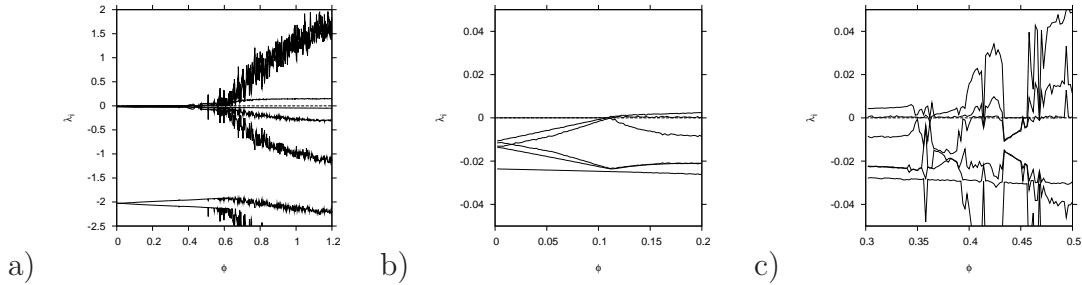


Figure 4.5: For the low seasonal system, where temporary cross-immunity rate  $\alpha = 2y^{-1}$ , the recovery rate  $\gamma = 52y^{-1}$ , the infection rate  $\beta_0 = 2 \cdot \gamma$ , the degree of seasonality  $\eta = 0.1$  and birth and death rate  $\mu = 1/65y$ , in a) the Lyapunov spectrum for the ratio of secondary infection contribution to the force of infection  $\phi \in [0, 1.2]$ , the whole parameter region of interest, in b) Lyapunov exponents for small values of the ratio of secondary infection contribution to the force of infection  $\phi \in [0, 0.2]$ , and in c) Lyapunov exponents for the ratio of secondary infection contribution to the force of infection  $\phi \in [0.3, 0.5]$ , the parameter region of onset of complexity.



up to  $\lambda = 2$  where the prediction horizon of the monthly peaks in the time series is in the range of half a year. In Figure 4.5b) the Lyapunov exponents are depicted in the parameter range  $\phi \in [0, 0.2]$ . There is a stable periodic solution which becomes unstable at a torus bifurcation. Using AUTO we calculated a torus bifurcation  $TR$  at  $\phi = 0.1145$ , slightly above the Hopf bifurcation of the non-seasonal system at ( $\phi = 0.1133$ ). Observe that the torus bifurcation  $TR$  in the seasonally forced system is close to the Hopf bifurcation for the non-seasonal system. This is reasonable since seasonal forcing adds complexity to the dynamics behavior, i.e. an equilibrium becomes a periodic solution and a limit cycle becomes a solution on a torus, whether periodic (one Lyapunov exponent zero), aperiodic (two Lyapunov exponents zero) or chaotic (one Lyapunov exponent zero and at least one positive). For higher  $\phi$  values the solution is restricted to the torus or a chaotic attractor.

In Figure 4.5c) the Lyapunov exponents are depicted in the parameter range  $\phi \in [0.3, 0.5]$  for the same low seasonal case of  $\eta = 0.1$ . There is a window in the chaotic region for  $\phi$ -values above the torus bifurcation  $TR$  around  $\phi = 0.44$  where there is a single Lyapunov exponent equal to zero, suggesting the existence of a stable limit cycle, which implies phase-locking. Continuation of this solution with  $\phi$  as free parameter reveals that this cycle, that is a period-13 cycle, possesses a tangent bifurcation at  $\phi = 0.431$  and a torus bifurcation at  $\phi = 0.471$ . These two critical points enclose the period-13 window of stable periodic solutions. For detailed analysis on the attractors in state space for the low seasonal seasonal, see Appendix 4.B.2.

### **Bifurcation analysis of the high seasonal model with import**

In the analysis of the high seasonal model ( $\eta = 0.35$ ) with low import of infected individuals ( $\rho = 10^{-10}$ ), AUTO predicted a torus bifurcation  $TR$  at  $\phi = 0.13$ . In Figure 4.6a) a little below that point the DLEs become positive, indicating chaos. The discrepancies between the continuation versus Lyapunov exponents calculation techniques happen due to long transients and consequently long sampling times in the Lyapunov exponents calculation near bifurcation points where one exponent becomes close to zero.

Another interesting range of  $\phi$  is a window in the chaotic region around  $\phi = 0.44$  where a stable limit cycle with period 12 exists. Hence in this region phase-locking occurs. With AUTO we calculated a tangent bifurcation at  $\phi = 0.406$  and a torus bifurcation at  $\phi = 0.522$ . The torus bifurcation is also predicted very well comparing the results given in Figure 4.6b), where the second zero Lyapunov exponent appears at  $\phi = 0.522$ . The position of the tangent bifurcation at  $\phi = 0.406$  is less clear from this figure obviously due to numerical inaccuracies prone to the detection of bifurcation points via integration in time instead of the calculation of the limit cycle by using a boundary value problem and the calculation of the Floquet multipliers.



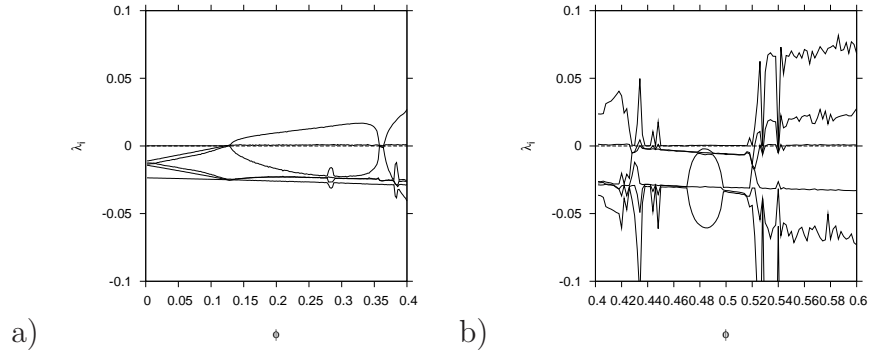


Figure 4.6: For the high seasonal system ( $\eta = 0.35$ ) with a low import of infected ( $\rho = 10^{-10}$ ), in a) Lyapunov exponents for the ratio of secondary infection contribution to the force of infection  $\phi \in [0, 0.4]$ . The second zero Lyapunov exponent is at  $\phi = 0.128$ , just before the torus bifurcation point calculated by AUTO at  $\phi = 0.13$ . In b) Lyapunov exponents for the ratio of secondary infection contribution to the force of infection  $\phi \in [0.4, 0.6]$ . In this region a tangent bifurcation at  $\phi = 0.406$  and a torus bifurcation at  $\phi = 0.522$  is predicted by AUTO.

In the limiting case where the amplitude of the seasonal forcing is zero, the torus bifurcation  $TR$  of the seasonally forced system coincides with the Hopf bifurcation  $H$  of the non-seasonal system. The larger the amplitude of the seasonal forcing  $\eta$  the higher the effects where the torus bifurcation occurs at higher  $\phi$  values. The same effect is found when adding the import factor of infected  $\rho$  into the seasonal system. For detailed analysis on the attractors in state space for the high seasonal seasonal model with import, see Appendix 4.B.3.

## 4.5 Time series

This study is completed with a time series analysis where the results are shown, leading to a discussion on its implications for data analysis. For the seasonal forcing to be inserted into system Eq. (4.1) we use Eq. (4.2) with  $\omega = 2\pi \cdot \frac{1}{T}$  and  $T = 1$  year as monitoring data of dengue suggest. For the moment we assume perfect sinusoidal forcing without any phase shift, hence  $\varphi = 0$ .

In this section, we compare the time series simulations and respective state space plots for the number of susceptible versus logarithm of the overall infected for the non-seasonal and seasonal scenarios. For a population  $N = 100$ , where the initial conditions are given by  $S = 70$ ,  $I_1 = 20$ ,  $I_2 = 10$ , and  $R_1, R_2, S_1, S_2, I_{12}, I_{21}, R = 0$ , fulfilling the condition of constant population size  $N = S + I_1 + I_2 + R_1 + R_2 + S_1 + S_2 + I_{12} + I_{21} + R$ , we discarded 5000 years of transients. The following parameters are fixed as shown in Table 4.1, temporary cross-immunity rate  $\alpha = 2y^{-1}$ , recovery rate  $\gamma = 52y^{-1}$ , infection rate  $\beta_0 = 2 \cdot \gamma$ , seasonality  $\eta = 0.35$ , import factor  $\rho = 10^{-10}$ , birth and death rate  $\mu = 1/65y$

and the ratio of secondary infection contribution to the force of infection  $\phi = 0.9$ , as initial attempt for the parameter estimation (Aguiar et al., 2011 b).

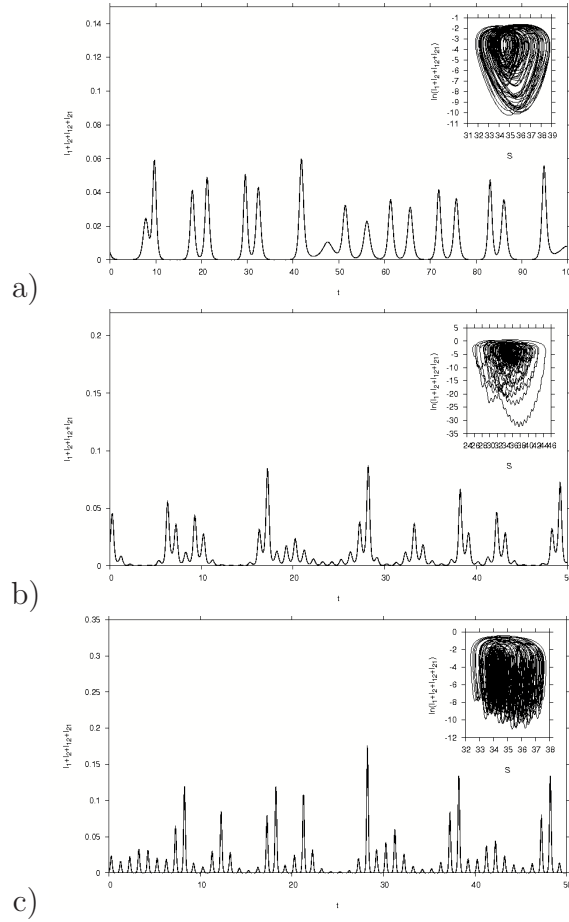


Figure 4.7: Time series simulations. In a) time series simulation for the non-seasonal model ( $\eta = 0$ ). In b) time series simulation for the low seasonal model, with seasonality  $\eta = 0.1$ . In c) time series simulation for the seasonal model with a low import of infected. Here, the degree of seasonality  $\eta = 0.35$  and the import of infected  $\rho = 10^{-10}$ . The absolute numbers on the y-axes indicate percentage of the total population.

In Fig. 4.7a) the time series simulation results for the total number of infected ( $I_1 + I_2 + I_{12} + I_{21}$ ) in the non-seasonal system ( $\eta = 0$ ), previously studied in (Aguiar et al., 2008), is shown. Besides showing an irregular pattern of outbreaks that happens every 5 years, the non-seasonal system and its time series are not able to represent dengue fever epidemiology that is characterized as a yearly cycle of incidences. By adding low seasonality ( $\eta = 0.1$ ) into the system, the epidemic outbreaks appear every year (see Fig. 4.7b)). However, between two large outbreaks there is a very low number of cases in subsequent years, which is also not data alike (see Fig. 4.9a), for example).

In Fig. 4.7c), the time series simulation in the high seasonal ( $\eta = 0.35$ ) system with a low import ( $\rho = 10^{-10}$ ) of infected contributing to the force of infection is shown. The addition of import into the seasonal system gives a much more realistic pattern of dengue fever epidemics, with irregular, yearly and smooth outbreaks. The system has a reasonable size (the number of infected stays quite away from zero), avoiding the chance of extinction in stochastic systems. Observe that very high import of infected only leads to periodic solution, whereas for import of  $\ln(\rho) \approx -18$  and below, complex behavior is observed (see Appendix 4.D, Fig. 4.16).

### 4.5.1 Lyapunov exponents and predictability:

In this section, the Lyapunov spectrum for both the non-seasonal model and the seasonal model with import are shown and compared concerning the prediction horizon of the monthly peaks in the multi-strain dengue model time series. We take as an example the DLE for  $\phi = 0.9$  in the region where the system is chaotic (positive DLE). Figure 4.8a) shows the Lyapunov spectrum for the non-seasonal system previously studied in (Aguiar et al., 2008, 2009). There are only negative exponents where the ratio of secondary infection contribution to the force of infection is in the interval  $\phi \in [0, 0.106]$  indicating a steady state point dynamic. At  $\phi = 0.108$  the DLE is zero (up to certain numerical accuracy of order  $10^{-5}$ ), indicating a periodic solution (period one or limit cycle dynamic). At  $\phi = 0.516$  the DLE becomes consistently positive, indicating chaotic behavior up to  $\phi = 0.994$ . The low noisy level of the second largest Lyapunov exponent around its theoretical value of zero, indicates that the DLE is really positive. For  $\phi$  in the interval  $\phi \in [0.994, 1.2]$  the system gets stabilized again, showing only periodic solutions (zero DLE). For the chaotic region of  $\phi = 0.9$ , the DLE = 0.04 giving approximately 25 years of prediction horizon in the monthly time series (see Fig. 4.8b)). In order to get a qualitative insight into the predictability in the monthly sampled time series, i.e. to show how the original system behaves under a small perturbation, we plot two different trajectories of the same system (for the non-seasonal model in Fig. 4.8b), and for the high seasonal model with a low import of infected in Fig. 4.8d)), where the perturbed system (black line) is compared with the original model simulation (red line). To get the trajectory of the perturbed system, we kept the last point of the transient of the original system and use those values as starting values to compute the new and perturbed trajectory. The perturbation is given by  $S_p = S + R \cdot \epsilon$  and  $R_p = R \cdot (1.0 - \epsilon)$ , where  $\epsilon = 0.001$ .

The same exercise was done for the seasonal model with low import of infected (see Fig. 4.8c) and Fig. 4.8d)). For the seasonal system with import, the zero Lyapunov exponent is visible indicating a period one dynamic from  $\phi$  between 0 to 0.122 where another slightly positive exponent appears ( $\lambda = 0.000145$ ). From  $\phi$  between 0.122 to 1.2 we have complex dynamics with torus bifurcations (2

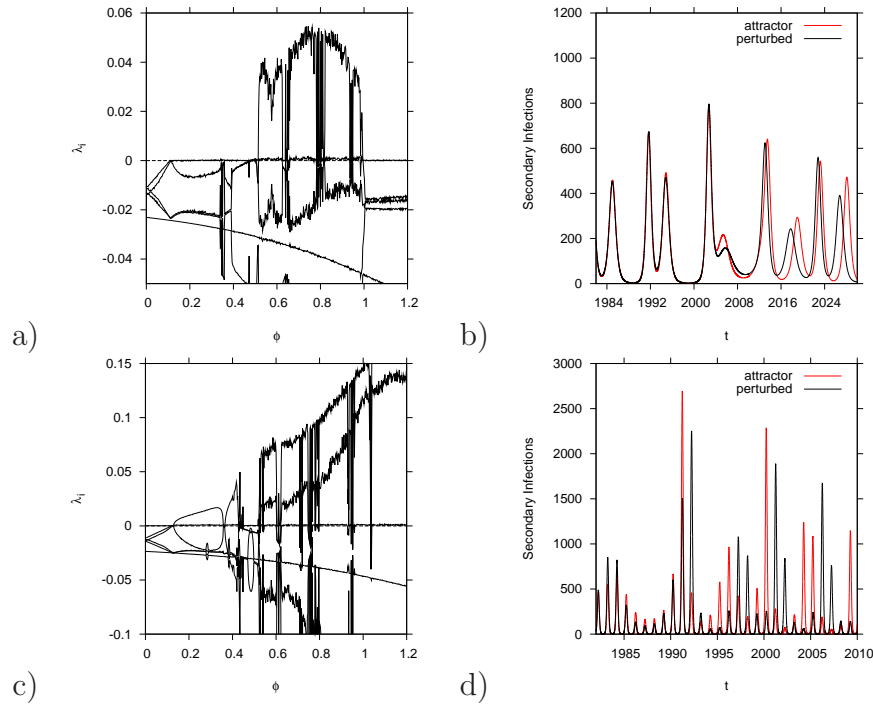


Figure 4.8: Qualitative insight into the predictability in the monthly time series. In a) we show the Lyapunov spectrum for the non-seasonally forced dengue model where the first 5 Lyapunov exponents are given. The DLE in the chaotic region of the ratio of secondary infection contribution to the force of infection  $\phi = 0.9$  is  $\lambda = 0.04$  giving  $\approx 25$  years of prediction horizon in the monthly time series. In b) the monthly time series simulation for  $\phi = 0.9$  is shown where the original trajectory (red line) is compared with the perturbed trajectory (black line). In c) we show the Lyapunov spectrum for the high seasonal model ( $\eta = 0.35$ ) with low import factor ( $\rho = 10^{-10}$ ) where the first 5 Lyapunov exponents are given. Here, the DLE in the chaotic region of the ratio of secondary infection contribution to the force of infection  $\phi = 0.9$  is  $\lambda = 0.118$  giving  $\approx 8.5$  years of prediction horizon in the monthly time series. In d) we show the monthly time series simulation for  $\phi = 0.9$  where the original trajectory (red line) is compared with the perturbed trajectory (black line). For the other parameter values used here see Table 4.1.

zero exponents) up to hyperchaos (2 positive exponents). The chaotic region of  $\phi = 0.9$ , shows the DLE= 0.118 giving approximately 8.5 years of prediction horizon in the monthly time series. It is clear that the addition of seasonal forcing into the system by itself decreases the practical predictability (see Fig. 4.5a)), however, the addition of a low import into the seasonally forced system helps to get a more complex dynamics and a better prediction horizon in the monthly time series.

### 4.5.2 Implications for data analysis:

Physicians in Thailand are trained to recognize and treat dengue fever and practically all cases of DHF and DSS are hospitalized. A system for reporting communicable diseases including DHF/DSS was considered fully installed in 1974 and the data bank of DHF and DSS is available at the Ministry of Public Health, Bangkok (Chareonsook et al., 1999). Thailand is the world's 50th largest country in terms of total area, and the 20th most-populous country, with approximately 66 million people. Thailand is divided into 75 provinces (changwat) plus the capital Bangkok which is a special administrative area. The provinces are geographically grouped into 6 regions, North, North-East, West, Central, East, and South (Wikipedia, 2011). The inspection of the available DHF incidence data in Thailand shows a smooth behavior with a well defined maximum each year of irregular height, for the North, North-East, and West Provinces (see Fig. 4.9a) for example, the DHF incidence data for Chiang Mai Province) whereas for the Central, East, and South Provinces the data is very noisy linked with a low endemicity of DHF cases. We take the Province of Chiang Mai as a case study where the empirical DHF incidence data and the time series simulation for the seasonal model with import (see Fig. 4.9b)) are compared (see Fig. 4.10).

The seasonal model with import shows complex dynamics and qualitatively a very good result when comparing empirical DHF data and simulation results (see Fig. 4.10). However, the extended model needs to be parametrized on data referring to incidence of severe disease (Aguiar et al., 2011 b). The ability to predict the future of the dengue outbreaks by analyzing the available epidemiological data via mathematical models ultimately aims to provide a tool to guide policies of prevention and control of the dengue virus transmission, including the implementation of vaccination programs when the dengue fever vaccine will be accessible.

## 4.6 Discussion and conclusions

In this manuscript a comparative study between three different scenarios (non-seasonal, low seasonal and high seasonal with a low import of infected individuals) was performed. The role of seasonality and import of infected individuals in such

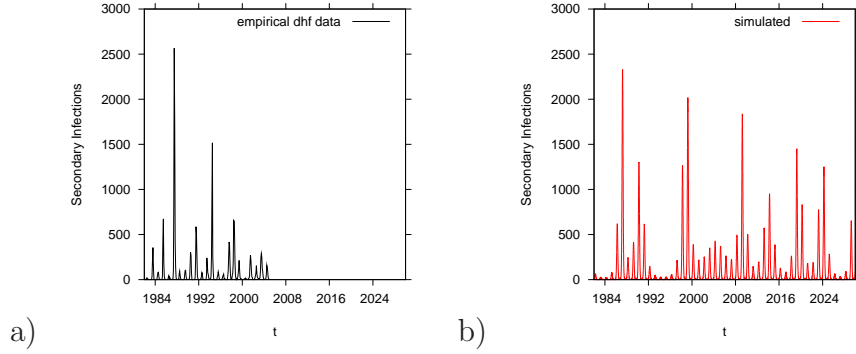


Figure 4.9: In a) we show the time series of DHF incidence in the Province of Chiang Mai in the North of Thailand. The population size is 1649457 (Chareonsook et al., 1999). In b) we show a simulation for the seasonal dengue model with import. We plot the secondary infections ( $I_{12} + I_{21}$ ) over time. The initial conditions and parameters were fixed as it follows.  $N = 1650000$ ,  $S = 1.250.000$ ,  $I_1 = 250000$ . 5000 years of transients were discarded. The temporary cross-immunity rate is  $\alpha = 2y^{-1}$ , the recovery rate  $\gamma = 52y^{-1}$ , the infection rate  $\beta_0 = 2 \cdot \gamma$ , the ratio of secondary infection contribution to the force of infection  $\phi = 0.9$ , the birth and death rate  $\mu = 1/65y$ , seasonality  $\eta = 0.35$ , the phase  $\varphi = 0$ , and the import factor  $\rho = 10^{-10}$ .

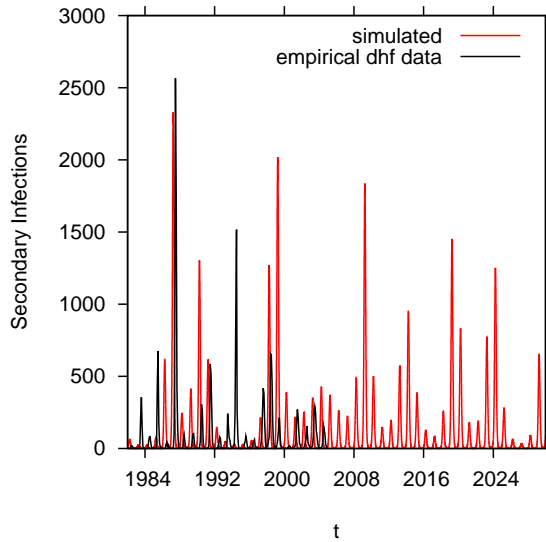


Figure 4.10: Empirical DHF incidence data are matched with the seasonal two-strain model with import simulation.

systems were considered as biologically relevant effects determining the dynamical behavior of the system.

We integrated the use of numerical bifurcation analysis and time series analysis techniques for the study of the long term dynamics of the non-autonomous system. Then the Lyapunov exponent, which is a generalization of both an eigenvalue and a Floquet multiplier being used for the stability analysis of respectively equilibria and limit cycles, were used directly for the determination of aperiodic or chaotic attractors.

Different extensions of the classical single-strain SIR model show a rich dynamic behavior. Multi-strain dynamics has previously been demonstrated to show critical fluctuations with power law distributions of disease cases, exemplified in meningitis epidemiology (Stollenwerk & Jansen, 2003 a; Stollenwerk et al., 2004). Dengue models including multi-strain interactions via ADE but without temporary cross-immunity period e.g. (Ferguson et al., 1999; Schwartz et al., 2005; Billings et al., 2007) have also shown deterministic chaos when strong infectivity on secondary infection was assumed ( $\phi \gg 1$ ). The addition of temporary cross-immunity period in such models, shows also a new deterministically chaotic attractor in an unexpected parameter region of reduced infectivity on secondary infection ( $\phi < 1$ ) (Aguiar & Stollenwerk, 2007; Aguiar et al., 2008, 2009), i.e. deterministic chaos was found in a wider parameter regions. When a low import of infected individuals is introduced into this system, the chaotic dynamics for  $\phi > 1$  disappears, whereas for the parameter region of  $\phi < 1$  the chaotic dynamics remains (see Appendix 4.C, Fig. 4.15).

In (Stone et al., 2007) the seasonally forced SIR system can show already deterministic chaos. Similarly, the introduction of seasonally forcing widens the parameter range of  $\phi$  where chaotic dynamics occurs, again also for  $\phi > 1$ . Therefore, it is clear that the addition of seasonal forcing into the system decreases the practical predictability of the dynamical system (see subsection 4.5.1). However, in order to be able to reproduce signals of a yearly cycle in dengue incidence, the addition of seasonal forcing is essential. Using the same parameter set as in (Aguiar et al., 2008) and including a seasonal forcing and a low import of infected individuals into our previous model (Aguiar et al., 2008) we get already a qualitatively very good result when comparing empirical DHF data and simulation results. Together with an import of  $\ln(\rho) \approx -18$  and below, the system shows the expected complex dynamics (see Appendix 4.D, Fig. 4.16) to explain the fluctuations observed in the available empirical data (see Fig. 4.10).

This suggests that this parameter set can be the starting set for a more detailed parameter estimation procedure. Such a technical parameter estimation is notoriously difficult for chaotic time series but temporally local approaches are possible (Ionides et al., 2006; He et al., 2010).

Being able to predict future outbreaks of dengue in the absence of human interventions is a major goal if one wants to understand the effects of control measures. Even after a dengue virus vaccine has become accessible, this holds

true for the implementation of a vaccination program. For example, to perform a vaccine trial in a year with normally low numbers of cases would make statistical tests of vaccine efficacy much more difficult than when it was performed in a year with naturally high numbers of cases. Thus predictability of the next season's height of the dengue peak on the basis of deterministic balance of infected and susceptible would be of major practical use.

## 4.A Seasonal forcing

In order to be able to use computer packages for autonomous systems such as AUTO (AUTO, 2009), the ODE equation system (4.1) can be augmented with the following two equations

$$\begin{aligned}\dot{x} &= -\omega y + c \cdot x(\eta^2 - (x^2 + y^2)) \\ \dot{y} &= \omega x + c \cdot y(\eta^2 - (x^2 + y^2))\end{aligned}\tag{4.4}$$

hence, a Hopf oscillator. The stable periodic solution of system Eq. (4.4) reads

$$x(t) = \eta \cdot \cos(\omega t) \quad , \quad y(t) = \eta \cdot \sin(\omega t)\tag{4.5}$$

and is without shift ( $\varphi = 0$ ) when choosing appropriate initial conditions ( $x(t_0) = \eta$ ,  $y(t_0) = 0$ ). This sinusoidal signal  $x(t)$  is fed into the epidemic model (system Eq. (4.1)) as

$$\beta(t) = \beta_0 \cdot (1 + x(t)) \quad .\tag{4.6}$$

The system Eq. 4.1) augmented with system Eq. (4.4) is  $\mathbb{Z}_2$ -symmetric just as the original non-seasonal and seasonal system.

The constant  $c > 0$  in the Hopf oscillator does not influence the solution  $(x(t), y(t))$  in stationarity, but only the convergence toward it, hence controls the stability of the Hopf oscillation and leaves the system Eq. (4.1) unchanged. The Hopf oscillator can be solved explicitly in polar coordinates, hence  $x = r \cdot \cos(\vartheta)$  and  $y = r \cdot \sin(\vartheta)$ , or inverted  $r = \sqrt{x^2 + y^2}$  and  $\vartheta = \arctan(y/x)$ .

The ODE system is in polar coordinates given by

$$\dot{r} = c \cdot r(\eta^2 - r^2)\tag{4.7}$$

$$\dot{\vartheta} = \omega\tag{4.8}$$

and solutions are

$$r(t) = \eta \left( 1 - \left( 1 - \frac{\eta^2}{r_0^2} \right) e^{-2\eta^2 c(t-t_0)} \right)^{-\frac{1}{2}}\tag{4.9}$$

$$\vartheta(t) = \vartheta_0 + \omega(t - t_0) \quad .\tag{4.10}$$



From this we can get the solution in Cartesian coordinates

$$\tilde{x}(t) = \eta \cdot \cos(\vartheta(t)) \quad \tilde{y}(t) = \eta \cdot \sin(\vartheta(t)) \quad (4.11)$$

with  $0 \leq t \leq T$  where  $T = 2\pi$ . This periodic solution is stable because we have  $\lim_{t \rightarrow \infty} r(t) = \eta$ , independent of  $r_0 > 0$ .

In AUTO (AUTO, 2009) the stability of the periodic solution  $\tilde{x}(t), \tilde{y}(t)$ ,  $0 \leq t \leq T$ , may be analyzed within the framework of Floquet theory by calculation of the multipliers, the eigenvalues of the so called monodromy matrix. For a detailed discussion the interested reader is referred to (Kuznetsov, 2004). We continue with the analysis of the so called Poincaré map. Since the system is periodically forced this map is also called a stroboscopic map. The analytical expression reads

$$r_{n+1} = \eta \left( 1 - \left( 1 - \frac{\eta^2}{r_n^2} \right) e^{-4\pi\eta^2 c} \right)^{-\frac{1}{2}} \quad (4.12)$$

where  $n \in \mathbb{N}$  and initially for  $n = 0$  we have  $r_0 > 0$ . Asymptotically we get for large  $n$ :  $r_n \approx \eta$  and therefore the multiplier equals the derivative evaluated at  $r = \eta$

$$\lambda = \eta e^{-4\pi\eta^2 c} \quad (4.13)$$

This single multiplier is less than 1 and therefore the periodic solution is stable.

Since this Hopf-system is decoupled from the system (4.1)

and therefore the Lyapunov exponents of the augmented system are those of the original system (4.1) together with zero (Haken, 1983) and expression (4.13). For the Lyapunov spectrum of the seasonal dengue models with parameter  $\phi$  between  $\phi = 0$  and  $\phi = 1.2$ , we plot the first 6 exponents coupled with the Hopf oscillator where the parameters are  $\eta = 0.1$ ,  $\omega = 2 \cdot \pi$  and contraction rate  $c = 5000$ , hence from the Hopf oscillator the Lyapunov exponent are  $\lambda_1 = -2c\eta^2 = -100$  and  $\lambda_2 = 0$ .

## 4.B Attractors in state space

In this section we show the transitions between different attractors in state space plot for the three studied scenarios, the non-seasonal model (see 4.B.1), the low seasonal model (see Appendix 4.B.2) and the seasonal model with import of infected (see Appendix 4.B.3). The parameters are given in Table 4.1. We plot the susceptibles  $S$  over the logarithm of total number of infected  $\ln(I_1 + I_2 + I_{12} + I_{21})$ .

### 4.B.1 Attractors in state space for the non-seasonal multi-strain dengue model

Figures 4.11 and 4.12 show the attractors in state space plot for the non-seasonal model.

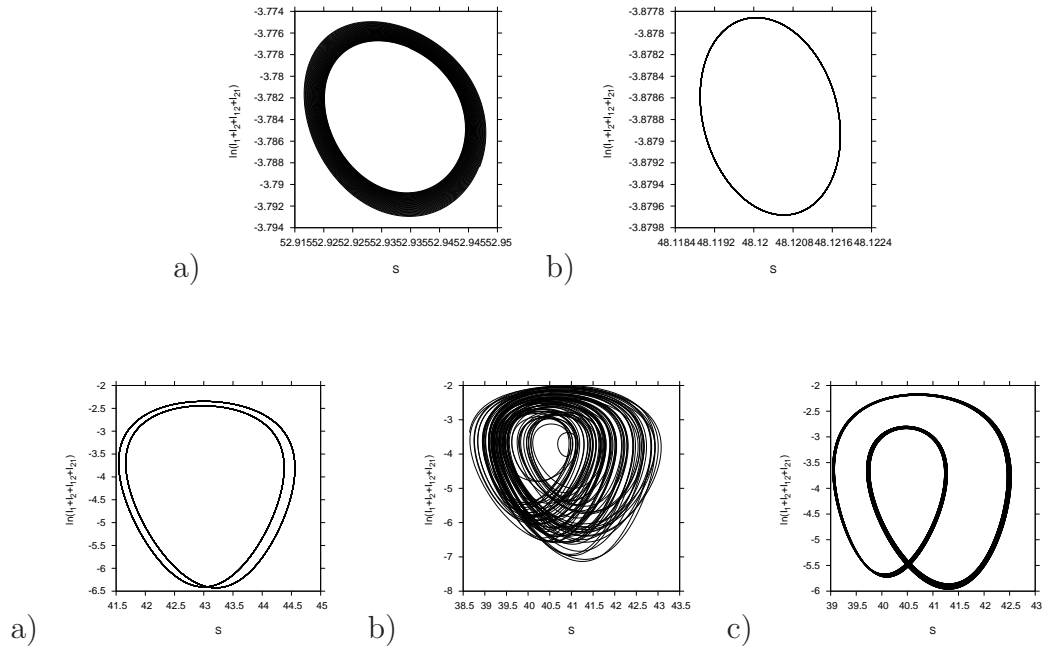


Figure 4.11: In a) the state space plot for  $\phi = 0.1133$ , the Hopf bifurcation point calculated by AUTO. 2000 years of transients were discarded, insufficient to obtain the expected simple limit cycle. In b) the attractor for  $\phi = 0.1133$ . It is really a limit cycle after discarding a sufficiently long transient of 40000 years. In c) the attractor for  $\phi = 0.4115$  with 2000 years of transients discarded, the pitchfork bifurcation point calculated by AUTO. In d) a chaotic attractor, and in e) a torus attractor both found for  $\phi = 0.5507$ . Those attractors were stable for very long transients of 10000 years suggesting a coexistence of attractors.

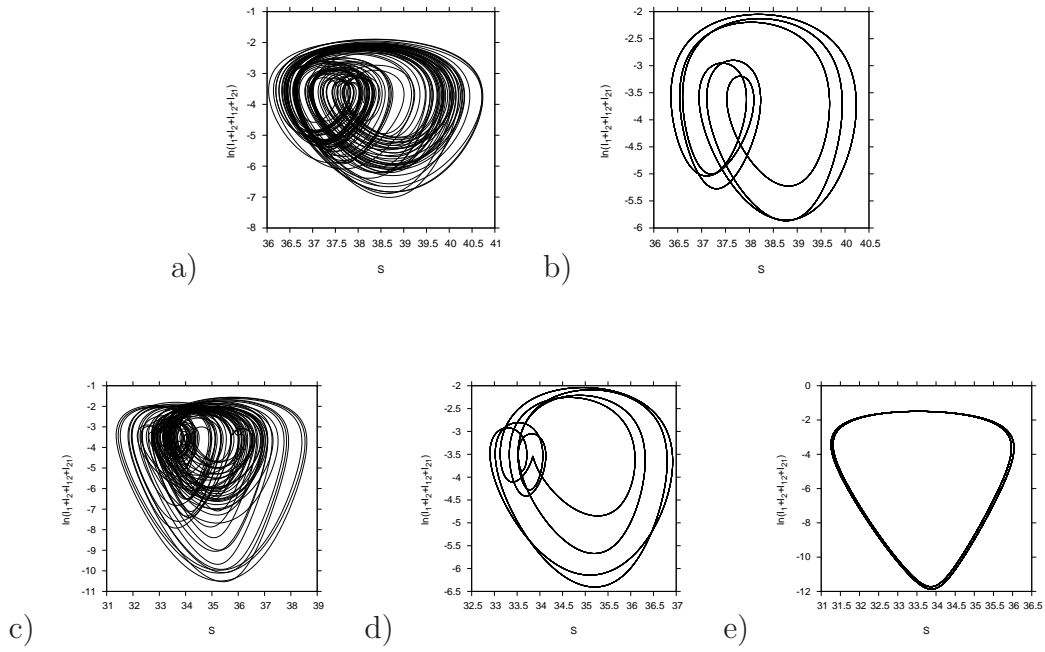


Figure 4.12: In a) the chaotic attractor from the main bifurcation branch, and in b) a coexisting attractor for in the isola region, both when  $\phi = 0.71$ . The coexistence of attractors was found when changing the initial conditions. In c) the chaotic attractor, in d) the coexisting attractor at  $\phi = 0.934$ . The coexistence of attractors was found when changing the initial conditions. In e) attractor with two limit cycles coexisting in  $\phi = 0.9921$ , the pitchfork bifurcation point calculated by AUTO.

## 4.B.2 Attractors in state space for the low seasonal multi-strain dengue model

Figure 4.13 shows the attractors in state space plot for the low seasonal model.

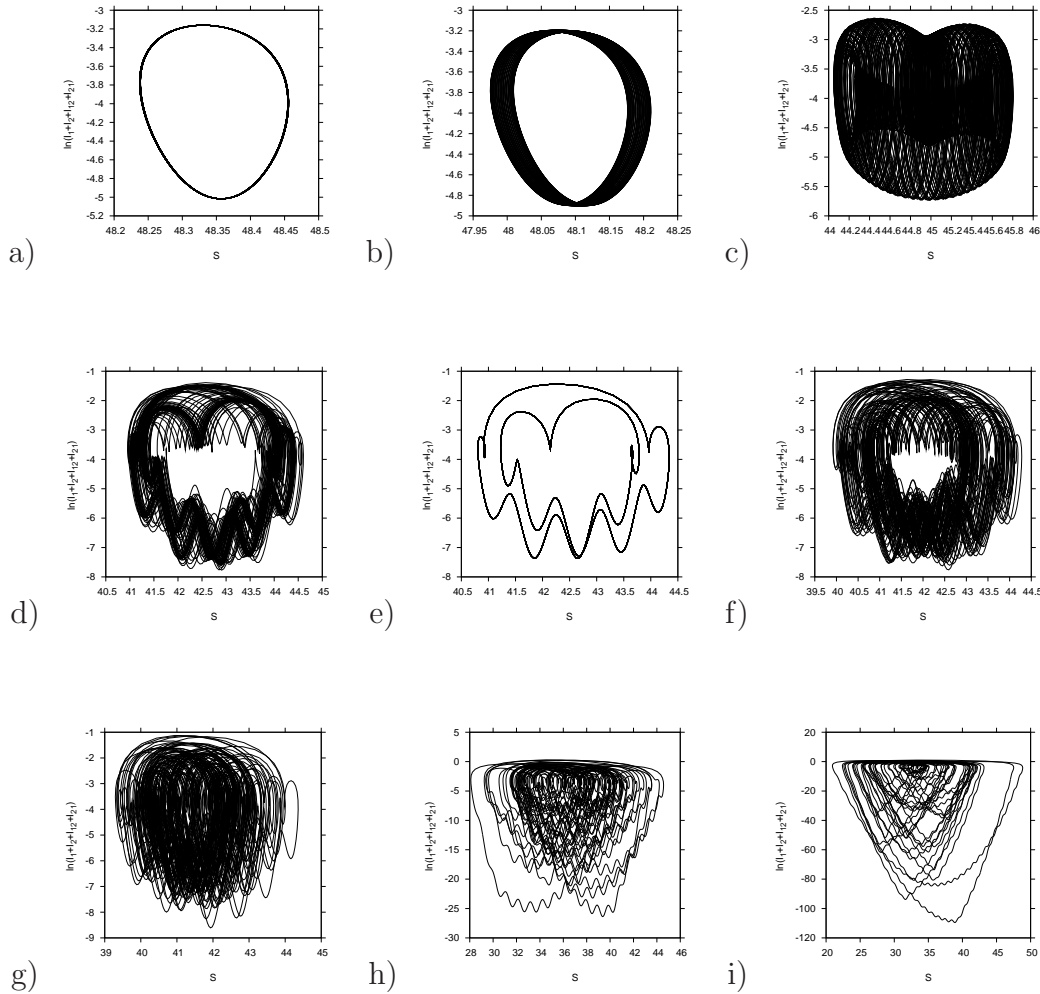


Figure 4.13: Attractors in state space plot for the low seasonal model. In a) the period one attractor for  $\phi = 0.1$ , in b) the torus attractor for  $\phi = 0.114535$ , the torus bifurcation point calculated by AUTO. In c) the torus attractor for  $\phi = 0.3$ . In d) the attractor for  $\phi = 0.431$ , in e) the period 13 attractor for  $\phi = 0.44$  and in f) the torus attractor for  $\phi = 0.471$ . In g) the chaotic attractor for  $\phi = 0.5$ , in h) the chaotic attractor for  $\phi = 0.8$  and in i) the chaotic attractor for  $\phi = 1$ .

### 4.B.3 Attractors in state space for the seasonal multi-strain dengue model with import of infected

Figure 4.14 shows the attractors in state space plot for the the seasonal model with import of infected.

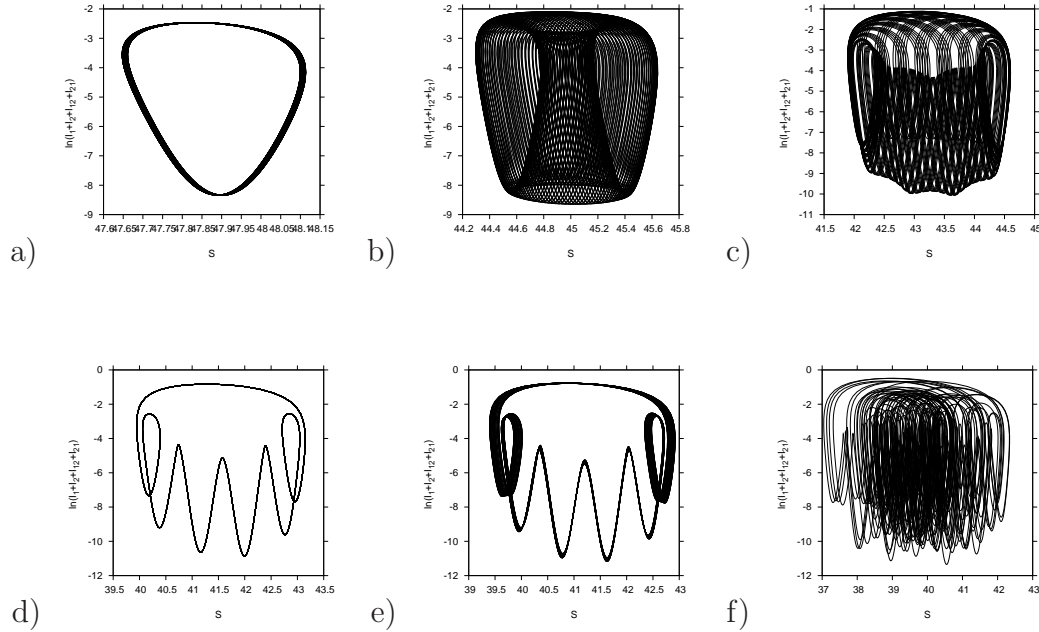


Figure 4.14: Attractors in state space plot for the the seasonal model with import of infected. In a) the torus attractor for  $\phi = 0.13$ , the torus bifurcation point calculated by AUTO. In b) and in c) the torus attractor for  $\phi = 0.3$  and  $\phi = 0.4$  respectively. For those  $\phi$  values, the Lyapunov spectrum shows a slightly positive exponent indicating chaos in the torus. In d) the attractor for  $\phi = 0.5$ , in e) torus attractor for  $\phi = 0.522165$ , the torus bifurcation calculated by AUTO, and in f) the chaotic attractor found in the region of  $\phi$  between 0.5 to 1. Here for  $\phi = 0.6$ .

## 4.C The non-seasonal model with import factor versus the low seasonal model with import factor

In this section we show the bifurcation diagram comparison between the original non-seasonal model Aguiar et al. (2008), the non-seasonal model with import and the low seasonal model with import. The addition of a low import factor into the original non-seasonal system gives a stable limit cycle as the unique attractor (see Fig. 4.15b)), in contrast with the results for the original non-seasonal models analyzed in (Ferguson et al., 1999; Aguiar et al., 2008, 2009), where two chaotic windows were found (see Fig. 4.15a)) just by assuming temporary cross-immunity period between recurrent dengue infections. Adding low seasonality to this system brings the chaotic attractors back for even larger parameter regions (see Fig. 4.15c)). These results are important since we expect complex dynamics to explain the fluctuations observed in empirical data, when the ratio of secondary infection contribution to the force of infection could be slightly smaller or larger 1, not needing to restrict the ADE effect to one or another region in parameter space.

## 4.D Lyapunov exponents and import factor

In this section we extend the analysis of the seasonal model with import of infected by presenting a bifurcation analysis where the import parameter  $\rho$  is varying. The Lyapunov spectrum together with the bifurcation diagram confirm the importance of adding import into the dynamical model. An import factor  $\ln(\rho) = -18$  or less leads to complex behavior while with a very high import factor of infected periodic solutions are observed (see Fig. 4.16). The understanding of such complex scenario opens possibilities to analyze the available data.

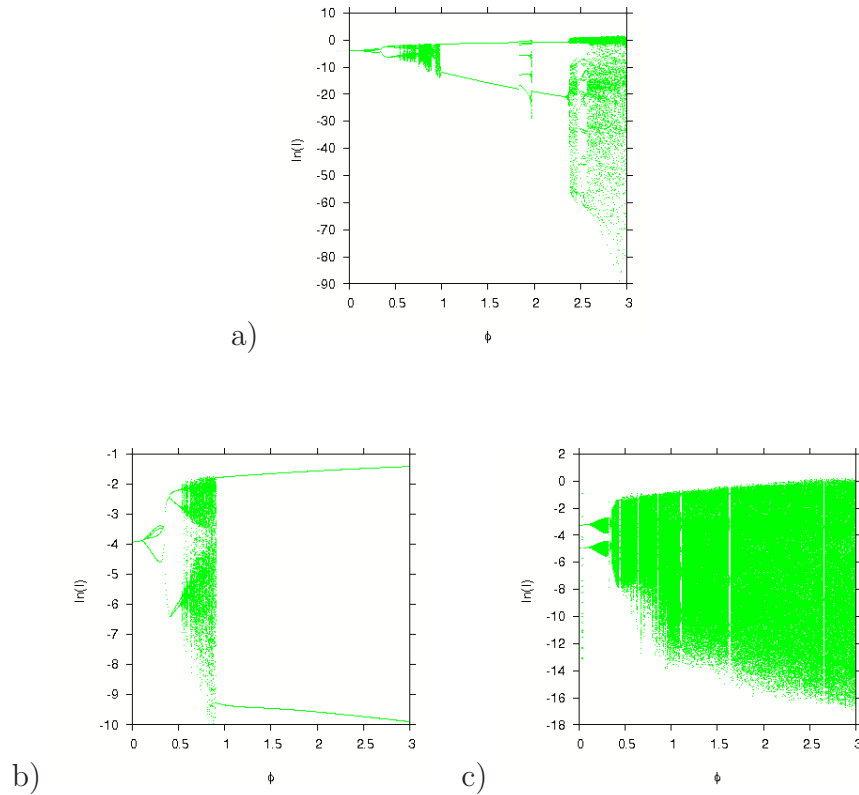


Figure 4.15: Bifurcation diagram comparison between the non-seasonal model, the non-seasonal model with import and the low seasonal model with import. In a) we show the bifurcation diagram for the original non-seasonal model previously studied in (Aguiar & Stollenwerk, 2007; Aguiar et al., 2008, 2009), where two chaotic windows were found. A new chaotic window in a  $\phi$  region where the ratio of secondary infection contribution to the force of infection is smaller than 1 and also the classical chaotic window found previously in (Ferguson et al., 1999; Aguiar et al., 2008), where the ratio of secondary infection contribution to the force of infection is much larger than 1, actually  $\approx 3$ . In b) we show the bifurcation diagram for the non-seasonal model described in (Aguiar et al., 2008) with addition of a low import of infected. Here we see that the import removes the complex dynamics in the region of  $\phi$  larger 1 where the stable limit cycle (crossing the right boundary of Fig. 4.2b) is the unique attractor. In c) we show the bifurcation diagram for the extended multi-strain model, the low seasonal ( $\eta = 0.1$ ) model with import ( $\rho = 10^{-10}$ ), where the chaotic attractors are back for even larger parameter regions.

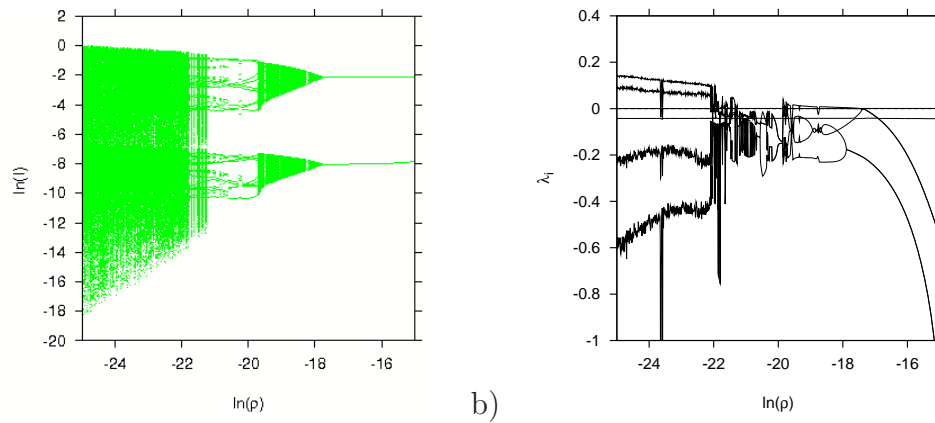


Figure 4.16: Bifurcation diagram for the import parameter and its Lyapunov spectrum. Here we vary the import factor  $\rho$  (in log scale). The other parameters are fixed as it follows: temporary cross-immunity  $\alpha = 2y^{-1}$ , recovery rate  $\gamma = 52y^{-1}$ , secondary infection contribution to the force of infection  $\phi = 0.9$ , the infection rate  $\beta_0 = 2 \cdot \gamma$ , degree of seasonality  $\eta = 0.35$ , and birth and death rate  $\mu = 1/65y$ .





# Chapter 5

## Scaling of stochasticity in dengue hemorrhagic fever epidemics

Maíra Aguiar, Bob W. Kooi and Nico Stollenwerk (2011)  
*Submitted.*

In this paper we analyze the stochastic version of a minimalistic multi-strain model, which captures essential differences between primary and secondary infections in dengue fever epidemiology, and investigate the interplay between stochasticity, seasonality and import. The introduction of stochasticity is needed to explain the fluctuations observed in some of the available data sets, revealing a scenario where noise and complex deterministic skeleton strongly interact. For large enough population size, the stochastic system can be well described by the deterministic skeleton gaining insight on the relevant parameter values purely on topological information of the dynamics, rather than classical parameter estimation of which application is in general restricted to fairly simple dynamical scenarios.

### 5.1 Introduction

Recently, we have investigated an epidemic multi-strain model motivated by dengue fever epidemiology, which shows deterministic chaos in wide parameter regions (Aguiar et al., 2008, 2009). The addition of seasonal forcing, mimicking the vectorial dynamics, and a low import of infected individuals, which is realistic in the dynamics of infectious diseases epidemics, showed complex dynamics and qualitatively a good agreement between empirical DHF monitoring data and the obtained model simulation (Aguiar et al., 2011 a).

Classical examples of chaos in epidemiological models are childhood diseases with extremely high infection rates so that a moderate seasonal forcing can gen-

erate Feigenbaum sequences of period doubling bifurcations into chaos. In other infectious diseases, much lower forces of infection have to be considered leading to further conceptual problems with noise affecting the system more than the deterministic part, leading even to critical fluctuations with power law behavior, when considering evolutionary processes of harmless strains of pathogens versus occasional accidents of pathogenic mutants (Stollenwerk & Jansen, 2003 b). Only explicitly stochastic models, of which the classical ODE models are mean field versions, can capture the fluctuations observed in time series data (Stollenwerk et al., 2004).

In this paper, we investigate the role of dynamic noise in understanding epidemiological systems, such as dengue fever, by deriving a stochastic version of ordinary differential equations from Markov processes for discrete populations. Our model has the minimal degree of complexity to generate both primary and secondary dengue infections. The introduction of stochasticity is needed to explain the fluctuations observed in some of the available data sets, revealing a scenario where noise and complex deterministic skeleton strongly interact. For large enough population size, the stochastic system gives rise to the observed time series incidences. The classical parameter estimation and its application are generally restricted to fairly simple dynamical scenarios and therefore a qualitative analysis of epidemiological data would have good chances to give insights into the relevant parameter values purely on topological information of the dynamics.

## 5.2 Modeling dengue fever epidemiology

According to the estimates giving by (CDC, 2011), dengue infection is a leading cause of illness and death in the tropics and subtropics. More than one-third of the world's population are living in areas at risk of acquiring dengue infection and it is estimated that every year, there are 70 – 500 million dengue infections, generating 36 million cases of dengue fever (DF) and 2.1 million cases of dengue hemorrhagic fever (DHF) that without proper medical care the fatality rates can exceed 20% (PDVI, 2011; WHO, 2009). There are four antigenically distinct but closely related dengue viruses, belonging to the family Flaviviridae, designated by DEN-1, DEN-2, DEN-3, and DEN-4. Infection by one serotype confers life-long immunity to only that serotype and a short period of temporary cross-immunity to a subsequent infection with other serotypes (Halstead, 1994; Matheus et al., 2005; WHO, 2009). Field researchers in dengue have found that severe disease is 15 – 80 times more likely in secondary than in primary infections and was positively associated with antibody-dependent enhancement (ADE) of infection of mononuclear phagocytes. Infection by an antibody-virus complex suppresses innate immune responses, increasing intracellular infection and generating inflammatory cytokines and chemokines that, collectively, result in enhanced disease (Halstead, 1982, 1994, 2003; Mackenzie et al., 2004; WHO, 2009; Dejnirattisai et

al., 2010; Guzmán et al., 2010). Treatment of uncomplicated dengue cases is only supportive, and severe dengue cases require hospitalization and careful attention to fluid management and proactive treatment of hemorrhagic symptoms (CDC, 2011; WHO, 2009). At present, there is no vaccine for dengue viruses, although several candidates are at various stages of development.

Dengue epidemiology dynamics is well known to be particularly complex with large fluctuations of disease incidences. Mathematical models describing the transmission of dengue viruses have focused on the ADE effect and temporary cross-immunity trying to explain the irregular behavior of dengue epidemics. Besides the fact that disease propagation is an inherently stochastic phenomenon, dengue models are mainly expressed mathematically as a set of deterministic differential equations which are easier to analyze. The mean field approximation is a good approximation to be used in order to understand better the behavior of the stochastic systems in certain parameter regions, where the dynamics of the mean quantities are approximated by neglecting correlations. However, it is only stochastic, as opposed to deterministic, models that can capture the fluctuations observed in some of the available time series data.

### 5.3 The stochastic model

The various multi-strain models currently investigated are essentially of SIR-type. In the simple SIR epidemics without strain structure of the pathogens we have the following reaction scheme for the possible transitions from one to another disease related state, susceptibles  $S$ , infected  $I$  and recovered  $R$ ,



for a host population of  $N$  individuals, with contact and infection rate  $\beta$ , recovery rate  $\gamma$  and temporary immunity rate  $\alpha$ . The deterministic ODE model

$$\begin{aligned} \dot{S} &= \alpha R - \frac{\beta}{N} \cdot I \cdot S \\ \dot{I} &= \frac{\beta}{N} \cdot I \cdot S - \gamma I \\ \dot{R} &= \gamma I - \alpha R \end{aligned} \tag{5.2}$$

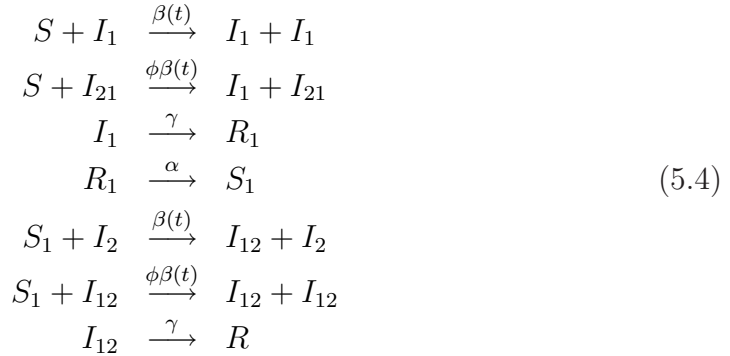
describes in mean field approximation  $\langle S \cdot I \rangle \approx \langle S \rangle \cdot \langle I \rangle$  the dynamics of the mean values, e.g.  $\langle I \rangle := \sum_{S=0}^N \sum_{I=0}^N I p(S, I, t)$ , where the initial values determine the time course of the system for all times. For more details on the calculations see e.g. (Stollenwerk & Jansen, 2011).

For the SIR model, the dynamics of probabilities in the form of a master equation (van Kampen, 1992) reads

$$\begin{aligned}
\frac{dp(S, I, t)}{dt} &= \frac{\beta}{N}(S+1)(I-1) p(S+1, I-1, t) \\
&+ \gamma(I+1) p(S, I+1, t) \\
&+ \alpha(N - (S-1) - I) p(S-1, I, t) \\
&- \left( \frac{\beta}{N}SI + \gamma I + \alpha(N - S - I) \right) p(S, I, t) .
\end{aligned} \tag{5.3}$$

This process can be simulated by e.g. the Gillespie algorithm (Gillespie, 1976, 1978) giving stochastic realizations. Only few stochastic processes can be solved explicitly, however, the mean field approximation is a good approximation to be used in order to understand the behavior of the stochastic systems in certain parameter regions.

Multi-strain dynamics are generally modeled with more extended with SIR-type models, dividing the host population into susceptible, infected and recovered individuals with subscripts for the respective strains. The stochastic version of the multi-strain dengue model is now in complete analogy to the previously described SIR model, and the mean field ODE system for the multi-strain dengue model can be read from the following reaction scheme



describing the transitions for first infection with strain 1 and secondary infection with strain 2. For the reverse process, where the first infection is caused by strain 2 and the secondary infection is caused by strain 1, the same reaction scheme can be used to describe the transitions by just changing labels. The demographic transitions are  $S, I_1, I_2, R_1, R_2, S_1, S_2, I_{12}, I_{21}, R \xrightarrow{\mu} S$  defining the system of two strains completely (for more information on the deterministic ODE system and its parametrization, see (Aguiar et al., 2008, 2011 a)). The parameter  $\beta$  takes the seasonal forcing into account as a cosine function,  $\beta(t) = \beta_0(1 + \eta \cos(\omega t))$ , where  $\beta_0$  is the basic infection rate and  $\eta$  is the degree of seasonality. The parameter  $\gamma$  is the recovery rate,  $\alpha$  is the temporary cross-immunity rate and  $\phi$  is the ratio

of secondary infection contribution to the force of infection. A low import factor is also included ( $S \xrightarrow{\rho} I$ ) where  $S$  can be any susceptible like  $S, S_1$  or  $S_2$  and  $I$  respectively  $I_1, I_2, I_{12}$  or  $I_{21}$ . In the simple SIR system, system Eq. (5.2), this gives  $\dot{S} = \alpha R - \frac{\beta}{N}S(I + \rho N)$  etc.

We assume no epidemiological asymmetry between strains, i.e. infections with strain one followed by strain two or vice versa contribute in the same way to the force of infection. Here, the only relevant difference concerning disease transmissibility is that the force of infection varies accordingly to the number of previous infections the hosts have experienced. In a primary infection the individuals transmit the disease with a force of infection  $\frac{\beta I}{N}$  whereas in a secondary infection the transmission is given with a force of infection  $\frac{\phi \beta I}{N}$  where  $\phi$  can be larger or smaller than unit, i.e. increasing or decreasing the transmission rate. For the stochastic simulations the parameter values are given in Table 5.1, if not otherwise explicitly stated.

Table 5.1: Parameter set, rates given in units per year, ratio without unit

Par.	Description	Values	Ref
$\mu$	new born susceptible rate	$1/65y$	(UNWPP, 2011)
$\gamma$	recovery rate	$52y^{-1}$	(WHO, 2009)
$\beta_0$	infection rate	$\in [\gamma, 2\gamma]$	(Ferguson et al., 1999)
$\alpha$	temporary cross-immunity rate	$2y^{-1}$	(Matheus et al., 2005)
$\phi$	ratio of contrib. to force of inf.	0.9	(Aguiar et al., 2011 a)
$\eta$	degree of seasonality	$\in [0, 0.2]$	(Aguiar et al., 2011 a)
$\ln(\rho)$	import factor	$\in [-17, -15.5]$	(Aguiar et al., 2011 a)

The first recorded epidemic of DHF in Thailand (population of approximately 66 million people (Wikipedia, 2011)) was in 1958 (WHO, 2009). The co-circulation of all four dengue serotypes and their capacity to produce severe dengue disease was demonstrated as early as 1960 in Bangkok, Thailand (Halstead et al., 1969). DHF occurred first only in Bangkok, but was disseminated to the whole region during the 1970s (Gubler, 2002; Halstead et al., 1969; Chareonsook et al., 1999). Physicians in Thailand are trained to recognize and treat dengue fever and practically all cases of DHF and DSS are hospitalized. A system for reporting communicable diseases including DHF/DSS was considered fully installed in 1974 and the data bank of DHF and DSS is available at the Ministry of Public Health, Bangkok (Chareonsook et al., 1999).

The inspection of the available DHF incidence data in Thailand shows a smooth behavior with a well defined maximum each year of irregular height for the Northern Provinces as opposed to the Central and Southern Provinces where the data is very noisy linked with a low endemicity of DHF cases. In (Aguiar et

al., 2011 a) the Province of Chiang Mai was taken as a case study and the empirical DHF incidence data was compared with the time series simulation obtained from the seasonal multi-strain model with import giving qualitatively a very good result, suggesting that the used parameter set could be the starting set for a more detailed parameter estimation procedure. However, in order to describe the noisy dynamics in Bangkok for example the introduction of stochasticity is even more important.

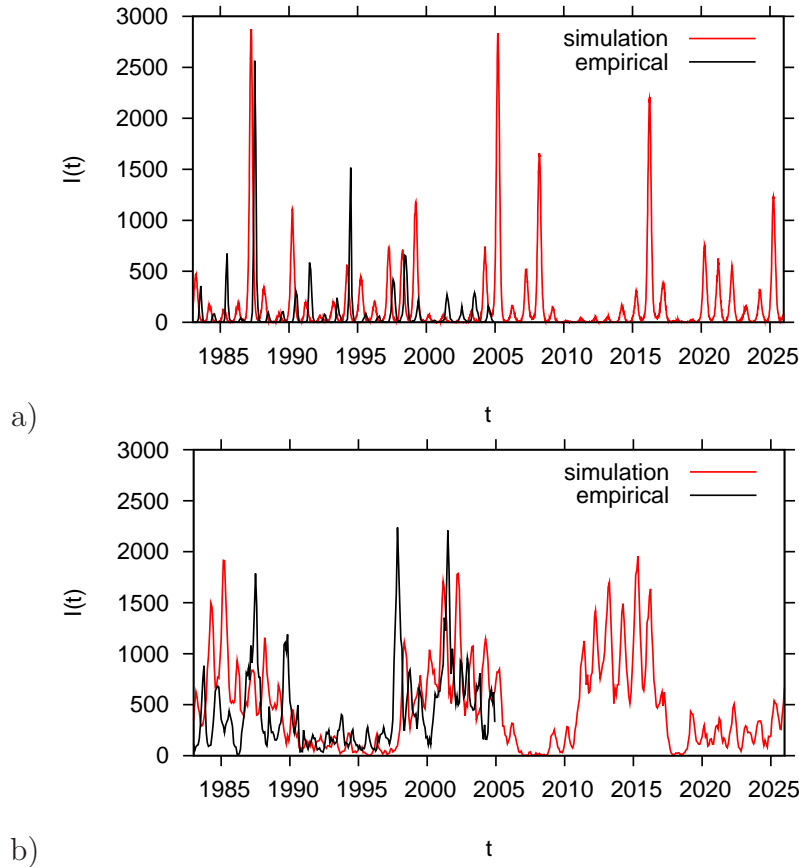


Figure 5.1: Empirical DHF incidence data (in black) matched with one stochastic realization (in red) for the seasonal multi-strain dengue model with import. In a) we show the incidences for Chaing Mai. For the stochastic simulation the infection rate is  $\beta_0 = 2\gamma$ , the degree of seasonality  $\eta = 0.2$  and the import  $\ln(\rho) = -15.7$ . In b) we show the incidences for Bangkok. For the stochastic simulation the infection rate is  $\beta_0 = 1.1 \cdot \gamma$ , the degree of seasonality  $\eta = 0.06$  and the import  $\ln(\rho) = -16.9$ . The other parameter values are listed in Table 5.1

In Fig. 5.1a) we show the DHF incidences for Chaing Mai (in black), one of the Northern Provinces of Thailand, with population size  $N = 1650000$  (UNWPP, 2011) compared with one stochastic realization for the multi-strain dengue model (in red) where the infection rate  $\beta_0 = 2\gamma$ , the degree of seasonality  $\eta = 0.2$  and the

import  $\ln(\rho) = -15.7$ . In Fig. 5.1b) the DHF incidences for Bangkok (in black), the capital of Thailand, with population size  $N = 6600000$  (UNWPP, 2011) is compared with one stochastic realization for the multi-strain dengue model (in red) where the infection rate  $\beta_0 = 1.1$ , the degree of seasonality  $\eta = 0.06$  and the import  $\ln(\rho) = -16.9$ . The stochastic approach is able to describe both types of the dynamics, the smooth data with a well defined maximum each year of irregular height, found in the high endemic regions of Thailand, e.g. in the Chiang Mai Province (see Fig. 5.1a)) and also the noisy data found mainly in low endemic regions of Thailand, e.g. in Bangkok (see Fig. 5.1b)).

Using the same values for the biological parameters given in (Aguiar et al., 2008, 2011 a), the fluctuations observed in the empirical data were qualitatively well described in the stochastic model. Under population noise low seasonal forcing was needed to represent the DHF incidences in the Province of Chiang Mai as opposed to the deterministic approach where the combination seasonality and import showed complex dynamics. For the representation of the DHF incidences in Bangkok, only the stochastic model could capture the noisy behavior where even lower seasonal forcing was needed as well a low infection rate. A value of  $\beta_0 = 1.1 \cdot \gamma$  is qualitatively in good agreement with the data (see Fig. 5.1b)) and hence the import factor  $\rho$  is here, more than the direct infectivity  $\beta$ , the driving force of the epidemic pattern in such a low endemic region.

## 5.4 The role of import

In our model, the parameter  $\rho$  is the import factor, related with the possibility of an individual to get infected outside the studied population and then bring the infection into the population that this individual belongs to, mimicking the imported cases of the disease in a defined population. Equivalently an infected visitor to the region under consideration who passes the infection to a susceptible in the population of size  $N$  has the same effect on the studied population. Hence, we do not need to distinguish this two scenarios of susceptibles traveling outside or infected traveling inside the region under consideration. In total, this captures the imported infection that comes from an external source.

In Figure 5.2 we present the bifurcation diagram comparison between the non-seasonal model, the non-seasonal model with import and the seasonal model with import. The bifurcation diagram for the original non-seasonal model previously studied in (Aguiar & Stollenwerk, 2007; Aguilar et al., 2008, 2009), shows two chaotic windows, a new chaotic window in a  $\phi$  region where the ratio of secondary infection contribution to the force of infection is smaller than 1 and also the classical chaotic window found previously in (Ferguson et al., 1999; Aguilar et al., 2008), where the ratio of secondary infection contribution to the force of infection is much larger than 1, actually around  $\phi = 3$  (see Fig. 5.2a)). The bifurcation diagram for the non-seasonal model described in (Aguilar et al., 2008)



with addition of a low import of infected shows that the addition of import in such a system removes the complex dynamics in the region of  $\phi$  larger 1 where the stable limit cycle is the unique attractor (see Fig. 5.2b)). The bifurcation diagram for the seasonal model with import described in (Aguiar et al., 2011 a), shows that the combination of seasonality and import brings back the chaotic attractors for even larger parameter regions (see Fig. 5.2b)).

These results are important since we expect complex dynamics to explain the fluctuations observed in empirical data, when the ratio of secondary infection contribution to the force of infection could be slightly smaller or larger 1, not needing to restrict the ADE effect to one or another region in parameter space.

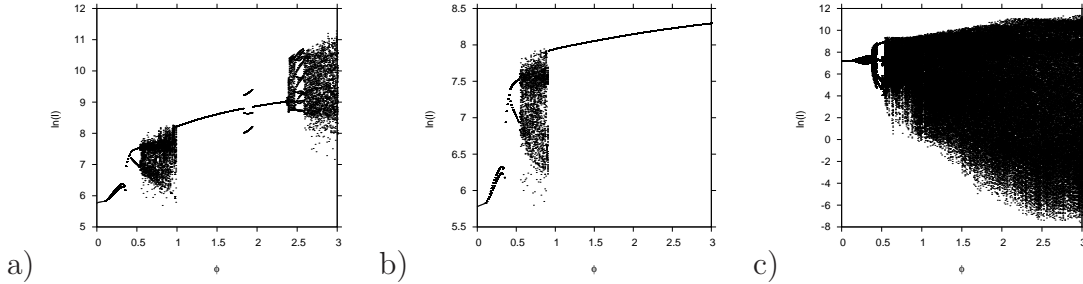


Figure 5.2: Bifurcation diagram comparison between the non-seasonal model, the non-seasonal model with import and the seasonal model with import. Here, the local maxima of the logarithm of the total number of infected  $\ln(I) = \ln(I_1 + I_2 + I_{12} + I_{21})$  are plotted against the ratio of the contribution of the secondary infections  $\phi$  to the force of infection. In a) we show the bifurcation diagram for the original non-seasonal model previously studied in (Aguiar et al., 2008, 2009), in b) we show the bifurcation diagram for the non-seasonal model described in (Aguiar et al., 2008) with addition of a low import of infected and in c) we show the bifurcation diagram for the seasonal model with import described in (Aguiar et al., 2011 a).

In the multi-strain dengue model the susceptible individuals without a previous dengue infection can get infected with two different infection rates, due to the ADE effect leading to severe disease requiring hospitalization. Individuals in the first infection would then transmit more than individuals in the secondary infection. For more information on the parametrization of the two-strain dengue model, see (Aguiar et al., 2008, 2011 a). Individuals infected for the first time become recovered and life long immune to that strain and, after a period of temporary cross-immunity, are again susceptible, however with an experienced previous infection. The second infection can only happen with a different strain. Individuals infected for the second time would more likely need to be hospitalized due to the severity of the disease. They recover and then become life long immune to the other strain. There is no epidemiological asymmetry between strains, i.e. infections with strain one followed by strain two or vice versa con-

tribute in the same way to the force of infection, so the notion of two different strains is enough to describe differences between primary infections, often asymptomatic, and secondary infection, associated with the severe form of the disease. The death rates coming out of all classes go into the class of susceptible without experiencing previous dengue infection as a birth rate. Since the demographic events often occur at a much slower rate than the infection, the disease has to be necessarily maintained by constant external infections to avoid the repeated stochastic disease extinction and re-introduction (Alonso et al., 2006; Keeling & Ross, 2008)).

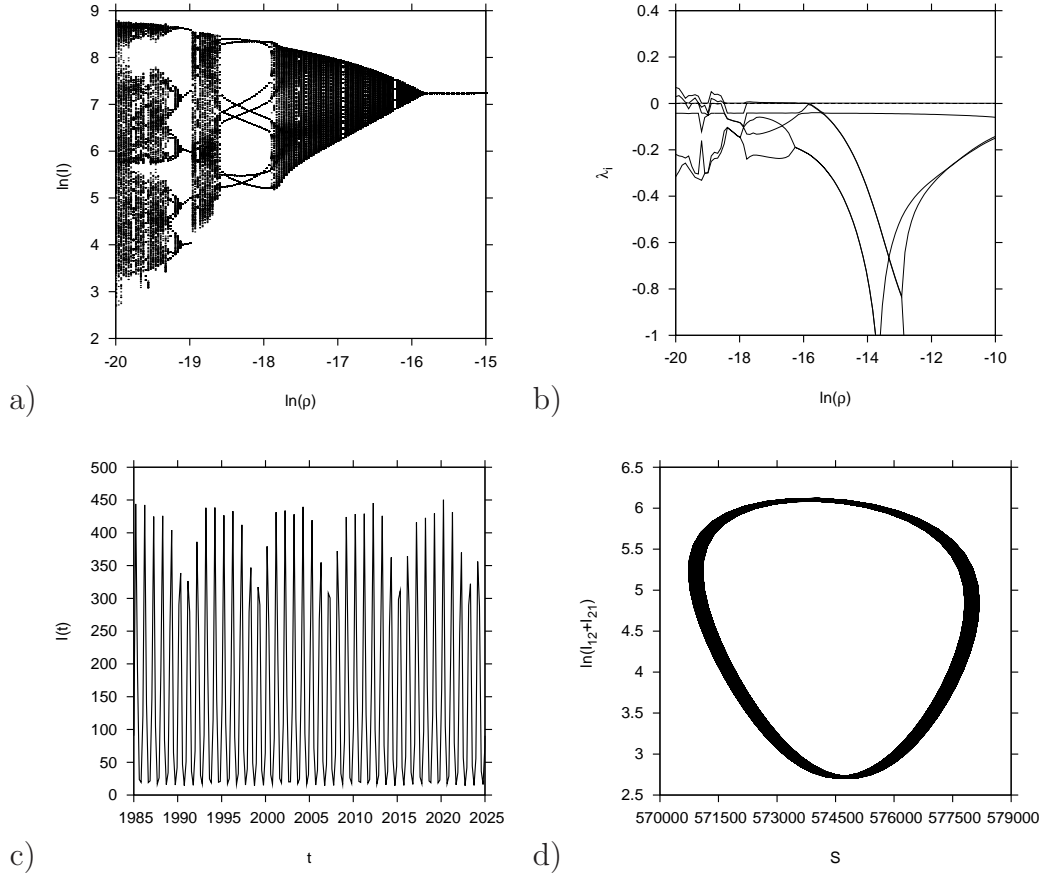


Figure 5.3: Numerical simulations for the province of Chiang Mai with population size  $N = 1650000$ . The parameter values are fixed as follows: Temporary cross-immunity  $\alpha = 2y^{-1}$ , infection rate  $\beta_0 = 2\gamma$ , recovery rate  $\gamma = 52y^{-1}$ , ratio of the contribution of the secondary infections to the force of infection  $\phi = 0.9$ , seasonal forcing  $\eta = 0.2$  and import  $\ln(\rho) = -15.85$ . In a) the bifurcation diagram varying the import parameter is shown. In b) the Lyapunov spectrum varying the import parameter, in c) the time series simulation and in d) the state space plot are shown. The torus attractor is visible here.

For the deterministic system a torus bifurcation  $TR$  was the first bifurcation

happening for a region of import factor  $\ln(\rho) = -15.85$  (see Fig. 5.3a)). Lyapunov exponents were calculated along the trajectory and the Lyapunov spectrum is shown in Fig. 5.3b), where two dominant zero Lyapunov exponents at  $\ln(\rho) = -15.85$  shows a quasi-periodicity (for instance on a torus). The appearance of this bifurcation for  $\ln(\rho) = -15.84$  is also predicted by AUTO (AUTO, 2009). In order to illustrate the infected dynamics on the deterministic approach we show the time series and its state space plot in Fig. 5.3c) and Fig. 5.3d).

Using the same parameter values as used for the deterministic simulations, the quasi-periodicity becomes more irregular resembling a chaotic behavior in the stochastic modeling approach. Figure 5.4a) shows one stochastic realization for the multi-strain dengue model which could describe very well the dynamics of the DHF incidences in Chiang Mai Province, North of Thailand (see Fig. 5.1a)). Such pattern would be most likely be described as being the chaotic transients towards the quasi-periodic torus of the deterministic skeleton (see 5.4b)) that got stabilized due to the noise.

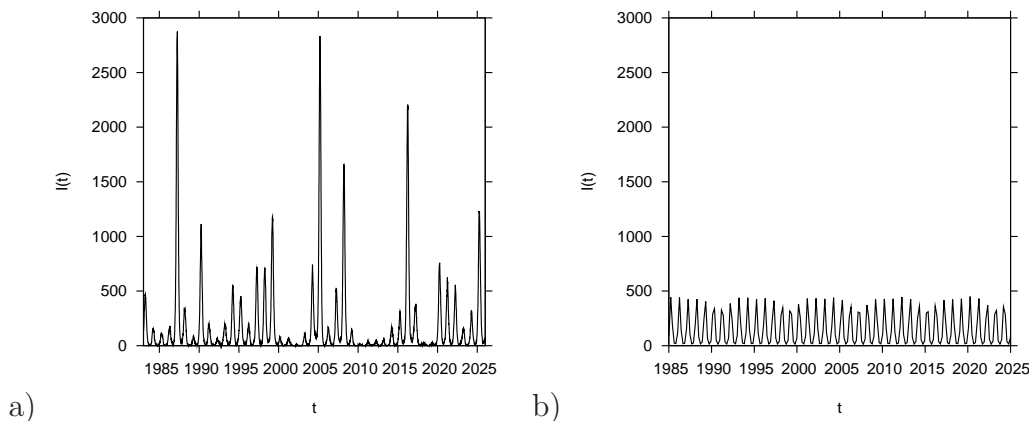


Figure 5.4: Stochastic and deterministic system's comparison. In a) One stochastic realization for a population size  $N = 1650000$ , temporary cross-immunity  $\alpha = 2y^{-1}$ , infection rate  $\beta_0 = 2\gamma$ , recovery rate  $\gamma = 52y^{-1}$ , ratio of the contribution of the secondary infections to the force of infection  $\phi = 0.9$ , seasonal forcing  $\eta = 0.2$  and import  $\ln(\rho) = -15.85$ . In b) the deterministic time series simulation as shown in Fig. 5.3c), scaled up to be properly compared with the stochastic time series simulation in Fig. 5.4a).

## 5.5 Scaling of stochasticity

It is known that stochastic simulations, using a finite size population, involve extinction phenomena operating through demographic stochasticity which acts drastically on small populations, as opposed for the deterministic models that do not handle extinction through population noise, leading to populations with

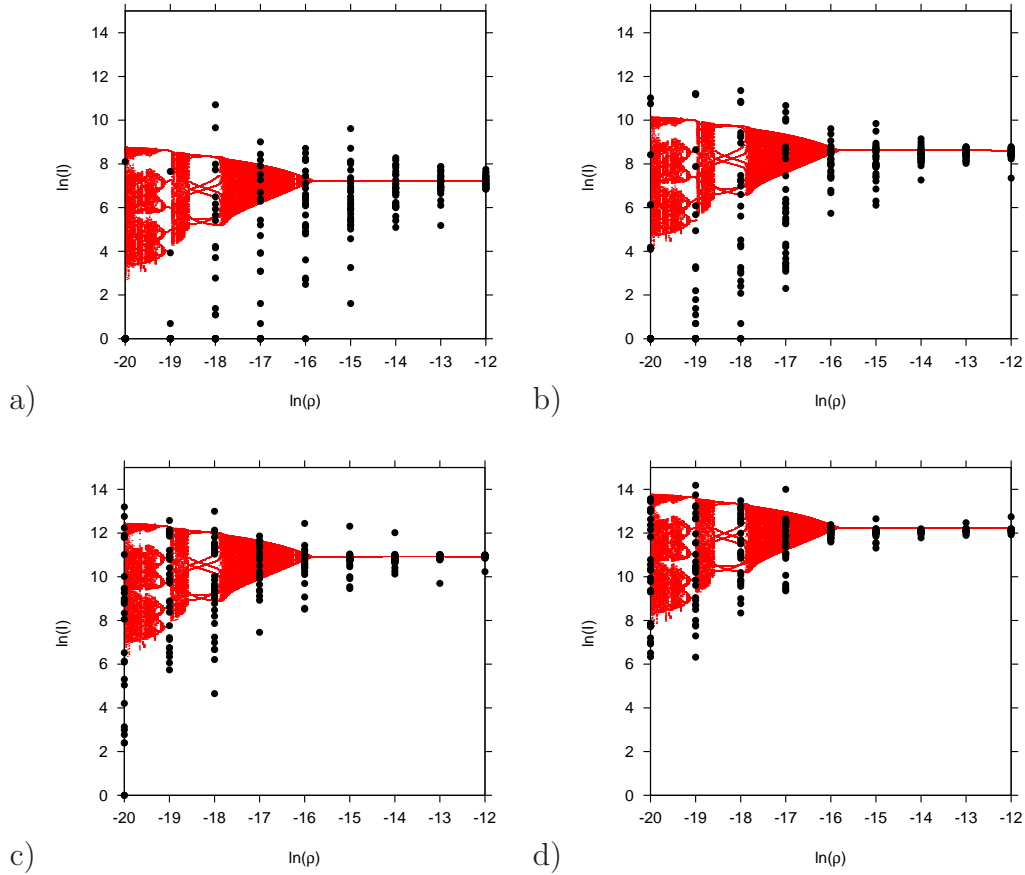


Figure 5.5: Stochastic and deterministic system's interaction. For the same parameter values used in Fig. 5.4, we show the bifurcation diagram for the import parameter for different population sizes  $N$ . In red the deterministic model and in black the stochastic model. In a) the Chiang Mai population size  $N = 1.65 \cdot 10^6$ , in b) North of Thailand population size  $N = 6 \cdot 10^6$ , in c) Thailand population size  $N = 66 \cdot 10^6$  and in d) a larger system size, where the population of some countries surrounding Thailand, for instance Burma, Laos, Vietnam and Cambodia, were counted together giving a system where the population size is  $N = 230 \cdot 10^6$ .

very few individuals or even fractions of individuals. In Fig. 5.5 we compare the deterministic and stochastic dynamics and we see that the magnitude of stochastic fluctuations decreases when the population size increases. We compare the interplay between the stochastic model and the deterministic skeleton in 4 different systems sizes. In Fig. 5.5a) we show the stochastic and deterministic system's interaction for a system where the population size  $N = 1.65 \cdot 10^6$ , mimicking the Province of Chiang Mai. The system with small population size shows very large fluctuations around the deterministic skeleton, hence an extreme noise amplification. In Fig. 5.5b) we show the stochastic and deterministic system's interaction for a system where the population size  $N = 6 \cdot 10^6$ , as it would be for the North of Thailand. In Fig. 5.5c) the system has the population size of Thailand,  $N = 66 \cdot 10^6$  and in Fig. 5.5d) a larger system size, where the population of some countries surrounding Thailand, for instance Burma, Laos, Vietnam and Cambodia, were counted together giving a system where the population size is  $N = 230 \cdot 10^6$ . For such large system, the stochastic fluctuations follow quite well the deterministic approach, where the noise is not much amplified anymore.

We see that the magnitude of the stochastic fluctuations decreases when the population size increases and more importantly, that for large enough population size, the stochastic system can be well described by the deterministic skeleton, where the essential dynamics are captured.

## 5.6 Conclusions

Multi-strain dynamics are generally modeled with SIR-type models, dividing the host population into susceptible, infected and recovered individuals with subscripts for the respective strains. We have considered the stochastic version of a multi-strain model with a minimal degree of complexity to generate both primary and secondary infections, motivated by dengue fever epidemiology. Besides the fact that disease propagation is an inherently stochastic phenomenon, dengue models are mainly expressed mathematically as a set of deterministic differential equations which are easier to analyze, however, it is only stochastic, as opposed to deterministic, models that can capture the fluctuations observed in some of the available time series data.

For the minimalistic multi-strain dengue model, the individuals can be susceptibles without a previous dengue infection, infected and recovered for the first time, susceptible with an experienced previous infection and infected for the second time, now with a different strain, and more likely been hospitalized due to the ADE effect leading to severe disease. Since the demographic events often occur at a much slower rate than the infection, the disease has to be necessarily maintained by the import of external infections to avoid the repeated stochastic disease extinction and re-introduction.

The stochastic realizations of infected in time were obtained by the Gillespie

algorithm. By considering stochasticity and external infections, we have shown that the introduction of stochasticity was needed to explain the fluctuations observed in some of the available data sets, revealing a scenario where noise and complex deterministic skeleton strongly interact. For large enough population size, the stochastic system could be well described by the deterministic skeleton, where the essential dynamics are captured, gaining insight into the relevant parameter values purely on topological information of the dynamics.

Understanding the dynamics of stochastic populations, and how they interact with the deterministic components of epidemiological models have maximum benefit on the practical predictability of the dynamical system by analyzing the available epidemiological data via mathematical models, since the classical parameter estimation and its application are generally restricted to fairly simple dynamical scenarios. The ability to predict the future dengue outbreaks via mathematical models would provide a tool to guide policies of prevention and control of the dengue virus transmission, including the implementation of vaccination programs when the dengue fever vaccine will be accessible.



## Chapter 6

# Irregularity in dengue fever epidemics: difference between first and secondary infections drives the rich dynamics more than the detailed number of strains

Maíra Aguiar, Bob W. Kooi, Filipe Rocha and Nico Stollenwerk (2011)  
*Submitted.*

Different extensions of the classical single-strain SIR model for the host population, motivated by modeling dengue fever epidemiology, have reported a rich dynamic structure including deterministic chaos which was able to explain the large fluctuations of disease incidences. A comparison between the basic two-strain dengue model, which already captures differences between primary and secondary infections, with the four-strain dengue model, that introduces the idea of competition of multiple strains in dengue epidemics shows that the difference between first and secondary infections drives the rich dynamics more than the detailed number of strains to be considered in the model structure. Chaotic dynamics were found to happen at the same parameter region of interest, for both the two and the four-strain models, able to explain the fluctuations observed in empirical data and showing a qualitatively good agreement between empirical data and model simulation. Since the law of parsimony favors the simplest of two competing models, the two-strain model would be the better candidate to be analyzed, giving the expected complex behavior to explain the fluctuations



observed in empirical data, and indeed the better option for estimating all initial conditions as well as the few model parameters based on the available incidence data.

## 6.1 Introduction

Dengue is a viral mosquito-borne infection, a leading cause of illness and death in the tropics and subtropics. There are four antigenically distinct but closely related dengue viruses, designated DEN-1, DEN-2, DEN-3, and DEN-4. Infection by one serotype confers life-long immunity to that serotype and a short period of temporary cross-immunity to other serotypes. Two forms of the disease exist: (DF) dengue fever, and (DHF) dengue hemorrhagic fever which has been associated with secondary dengue infection due to the (ADE) antibody-dependent enhancement process, where the pre-existing antibodies to previous dengue infection cannot neutralize but rather enhance the new infection. In the first dengue infection virus particles are captured and processed by so-called antigen presenting cells. T-cells become activated, likewise B-cells that produce antibodies used to inactivate the viruses. In a secondary infection the antibodies from the first infection attaches to the virus particles but does not inactivate them. The antibody-virus complex suppresses innate immune responses, increasing intracellular infection and generating inflammatory cytokines and chemokines that, collectively, result in enhanced disease (Halstead, 1982; Guzmán et al., 2010; Dejnirattisai et al., 2010).

Dengue fever dynamics is well known to be particularly complex with large fluctuations of disease incidences. Several mathematical models found in the literature have been formulated to describe the transmission of dengue fever. Multi-strain dengue dynamics are generally modeled with extended SIR-type models, and have demonstrated to show critical fluctuations with power law distributions of disease cases Massad et al. (2008) and deterministic chaos via ADE, but without temporary cross-immunity, Ferguson et al. (1999); Schwartz et al (2005); Billings et al. (2007), when strong infectivity on secondary infection was assumed. In these models, the recovered individuals could be immediately infected with another strain.

The combination of biological aspects such as temporary cross-immunity and ADE have been studied by several authors Wearing & Rohani (2006); Nagao & Koelle (2008); Recker et al. (2009) where four strains are involved, but again limiting the effect of ADE to increase the contribution of secondary cases to the force of infection. Aguiar et al. (2008) have investigated a two-strain dengue model, initially suggested and preliminarily analyzed in Ferguson et al. (1999), where deterministic chaos was found in a wider parameter regions when including temporary cross-immunity Aguiar et al. (2008), not needing to restrict the infectivity on secondary infection to one or another region in parameter space.

The two-strain model captures the essential differences between primary and secondary infections where the notion of two different strains is enough to describe primary infections, a mostly harmless form of illness, and secondary infection, associated with the severe form of the disease. It is a lower dimensional model as opposed to the multiple strain models, easier to be analyzed and still can attempt to estimate all initial conditions as well as the few model parameters.

In this manuscript we compare the basic two-strain dengue model, which already captures differences between primary and secondary infections, with the four-strain dengue model, that introduces the idea of competition of multiple strains in dengue epidemics. We perform a qualitative study in order to show how much complexity we really need to add into epidemiological models to be able to explain the fluctuations observed in empirical dengue hemorrhagic fever incidence data.

## 6.2 Two competing multi-strain models: a dimensional problem

A basic  $n$ -strain epidemiological model with primary and secondary infections can be written as follows.

$$\begin{aligned} \dot{S} &= \mu(N - S) \\ &\quad - \sum_{i=1}^n \frac{\beta}{N} S \left( I_i + \rho \cdot N + \phi \left( \sum_{j=1, j \neq i}^n I_{ji} \right) \right) \end{aligned} \quad (6.1)$$

and for  $i = 1, \dots, n$

$$\begin{aligned} \dot{I}_i &= \frac{\beta}{N} \left( I_i + \rho \cdot N + \phi \left( \sum_{j=1, j \neq i}^n I_{ji} \right) \right) \\ &\quad - (\gamma + \mu) I_i \end{aligned} \quad (6.2)$$

$$\dot{R}_i = \gamma I_i - (\alpha + \mu) R_i \quad (6.3)$$

$$\begin{aligned} \dot{S}_i &= \alpha R_i \\ &\quad - \sum_{j=1, j \neq i}^n \frac{\beta}{N} S_i \left( I_j + \rho \cdot N + \phi \left( \sum_{k=1, k \neq j}^n I_{kj} \right) \right) \\ &\quad - \mu S_i \end{aligned} \quad (6.4)$$

and for  $i = 1, \dots, n$  and  $j = 1, \dots, n$  with  $j \neq i$

$$\begin{aligned} \dot{I}_{ij} = & \frac{\beta}{N} S_i \left( I_j + \rho \cdot N + \phi \left( \sum_{k=1, k \neq j}^n I_{kj} \right) \right) \\ & - (\gamma + \mu) I_{ij} \end{aligned} \quad (6.5)$$

and finally

$$\dot{R} = \gamma \left( \sum_{i=1}^n \sum_{j=1, j \neq i}^n I_{ij} \right) - \mu R \quad . \quad (6.6)$$

where the parameter  $\beta$  is given explicitly by

$$\beta(t) = \beta_0 \cdot (1 + \eta \cdot \cos((\omega \cdot t))) \quad (6.7)$$

where  $\beta_0$  is the infection rate and  $\eta$  is the degree of seasonality. The parameter  $\rho$  is the import factor, related to the possibility of an individual to get infected outside the studied population and then bring the infection into the population to which this individual belongs to, mimicking the imported cases of the disease in a defined population. Equivalently an infected visitor to the region under consideration who passes the infection to a susceptible in the population of size  $N$  has the same effect on the studied population. Hence, we do not need to distinguish these two scenarios of susceptibles traveling outside or infected traveling inside the region under consideration. In total, this captures the imported infection that comes from an external source.

For constant population size, the susceptibles individuals without a previous experienced dengue infection ( $S$ ) become infected for the first time with a given dengue strain ( $I_i$ ) with two possible infection rates, depending on who (individual on his primary or secondary infection) is transmitting the infection. The relevant difference concerning disease transmissibility is that the force of infection varies accordingly to the number of previous infections the hosts have experienced. Note that the number of dengue cases caused by a third or fourth dengue virus infection is extremely low and once confirmed, the risk for DHF relative to DF was not different for those experiencing third or fourth dengue virus infections over those experiencing a second dengue virus infection Endy et al. (2002); Gibbons et al. (2007); Halstead (2008). Therefore, individuals in a primary infection transmit the disease with a force of infection  $\frac{\beta I}{N}$  whereas in a secondary infection the transmission is given with a force of infection  $\frac{\phi \beta I}{N}$  where  $\phi$  can be larger or smaller than unit, i.e. increasing or decreasing the transmission rate, due to the ADE effect. Individuals infected for the first time become recovered and life long immune to that given strain ( $R_i$ ), with a recovery rate  $\gamma$  and after a period of temporary cross-immunity  $\alpha$ , are again susceptible with a previous experienced infection ( $S_i$ ). Individuals only get infected for the second time with

a different strain than the one acquired during the first infection ( $I_{ij}$ ), again with two possible infection rates, depending on who (individual on his primary or secondary infection) is transmitting the infection. Finally, they recover from the secondary infection ( $R$ ) with recovery rate  $\gamma$ . The death rates  $\mu$  coming out of all classes go into the class of susceptible without experiencing previous dengue infection as a birth rate.

### 6.2.1 The two-strain model versus the four-strain model

Concerning data availability, long term epidemiological information comes from the Ministry of Public Health in Thailand and consist on monthly incidences of hospitalized DHF cases. For such a data scenario, models that are able to generate both primary and secondary infection cases (with a different strain), without the need of considering differences on the dynamics of different co-circulating dengue serotypes, have show a good qualitative agreement between empirical data and model output Aguiar et al. (2011 a), just by combining ADE and temporary cross-immunity.

The two-strain model with temporary cross-immunity is a 9 dimensional system where the population  $N$  is divided into ten classes. For two different strains, named strain 1 and strain 2, we label the SIR classes for the hosts that have seen the individual strains, without epidemiological asymmetry between strains, i.e. infections with strain one followed by strain two or vice versa contribute in the same way to the force of infection. The complete system of ordinary differential equations (ODEs) for the two-strain epidemiological model can be written as follows.

$$\begin{aligned} \dot{S} &= \mu(N - S) \\ &\quad - \frac{\beta(t)}{N}S(I_1 + \rho \cdot N + \phi I_{21}) \\ &\quad - \frac{\beta(t)}{N}S(I_2 + \rho \cdot N + \phi I_{12}) \end{aligned} \quad (6.8)$$

$$\dot{I}_1 = \frac{\beta(t)}{N}S(I_1 + \rho \cdot N + \phi I_{21}) - (\gamma + \mu)I_1 \quad (6.9)$$

$$\dot{I}_2 = \frac{\beta(t)}{N}S(I_2 + \rho \cdot N + \phi I_{12}) - (\gamma + \mu)I_2 \quad (6.10)$$

$$\dot{R}_1 = \gamma I_1 - (\alpha + \mu)R_1 \quad (6.11)$$

$$\dot{R}_2 = \gamma I_2 - (\alpha + \mu)R_2 \quad (6.12)$$

$$\dot{S}_1 = \alpha R_1 - \frac{\beta(t)}{N}S_1(I_2 + \rho \cdot N + \phi I_{12}) - \mu S_1 \quad (6.13)$$

$$\dot{S}_2 = \alpha R_2 - \frac{\beta(t)}{N}S_2(I_1 + \rho \cdot N + \phi I_{21}) - \mu S_2 \quad (6.14)$$

$$\dot{I}_{12} = \frac{\beta(t)}{N} S_1(I_2 + \rho \cdot N + \phi I_{12}) - (\gamma + \mu) I_{12} \quad (6.15)$$

$$\dot{I}_{21} = \frac{\beta(t)}{N} S_2(I_1 + \rho \cdot N + \phi I_{21}) - (\gamma + \mu) I_{21} \quad (6.16)$$

$$\dot{R} = \gamma(I_{12} + I_{21}) - \mu R \quad (6.17)$$

The basic two-strain model shows a rich variety of dynamics through bifurcations up to deterministically chaotic behavior in wider and more biologically realistic parameter regions (see Fig 6.1a)) than previously anticipated when neglecting temporary cross-immunity. Two chaotic windows appear, one for  $\phi < 1$ , where this dynamical behavior has been described first in Aguiar et al. (2008), and also the one for  $\phi > 1$ , see e.g. Ferguson et al. (1999). There is good evidence that sequential infection increases the risk of developing DHF associated with ADE and since practically all cases of DHF are hospitalized Chareonsook et al. (1999), the irregular behavior in the parameter region of  $\phi < 1$ , where people in a secondary dengue infection do not contribute to the force of infections as much as people with first infection, was found to be more realistic for dengue fever epidemiology. The new chaotic window for  $\phi < 1$  disappears when neglecting the temporary cross-immunity, i.e. by putting  $\alpha \rightarrow \infty$  (see Fig 6.1b)). For detailed information on the basic two-strain dengue model, see Aguiar et al. (2008, 2009, 2011 a).

Differently from the minimalistic dengue model, the four-strain model is a 25 dimensional system, dividing the constant population  $N$  into twenty six classes. For four different strains, 1, 2, 3 and 4, we now label the SIR classes for the hosts that have seen the individual strains, again without epidemiological asymmetry between strains. The serotype data are recent and too short to give any realistic information concerning difference in biological parameters such as infection and recovery rates for a given strain. The four-strain model dynamics is described in a similar way as the two-strain model, where the relevant difference concerning disease transmissibility is that the force of infection varies accordingly to the number of previous infections the hosts have experienced. Since the secondary infection can only happen with a different strain from the first infection, here the individuals can get infected for the second time with strain one when the first infection was caused by strain two, three or four ( $I_{21}, I_{31}, I_{41}$ ). Individuals can get infected for the second time with strain two when the first infection was caused by strain one, three or four ( $I_{12}, I_{32}, I_{42}$ ). Individuals can get infected for the second time with strain three when the first infection was caused by strain one, two or four ( $I_{13}, I_{23}, I_{43}$ ) and individuals can get infected for the second time with strain four when the first infection was caused by strain one, two or three ( $I_{14}, I_{24}, I_{34}$ ). The model also captures the differences between primary and secondary infections, however, it is high dimensional so that the investigation of the possible dynamical structures cannot be easily performed.

The four-strain epidemiological model can be written as a system of 26 ODEs (for the complete ODE system, see electronic supplementary material). It can be simplified to a three or two-strain model only by neglecting the existence of specific strains. A three-strain model can be obtained by putting  $I_4 = 0$  at  $t_0$  and initially no secondary infected for example, where the complete system of ODEs would be reduced to a system of 17 ODEs, and by putting  $I_3 = 0, I_4 = 0$  at  $t_0$  and initially no secondary infected, we get back the original two-strain model without any loss of generality, a system of 10 ODEs.

### 6.3 Numerical analysis

In this section we start with a numerical bifurcation analysis where we compare the results for the non-seasonal two-strain model to that of the non-seasonal four-strain model. First we compare the bifurcation diagrams obtained for both models when assuming and neglecting the temporary cross-immunity parametrized by  $\alpha$ . This study is completed with a time series analysis in which we compare the qualitative agreement between the models simulations and empirical DHF data. The parameter description and respective values for dengue fever epidemiology are given in Table 6.1.

The bifurcation diagrams were obtained plotting the local maxima of the logarithm of the total number of infected  $\ln(I)$  against the ratio of the contribution of the secondary infections  $\phi$  to the force of infection (see Fig. 6.1). Fixed points appear as one dot per parameter value, limit cycles appear as two dots, double-limit cycles as four dots, more complicated limit cycles as more dots, and chaotic attractors as continuously distributed dots for a single  $\phi$  value Ruelle (1989).

In Fig 6.1a) and Fig 6.1b) we observe only one chaotic window for  $\phi > 1$ . For both models, when neglecting the temporary cross-immunity period, the complex dynamics were restricted to the parameter region  $\phi \gg 1$ , where individuals in the secondary dengue infection would contribute much more to the force of infection than individuals in the first infection. Consideration of temporary cross-immunity brings a new chaotic window, (see Fig 6.1c) and Fig 6.1d)), with a rich dynamical behavior from fixed point to limit cycles until completely irregular behavior for a more biologically realistic parameter region  $\phi < 1$ , in addition to the previously found chaotic window for  $\phi > 1$ .

Note that the addition of seasonal forcing (see Fig 6.2a)) and/or population noise brings complex behavior also for the region where only periodic dynamics are observed. It is clear that in order to obtain the complex behavior, the difference between first and secondary infection combined with the temporary cross-immunity period is more important than the addition of a detailed number of strains.

In Figure 6.2b) we present the bifurcation diagram comparison, for both two-strain and four-strain model, in the relevant parameter region of  $\phi < 1$ , when

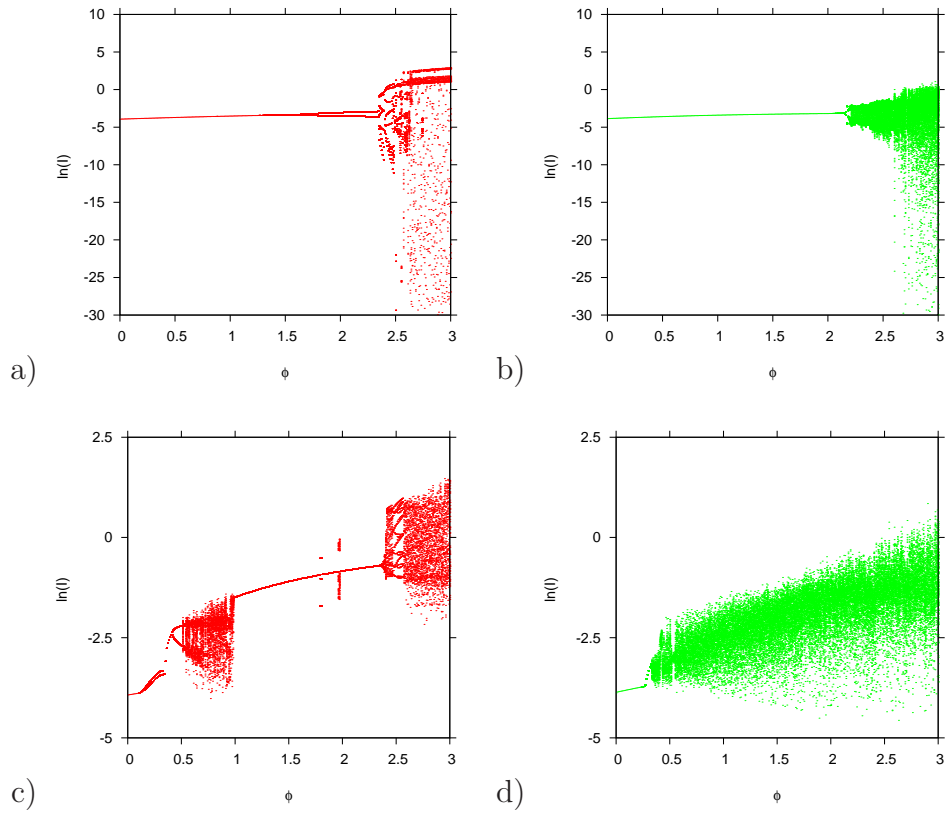


Figure 6.1: Bifurcation diagram comparison between multi-strain models. In red the non-seasonal two-strain model and in green the non-seasonal four-strain model. For neglecting temporary cross-immunity period ( $\alpha = 52y^{-1}$  or one week) we show in a) the two-strain model and in b) the four-strain model. For assuming temporary cross-immunity period ( $\alpha = 2y^{-1}$  or six months) we show in c) the two-strain model and in d) the four-strain model.

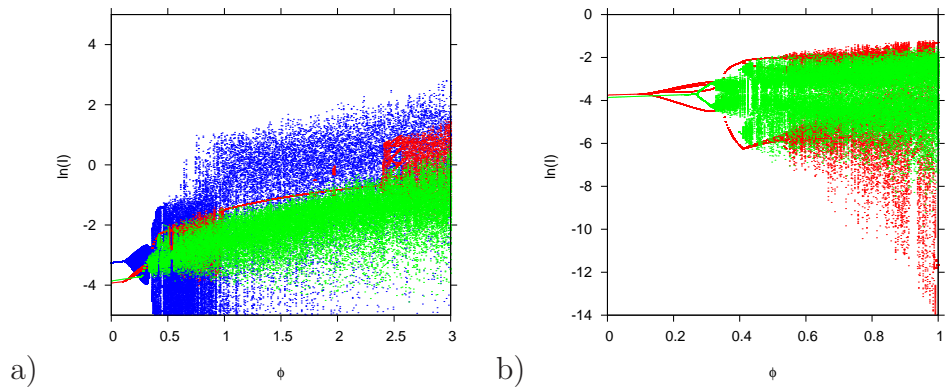


Figure 6.2: Bifurcation diagram comparison between multi-strain models. In red the non-seasonal two-strain model, in green the non-seasonal four-strain model and in blue the seasonal ( $\eta = 0.1$ ) two-strain model. In a) for the parameter region of  $0 < \phi < 3$  and in b) for the parameter region of  $\phi < 1$ .

Table 6.1: Parameter set for the basic multi-strain models.

Par.	Description	Values	Ref.
$N$	population size	$1.6 \times 10^6$	–
$\mu$	birth and death rate	$1/65y$	UNWPP (2011)
$\gamma$	recovery rate	$52y^{-1}$	WHO (2009); CDC (2011)
$\beta_0$	infection rate	$2 \cdot \gamma$	Ferguson et al. (1999)
$\eta$	degree of seasonality	$\in [0, 0.35]$	Aguiar et al. (2011 a)
$\rho$	import parameter	$\in [0, 10^{-10}]$	Aguiar et al. (2011 a)
$\alpha$	temporary cross immunity rate	$\in [2, 52]y^{-1}$	(Matheus et al., 2005)
$\phi$	ratio of secondary infections contributing to force of infection	$\in [0, 3]$	(Aguiar et al., 2008)

dengue patients in a secondary infection evolving to severe disease because of the ADE phenomenon contributing less to the force of infection, and not more, as previous models suggested. For the two-strain model a Hopf bifurcation was found to occur at  $\phi = 0.1133$  and a torus bifurcation, as a route to the chaotic behavior, was found to occur at  $\phi = 0.551$  whereas for the four-strain model the Hopf bifurcation occurs at  $\phi = 0.267$  followed by a torus bifurcation that occurs at  $\phi = 0.311$ . Qualitatively, the bifurcation points appear to happen at similar parameter regions, well below the region of interest  $\phi \approx 1$ . For both models the chaotic dynamics which are able to explain the fluctuations observed in empirical data were found at the same parameter region of interest and not only when assuming strong infectivity on secondary infection.

In order to illustrate the similarities on the dynamical behavior of non-seasonal multi-strain models better, we show in Fig 6.3 the bifurcation diagram where the temporary cross-immunity period  $\alpha$  is the varying parameter, and also the time series and its state-space plot for  $\phi = 0.6$ , where chaotic behavior was confirmed to happen in the non-seasonal models with two, three and four-strains. For more information on the quantification of unpredictability via Lyapunov exponents, see Aguiar et al. (2008, 2011 a).

The bifurcation diagram analysis (Fig 6.3a), 6.3b) and 6.3c)) shows that complex dynamics appears at the same parameter region of interest, i.e. when assuming temporary cross-immunity period between 3 – 9 months, for all of the possible non-seasonal multi-strain models, the two, three and four-strain models. These results confirm the fact that the difference between first and secondary infection (different forces of infections due to the hospitalization of the severe cases



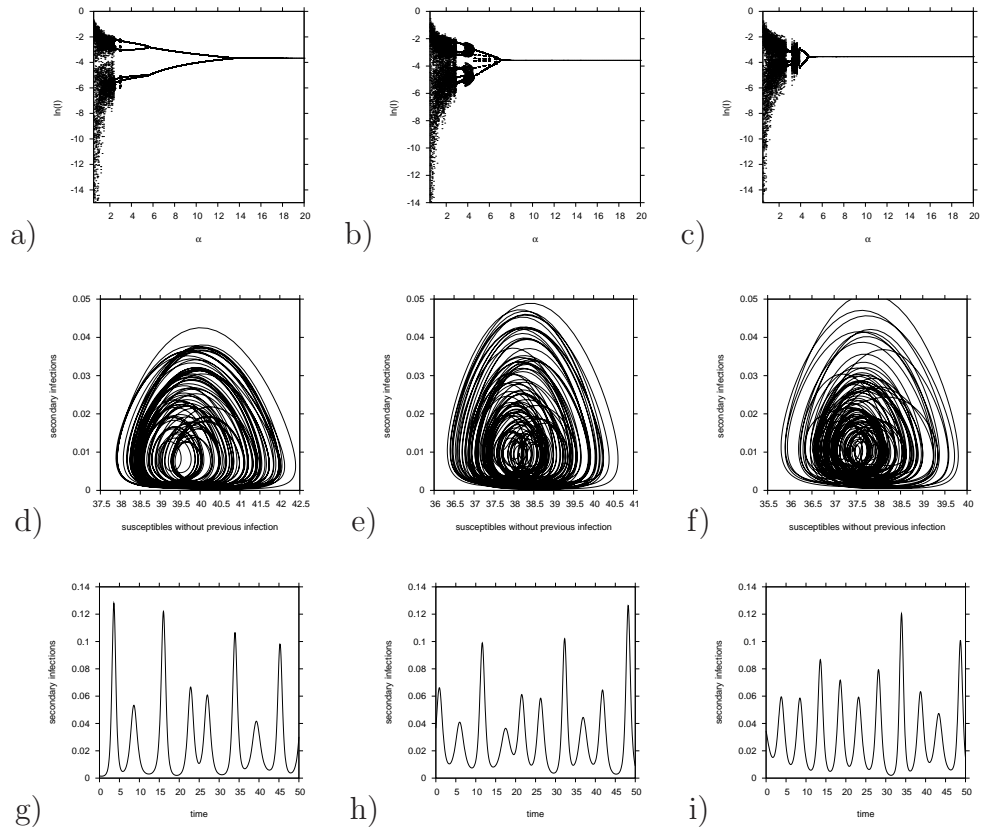


Figure 6.3: Similarities between non-seasonal multi-strain models. For  $\phi = 0.6$ , in a) we show the bifurcation diagram for the two-strain model, in b) the bifurcation diagram for the three-strain model and in c) the bifurcation diagram for the four-strain model. Here, the local maxima of the logarithm of the total number of infected  $\ln(I)$  is plotted against the temporary cross-immunity period  $\alpha$ . By fixing the temporary cross-immunity period  $\alpha = 2y^{-1}$ , in d) we show the state-space plot for the two-strain model, in e) the state-space plot for the three-strain model and in f) the state-space plot for the four-strain model. In g) we show the time series for the two-strain model, in h) the time series for the three-strain model and in i) the time series for the four-strain model.

of the disease), combined with temporary cross-immunity aspect (to be assumed between recurrent infections) are driving the complex dynamics in multi-strain models more than the specific number of strains to be considered into the model assumptions. The time series and the respective state-space plots are also shown (see Fig 6.3d)-6.3f)) for each one of the presented models, where the similarities on the chaotic parameter region is confirmed.

The addition of seasonal forcing and import of infected have shown a qualitatively very good result when comparing empirical DHF data and simulation results, again for both the two-strain model Aguiar et al. (2011 a) (see Fig 6.4a)) and the four-strain model (see Fig 6.4b)), where patterns of the chaotic data were similarly found in the models simulations.

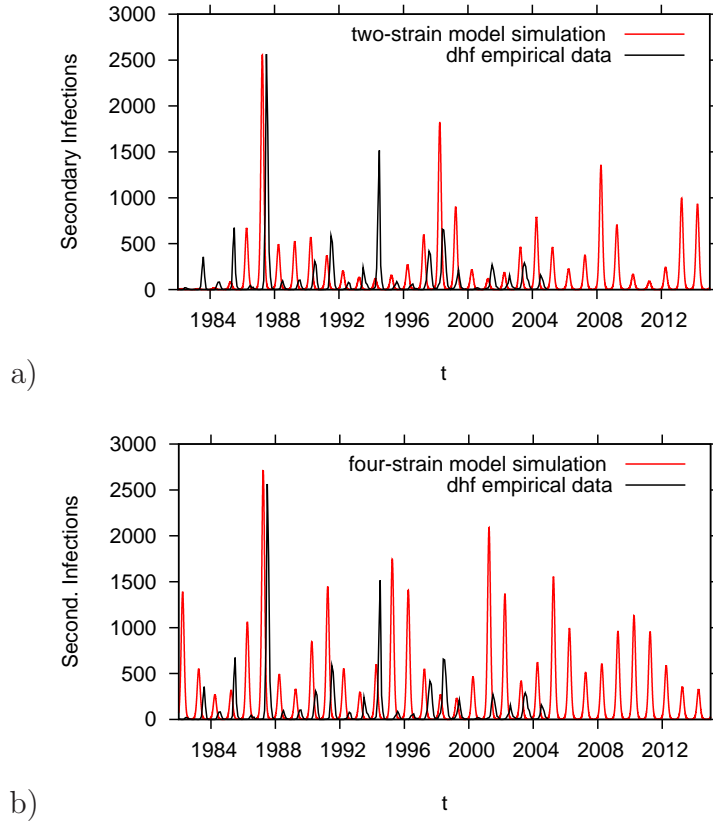


Figure 6.4: Using the same parameter set, empirical DHF incidence data (in black) for the Province of Chiang Mai in the North of Thailand are matched with simulations (in red) for the seasonal multi-strain models with import of infected. In a) two-strain model and in b) the four-strain model. Here, the degree of seasonality  $\eta = 0.35$  and the import factor  $\rho = 10^{-10}$ . The other parameter values are given in Table 6.1.

The effective dimension of the two-strain model is 9 while of the four-strain model 25. The law of parsimony that recommends selecting the hypothesis that

makes the fewest assumptions, implies that the 9 dimensional two-strain model would be the better candidate than the 25 dimensional four-strain model to be analyzed, capturing the essential differences of primary versus secondary infection without needing to restrict the ADE effect to one or another region in parameter space.

The two-strain model in its simplicity is a good model to be analyzed, giving the expected complex behavior to explain the fluctuations observed in empirical data, and would be indeed the best option to be used for parameter estimation, which is notoriously difficult for chaotic time series, based on the available incidence data. Only the two-strain model could attempt to estimate all initial conditions as well as the few model parameters, as opposed of the four-strain model.

## 6.4 Discussion and Remarks

In this manuscript we presented the results obtained from a qualitative analysis of multi-strain dynamical system motivated by dengue fever epidemiology. The comparison between the basic two-strain dengue model, which already captures differences between primary and secondary infections, with the four-strain dengue model, that introduces the idea of competition of multiple strains in dengue epidemics have shown that the difference between first and secondary infection combined with the temporary cross-immunity period is driving more the complex dynamics, which is able to explain the large fluctuations observed in the empirical DHF incidence data, then the detailed number of strains to be considered into the model assumptions.

The numerical bifurcation analysis has showed that chaotic dynamics appear to happen at the same parameter region of interest, i.e. when assuming temporary cross-immunity period between 3 – 9 months, for all of the considered multi-strain models, and the addition of seasonal forcing and import of infected have shown a qualitatively very good result when comparing empirical DHF data and simulation results, where patterns of the data behavior were similarly found to happen, for both models, in the time series simulations.

Frequently the time series of empirical data are used as a qualitative check on model output, however, fitting every chaotic detail of the model to that of the empirical data is not possible. Parameter estimation based on empirical data to estimate initial conditions and model parameters have received great attention and is notoriously difficult for chaotic time series. Temporally local approaches are possible using iterated filtering algorithms Ionides et al. (2006); He et al. (2010), and at the moment only minimalistic models would have a chance to be qualitatively understood well and eventually tested against existing data.

The two-strain model in its simplicity is a good model to be analyzed, giving the expected complex behavior to explain the fluctuations observed in empirical

data. It is minimalistic in the sense that it can capture the essential differences of primary versus secondary infection without needing to restrict the ADE effect to one or another region in parameter space. For future parameter estimation only the two-strain model could attempt to estimate all initial conditions as well as the few model parameters. The two-strain model showed a qualitatively good result when comparing empirical DHF data and model simulations, giving insights into the relevant parameter values purely on topological information of the dynamics, and these relevant parameter values can be used for further refinement in formal parameter estimation based on the available data.

## 6.A Unpacking the n-strain model into a four-strain model

The basic n-strain epidemiological model motivated by dengue fever epidemiology, capturing difference between primary and secondary infections is shown in system Eq. (??-??), giving for  $n = 4$  a system with 26 ODEs in total. The complete system of ordinary differential equations for the four-strain epidemiological model can be written as follows.

$$\begin{aligned} \dot{S} &= \mu(N - S) & (6.18) \\ &- \frac{\beta}{N}S(I_1 + \rho \cdot N + \phi(I_{21} + I_{31} + I_{41})) \\ &- \frac{\beta}{N}S(I_2 + \rho \cdot N + \phi(I_{12} + I_{32} + I_{42})) \\ &- \frac{\beta}{N}S(I_3 + \rho \cdot N + \phi(I_{13} + I_{23} + I_{43})) \\ &- \frac{\beta}{N}S(I_4 + \rho \cdot N + \phi(I_{14} + I_{24} + I_{34})) \end{aligned}$$

$$\dot{I}_1 = \frac{\beta}{N}S(I_1 + \rho \cdot N + \phi(I_{21} + I_{31} + I_{41})) - (\gamma + \mu)I_1 \quad (6.19)$$

$$\dot{I}_2 = \frac{\beta}{N}S(I_2 + \rho \cdot N + \phi(I_{12} + I_{32} + I_{42})) - (\gamma + \mu)I_2 \quad (6.20)$$

$$\dot{I}_3 = \frac{\beta}{N}S(I_3 + \rho \cdot N + \phi(I_{13} + I_{23} + I_{43})) - (\gamma + \mu)I_3 \quad (6.21)$$

$$\dot{I}_4 = \frac{\beta}{N}S(I_4 + \rho \cdot N + \phi(I_{14} + I_{24} + I_{34})) - (\gamma + \mu)I_4 \quad (6.22)$$

$$\dot{R}_1 = \gamma I_1 - (\alpha + \mu)R_1 \quad (6.23)$$

$$\dot{R}_2 = \gamma I_2 - (\alpha + \mu)R_2 \quad (6.24)$$

$$\dot{R}_3 = \gamma I_3 - (\alpha + \mu)R_3 \quad (6.25)$$

$$\dot{R}_4 = \gamma I_4 - (\alpha + \mu)R_4 \quad (6.26)$$

$$\dot{S}_1 = \alpha R_1 \quad (6.27)$$

$$- \frac{\beta}{N} S_1 (I_2 + \rho \cdot N + \phi(I_{12} + I_{32} + I_{42}))$$

$$- \frac{\beta}{N} S_1 (I_3 + \rho \cdot N + \phi(I_{13} + I_{23} + I_{43}))$$

$$- \frac{\beta}{N} S_1 (I_4 + \rho \cdot N + \phi(I_{14} + I_{24} + I_{34}))$$

$$- \mu S_1$$

$$\dot{S}_2 = \alpha R_2 \quad (6.28)$$

$$- \frac{\beta}{N} S_2 (I_1 + \rho \cdot N + \phi(I_{21} + I_{31} + I_{41}))$$

$$- \frac{\beta}{N} S_2 (I_3 + \rho \cdot N + \phi(I_{13} + I_{23} + I_{43}))$$

$$- \frac{\beta}{N} S_2 (I_4 + \rho \cdot N + \phi(I_{14} + I_{24} + I_{34}))$$

$$- \mu S_2$$

$$\dot{S}_3 = \alpha R_3 \quad (6.29)$$

$$- \frac{\beta}{N} S_3 (I_1 + \rho \cdot N + \phi(I_{21} + I_{31} + I_{41}))$$

$$- \frac{\beta}{N} S_3 (I_2 + \rho \cdot N + \phi(I_{12} + I_{32} + I_{42}))$$

$$- \frac{\beta}{N} S_3 (I_4 + \rho \cdot N + \phi(I_{14} + I_{24} + I_{34}))$$

$$- \mu S_3$$

$$\dot{S}_4 = \alpha R_4 \quad (6.30)$$

$$- \frac{\beta}{N} S_3 (I_1 + \rho \cdot N + \phi(I_{21} + I_{31} + I_{41}))$$

$$- \frac{\beta}{N} S_4 (I_2 + \rho \cdot N + \phi(I_{12} + I_{32} + I_{42}))$$

$$- \frac{\beta}{N} S_4 (I_3 + \rho \cdot N + \phi(I_{13} + I_{23} + I_{43}))$$

$$- \mu S_4$$

$$\dot{I}_{12} = \frac{\beta}{N}S_1(I_2 + \rho \cdot N + \phi(I_{12} + I_{32} + I_{42})) - (\gamma + \mu)I_{12} \quad (6.31)$$

$$\dot{I}_{13} = \frac{\beta}{N}S_1(I_3 + \rho \cdot N + \phi(I_{13} + I_{23} + I_{43})) - (\gamma + \mu)I_{13} \quad (6.32)$$

$$\dot{I}_{14} = \frac{\beta}{N}S_1(I_4 + \rho \cdot N + \phi(I_{14} + I_{24} + I_{34})) - (\gamma + \mu)I_{14} \quad (6.33)$$

$$\dot{I}_{21} = \frac{\beta}{N}S_2(I_1 + \rho \cdot N + \phi(I_{21} + I_{31} + I_{41})) - (\gamma + \mu)I_{21} \quad (6.34)$$

$$\dot{I}_{23} = \frac{\beta}{N}S_2(I_3 + \rho \cdot N + \phi(I_{13} + I_{23} + I_{43})) - (\gamma + \mu)I_{23} \quad (6.35)$$

$$\dot{I}_{24} = \frac{\beta}{N}S_2(I_4 + \rho \cdot N + \phi(I_{14} + I_{24} + I_{34})) - (\gamma + \mu)I_{24} \quad (6.36)$$

$$\dot{I}_{31} = \frac{\beta}{N}S_3(I_1 + \rho \cdot N + \phi(I_{21} + I_{31} + I_{41})) - (\gamma + \mu)I_{31} \quad (6.37)$$

$$\dot{I}_{32} = \frac{\beta}{N}S_3(I_2 + \rho \cdot N + \phi(I_{12} + I_{32} + I_{42})) - (\gamma + \mu)I_{32} \quad (6.38)$$

$$\dot{I}_{34} = \frac{\beta}{N}S_3(I_4 + \rho \cdot N + \phi(I_{14} + I_{24} + I_{34})) - (\gamma + \mu)I_{34} \quad (6.39)$$

$$\dot{I}_{41} = \frac{\beta}{N}S_4(I_1 + \rho \cdot N + \phi(I_{21} + I_{31} + I_{41})) - (\gamma + \mu)I_{41} \quad (6.40)$$

$$\dot{I}_{42} = \frac{\beta}{N}S_4(I_2 + \rho \cdot N + \phi(I_{12} + I_{32} + I_{42})) - (\gamma + \mu)I_{42} \quad (6.41)$$

$$\dot{I}_{43} = \frac{\beta}{N}S_4(I_3 + \rho \cdot N + \phi(I_{13} + I_{23} + I_{43})) - (\gamma + \mu)I_{43} \quad (6.42)$$

$$\begin{aligned} \dot{R} = & \gamma(I_{12} + I_{13} + I_{14} + I_{21} + I_{23} + I_{24} + I_{31} \\ & + I_{32} + I_{34} + I_{41} + I_{42} + I_{43}) - \mu R \end{aligned} \quad (6.43)$$

It divides the population  $N$  into twenty six classes, a 25 dimensional dynamical system due to the constant population size. The dynamics are described in a similar way as the two-strain model. Susceptible individuals without a previous dengue infection  $S$  can possibly get the primary infection with strain one ( $I_1$ ), strain two ( $I_2$ ), strain three ( $I_3$ ) or strain four ( $I_4$ ), with two different infection rates, depending on whom (individual on his primary or secondary infection) is transmitting the infection. Remember that the relevant difference concerning disease transmissibility is that the force of infection varies accordingly to the number of previous infections the hosts have experienced. In a primary infection, individuals transmit the disease with a force of infection  $\beta I/N$  whereas in a secondary

infection the transmission is given with a force of infection  $\phi\beta I/N$ , where  $\phi$  can be larger or smaller than 1, i.e. increasing or decreasing the transmission rate, due to the ADE effect. Note that the number of dengue cases caused by a third or fourth dengue virus infection is extremely low and once confirmed, the risk for DHF relative to DF was not different for those experiencing third or fourth dengue virus infections over those experiencing a second dengue virus infection Endy et al. (2002); Gibbons et al. (2007); Halstead (2008).

Individuals infected for the first time become recovered, with strain one ( $R_1$ ), strain two ( $R_2$ ), strain three ( $R_3$ ) or strain four ( $R_4$ ), and life long immune to the given strain, with a recovery rate  $\gamma$ . After a period of temporary cross-immunity  $\alpha$ , the first recovered individuals are again susceptible, however with an experienced previous infection with strain one ( $S_1$ ), strain two ( $S_2$ ), strain three ( $S_3$ ) or strain four ( $S_4$ ). The secondary infection can only happen with a different strain, and therefore, individuals can get infected for the second time with strain one when the first infection was caused by strain two, three or four ( $I_{21}, I_{31}, I_{41}$ ). Individuals can get infected for the second time with strain two when the first infection was caused by strain one, three or four ( $I_{12}, I_{32}, I_{42}$ ). Individuals can get infected for the second time with strain three when the first infection was caused by strain one, two or four ( $I_{13}, I_{23}, I_{43}$ ) and individuals can get infected for the second time with strain four when the first infection was caused by strain one, two or three ( $I_{14}, I_{24}, I_{34}$ ). Finally, the individuals recover from the second infection ( $R$ ) with recovery rate  $\gamma$ . The death rates  $\mu$  coming out of all classes go into the class of susceptible without experiencing previous dengue infection as a birth rate. The model also captures the differences between primary and secondary infections, however, it is high dimensional so that the investigation of the possible dynamical structures cannot be easily performed.

# Bibliography

- Adams, B., & Boots, M. (2006). Modelling the relationship between antibody-dependent enhancement and immunological distance with application to dengue. *Journal of Theoretical Biology*, 242, 337–46.
- Adams, B., & Boots, M. (2007). The influence of immune cross-reaction on phase structure in resonant solutions of a multi-strain seasonal SIR model. *Journal of Theoretical Biology*, 248, 202–11.
- Albers, D., & Sprott, J. (2006). Routes to chaos in high-dimensional dynamical systems: A qualitative numerical study. *Physica D*, 223, 194–207.
- Aguiar, M., & Stollenwerk, N. (2007). A new chaotic attractor in a basic multi-strain epidemiological model with temporary cross-immunity. *arXiv:0704.3174v1 [nlin.CD]*.
- Aguiar, M., Kooi, B.W., & Stollenwerk, N. (2008). Epidemiology of Dengue Fever: A Model with Temporary Cross-Immunity and Possible Secondary Infection Shows Bifurcations and Chaotic Behaviour in Wide Parameter Regions (see **Chapter 2**). *Math. Model. Nat. Phenom.*, 4, 48–70.
- Aguiar, M., Stollenwerk, N., & Kooi, B.W. (2009). Torus bifurcations, isolas and chaotic attractors in a simple dengue model with ADE and temporary cross immunity (see **Chapter 3**). *International Journal of Computer Mathematics*, 86, 1867–1877.
- Aguiar, M., et al. (2011 a). The role of seasonality and import in a minimalistic multi-strain dengue model capturing differences between primary and secondary infections: complex dynamics and its implications for data analysis (see **Chapter 4**). *Journal of Theoretical Biology*, 289, 181–196.
- Aguiar, M., Ballesteros, S., Boto, J.P., Kooi, B.W., Mateus, L., Stollenwerk, N. (2011 b). Parameter estimation in epidemiology: from simple to complex dynamics. *AIP Conference Proceedings*, 1389, 1248–1251.
- Aguiar, M., Kooi B.W., & Stollenwerk N. (2011 c). Scaling of stochasticity in DHF epidemics. (see **Chapter 5**).



- Aguiar, M., Stollenwerk N., & Kooi B.W. (2011 d). Irregularity in dengue fever epidemics: difference between first and secondary infections drives the rich dynamics more than the detailed number of strains. (**see Chapter 6**).
- Alcon, S. et al. (2002). Enzyme-Linked Immunosorbent Assay Specific to Dengue Virus Type 1 Nonstructural Protein NS1 Reveals Circulation of the Antigen in the Blood during the Acute Phase of Disease in Patients Experiencing Primary or Secondary Infections. *Journal of Clinical Microbiology*, 40, 376–381.
- Alonso, D., McKane, A., & Pascual, M. (2006). Stochastic Amplification in Epidemics. *Journal of the Royal Society Interface*, 4, 575–582.
- Anderson, R. M., & May, R.M. (1979). Population biology of infectious diseases: Part I. *Nature*, 280, 361–67.
- Doedel J.E. & Oldeman, B. (2009). AUTO 07P Continuation and bifurcation software for ordinary differential equations. *Technical Report: Concordia University, Montreal, Canada*, Retrieved from <http://indy.cs.concordia.ca/auto/>
- Billings, L., et al. (2007). Instabilities in multiserotype disease models with antibody-dependent enhancement. *Journal of Theoretical Biology*, 246, 18–27.
- Boer, M.P., Kooi, B.W. & Kooijman, S.A.L.M. (1999). Homoclinic and heteroclinic orbits in a tri-trophic food chain. *Journal of Mathematical Biology*, 39, 19–38.
- Boer, M.P., Kooi, B.W. & Kooijman, S.A.L.M. (2001). Multiple attractors and boundary crises in a tri-trophic food chain. *Mathematical Biosciences*, 169, 109–128.
- Centers for Disease Control and Prevention. (2011). *Dengue*. Retrieved from <http://www.cdc.gov/dengue/>
- Chareonsook, O. et al. (1999). Changing epidemiology of dengue hemorrhagic fever in Thailand. *Epidemiol. Infect.*, 122, 161–166.
- Dejnirattisai, W. et al. (2010). Cross-Reacting Antibodies Enhance Dengue Virus Infection in Humans. *Science*, 328, 745–748.
- Drepper, F.R., Engbert, R., & Stollenwerk, N. (1994). Nonlinear time series analysis of empirical population dynamics. *Ecological Modelling*, 75/76, 171–181.
- Endy, T.P. et al. (2002). Spatial and Temporal Circulation of Dengue Virus Serotypes: A Prospective Study of Primary School Children in Kamphaeng Phet, Thailand. *Am. J. Epidemiol.*, 156, 52–59.

- Esteva, L. & Vargas, C. (1998). Analysis of a dengue disease transmission model. *Mathematical Biosciences*, 150, 131–151.
- Esteva, L. & Vargas, C. (2000) Influence of vertical and mechanical transmission on the dynamics of dengue disease. *Mathematical Biosciences*, 167, 51–64.
- Eckmann, J.P., Oliffson-Kamphorst, S., Ruelle, D., & Ciliberto, S. (1986). Liapunov exponents from time series. *Phys. Rev A.*, 34, 4971–9.
- Farmer, J.D., & Sidorowich, J.J. (1987). Predicting chaotic time series. *Phys. Rev. Lett.*, 95, 845–848.
- Favier, C., et al. (2005). Influence of spatial heterogeneity on an emerging infectious disease: the case of dengue epidemics. *Proc. Biol. Sci.*, 272, 1171–7.
- Ferguson, N., Anderson, R. & Gupta, S. (1999). The effect of antibody-dependent enhancement on the transmission dynamics and persistence of multiple-strain pathogens. *Proc. Natl. Acad. Sci. USA*, 96, 790–94.
- Fischer, D.B., & Halstead, S.B. (1970). Observations related to pathogenesis of dengue hemorrhagic fever. V. Examination of age specific sequential infection rates using a mathematical model. *J. Biol. Med.*, 42, 329–49.
- Gibbons, V.R. et al. (2007). Analysis of Repeat Hospital Admissions for Dengue to Estimate the Frequency of Third or Fourth Dengue Infections Resulting in Admissions and Dengue Hemorrhagic Fever, and Serotype Sequences. *Am. J. Trop. Med. Hyg.*, 77, 910–913.
- Gillespie, D.T. (1976). A general method for numerically simulating the stochastic time evolution of coupled chemical reactions. *Journal of Computational Physics*, 22, 403–434.
- Gillespie, D.T. (1978). Monte Carlo simulation of random walks with residence time dependent transition probability rates. *Journal of Computational Physics*, 28, 395–407.
- Golubitsky, M., & Schaeffer, D.G. (1985). *Singularities and groups in bifurcation theory*. (Springer, New York).
- Gubler, J.D., Suharyono, W., Tan, R., Abidin, M. & Sie, A. (1981). Viraemia in patients with naturally acquired dengue infection. *Bull World Health Organ.*, 59, 623–630.
- Gubler D.J., (2002). Epidemic dengue/dengue hemorrhagic fever as a public health, social and economic problem in the 21st century. *Trends in Microbiology*, 10, 100–103.

- Guckenheimer, J. & Holmes, P. (1985). *Nonlinear Oscillations, Dynamical Systems and Bifurcations of Vector Fields*. (Springer-Verlag, New York).
- Guzmán, M.G. et al. (2000). Epidemiologic Studies on Dengue in Santiago de Cuba, 1997. *Am. J. Epidemiol.*, 152, 793–799.
- Guzmán, M.G. et al. (2010). Dengue: a continuing global threat. *Nature Reviews Microbiology*, 8, S7–S16.
- Haken, H. (1983). At least one Lyapunov exponent vanishes if the trajectory of an attractor does not contain a fixed point, *Physics Letters*, 94A, 71–72.
- Halstead S.B., et al. (1969). Dengue and chikungunya virus infection in man in Thailand, 1962–1964. V. Epidemiologic observations outside Bangkok. *Am. J. Trop. Med. Hyg.* 18, 1022–33.
- Halstead, S.B., & Rourke, E.J. (1977). Dengue viruses and mononuclear phagocytes I: infection enhancement by non neutralizing antibody. *J. Exp. Med.*, 146, 201–17.
- Halstead, S.B. (1982). Immune enhancement of viral infection. *Progress in Allergy*, 31, 301–364.
- Halstead, S.B. (1994). Antibody-dependent Enhancement of Infection: A Mechanism for Indirect Virus Entry into Cells. *Cellular Receptors for Animal Viruses*, 28, Chapter 25, 493–516. (Cold Spring Harbor Laboratory Press).
- Halstead, S.B. (2003). Neutralization and antibody-dependent enhancement of dengue viruses. *Advances in Virus Research*, 60, 421–467.
- Halstead, S.B. (1994). Antibody-dependent Enhancement of Infection: A Mechanism for Indirect Virus Entry into Cells. *Cellular Receptor for Animal Viruses*, 28, Chapter 25, 493–516. Cold Spring Harbor Laboratory Press 0-87969-429-7/94.
- Halstead, S.B. (2008). Tropical Medicine: Science and Practice. *Dengue*, Volume 5, Chapter 7. (Imperial College Press).
- He, D., Ionides, E.L., King, A.A. (2010). Plug-and-play inference for disease dynamics: measles in large and small populations as a case study. *J. R. Soc. Interface*, 7, 271–283.
- Holzfuß, J., & Lauterborn, W. (1989). Liapunov exponents from a time series of acoustic chaos. *Physical Review A*, 39, 2146–2152.
- Holzfuß, J., & Parlitz, U. (1991). Lyapunov exponents from time series. *Lecture Notes in Mathematics*, 1486, 263–270.

- Ionides, E., Breto, C., & King, A.A. (2006). Inference for nonlinear dynamical systems. *Proc. Natl. Acad. Sci. USA*, 103, 18438–18443.
- Keeling, M.J. & Ross, J.V. (2008). On methods for studying stochastic disease dynamics. *Journal of the Royal Society Interface*, 5, 171–181.
- Kliks, S.C., Nisalak, A., Brandt, W.E., Wahl, L., & Burke, D.S. (1989). Antibody-dependent enhancement of dengue virus growth in human monocytes as a risk factor for dengue hemorrhagic fever. *Am. J. Trop. Med. Hyg.*, 40, 444–51.
- Kooi, B.W., & Boer, M.P. (2002). Chaotic behaviour of a predator-prey system. *Dynamics of Continuous, Discrete and Impulsive Systems, Series B: Applications and Algorithms*, 10, 259–272.
- Kooi, B.W., Kuijper, L.D.J., & Kooijman, S.A.L.M. (2004). Consequence of symbiosis for food web dynamics. *Journal of Mathematical Biology*, 49, 227–271.
- Kooi, B.W., v. Voorn, G.A.K. & pada Das, K. (2011). Stabilisation and complex dynamics in a predator-prey model with predator suffering from an infectious disease. *Ecological Complexity*, 8, 113–122.
- Kuznetsov, Y.A. (2004). *Elements of Applied Bifurcation Theory*. (Springer-Verlag, 3 edition, New York).
- Lourenço, J., & Recker, M. (2010). Viral and Epidemiological Determinants of the Invasion Dynamics of Novel Dengue Genotypes. *PLoS Negl. Trop. Dis.*, 4, e894.
- Malchow, H., Petrovskii, S.V. & Venturino, E. (2008). *Spatiotemporal Patterns in Ecology and Epidemiology: Theory, Models, and Simulation*. (Chapman & Hall/CRC Press edition).
- McKane, A.J., & Newman, T.J. (2005). Predator-prey cycles from resonant amplification of demographic stochasticity. *Phys. Rev. Lett.*, 94, 218102–7.
- Mackenzie, J.S., Gubler, D.J., & Petersen, L.R. (2004). Emerging flaviviruses: the spread and resurgence of Japanese encephalitis, West Nile and dengue viruses. *Nature Medicine Review*, 12, S98–S109.
- Massad, E., et al. (2008). Scale-free network of a dengue epidemic. *Applied Mathematics and Computation*, 195, 376–381.
- Matheus, S. et al. (2005). Discrimination between Primary and Secondary Dengue Virus Infection by an Immunoglobulin G Aviditnoy Test Using a Single Acute-Phase Serum Sample. *Journal of Clinical Microbiology*, 43, 2793–2797.

- Mattheij, R.M.M. and Molenaar, J. (1996). *Ordinary differential equations in theory and practice.*, ISBN 0-89871-531-8, (Wiley, Chichester and New York).
- Monath T.P., (1994). Dengue: The risk to developed and developing countries. *Proc. Natl. Acad. Sci. U.S.A.*, 91, 2395–2400.
- Nagao, Y., & Koelle, K.(2008). Decreases in dengue transmission may act to increase the incidence of dengue hemorrhagic fever. *Proc. Natl. Acad. Sci. USA*, 105, 2238–2243.
- Nisalak, A. et al. (2003). Serotype-specific dengue virus circulation and dengue disease in Bangkok, Thailand from 1973 to 1999. *Am. J. Trop. Med. Hyg.*, 68, 191–202.
- Ott, E. (1993). *Chaos in Dynamical Systems.* Cambridge University Press. (Cambridge University Press, Cambridge, 2nd edition).
- Packard, N.H., Crutchfield, J.P., Farmer, J.D., & Shaw, R.S. (1980). Geometry from a Time Series. *Phys. Rev. Lett.*, 45, 712–716.
- Pediatric Dengue Vaccine Initiative. International Vaccine Institute (IVI). *Global Burden of Dengue.* Retrieved from [http://www.pdvi.org/about\\_dengue/GBD.asp](http://www.pdvi.org/about_dengue/GBD.asp)
- Parlitz, U. (1992). Identification of true and spurious Lyapunov exponents from time series. *Int. J. Bif. Chaos*, 2, 155–165.
- Recker, M. et al. (2009). Immunological serotype interactions and their effect on the epidemiological pattern of dengue. *Proc. R. Soc. B.*, 276, 2541–2548.
- Rigau-Pérez, J.G., et al. (1998). Dengue and dengue haemorrhagic fever. *The Lancet*, 352, 971–77.
- Rosen, L. et al. (1983). Transovarial transmission of dengue viruses by mosquitoes: *A. albopictus* and *A. aegypti*. *Am. J. Trop. Med. Hyg.*, 32, 1108–19.
- Rothman, A.L. (2004) . Dengue: defining protective versus pathologic immunity. *Journal of Clinical Investigation*, 113, 946–51.
- Eckmann, J.-P., Kamphorst, O.S., Ruelle, D. & Ciliberto, S. (1986). Liapunov exponents from time series. *Physical Review A*, 34, 4971–4979.
- D. Ruelle. (1989). *Chaotic Evolution and Strange Attractors.* (Cambridge University Press, Cambridge).

- Pers comm.: Francisco Lemos, Secretaria de Estado de Saúde de Minas Gerais, Brazil; Sônia Diniz, Fundação Ezequiel Dias, Minas Gerais, Brazil and Scott Halstead, Pediatric Dengue Vaccine Initiative, Maryland, USA.
- Schwartz, I.B., et al. (2005). Chaotic desynchronization of multi-strain diseases. *Physical Review*, E 72, 066201–6.
- Seydel, R. (1994). *Practical bifurcation and stability analysis—from equilibrium to chaos*. (Springer-Verlag, New York).
- Stephenson, J.R., (2005). Understanding dengue pathogenesis: implications for vaccine design. *Bull. World Health Organ.*, 83, 308–14.
- Stiefs, D., Venturino, E. & Feudel, U. (2009). Evidence of chaos in eco-epidemic models. *Mathematical Biosciences and Engineering*, 6, 855–871.
- Stollenwerk, N., & Jansen, V.A.A. (2003). Meningitis, pathogenicity near criticality: the epidemiology of meningococcal disease as a model for accidental pathogens. *J. Theor. Biol.*, 222, 347–359.
- Stollenwerk, N., & Jansen, V.A.A. (2003). Evolution towards criticality in an epidemiological model for meningococcal disease. *Physics Letters A*, 317, 87–96.
- Stollenwerk, N., Maiden, M.C.J., & Jansen, V.A.A. (2004). Diversity in pathogenicity can cause outbreaks of meningococcal disease. *Proc. Natl. Acad. Sci. USA*, 101, 10229–10234.
- Stollenwerk, N., & Jansen, V. (2011). *Population biology and criticality* (Imperial College Press, London).
- Stollenwerk, N., van Noort, S., Martins, J., Aguiar, M., Hilker, F., Pinto, A., & Gomes G. (2010). A spatially stochastic epidemic model with partial immunization shows in mean field approximation the reinfection threshold. *Journal Of Biological Dynamics*, 4, 634–649.
- Stone, L., Olinky, R., & Amit Huppert, A. (2007). Seasonal dynamics of recurrent epidemics. *Nature*, 446, 533–36.
- Takens, F. (1980). *Detecting strange attractors in turbulence*. (Lecture Notes in Mathematics, Springer, Berlin).
- World Population Prospects: The 2008 Revision. *Population Database*. Retrieved from <http://esa.un.org/unpp/index.asp?panel=2>
- van Kampen, N.G. (1992). *Stochastic Processes in Physics and Chemistry*. (North-Holland, Amsterdam).

- David, W.V., Green, S., Kalayanarooj, S., Innis, L.B., Nimmannitya, S., Suntayakorn, S., Endy, P.T., Raengsakulrach, B., Rothman, L.A., Ennis, A.F., & Nisalak, A. (2000). Dengue viremia titer, Antibody Response Pattern, and Virus Serotype Correlate with Disease Severity. *J. Infect. Dis.*, 181, 2–9.
- Wearing, H.J., & Rohani, P. (2006). Ecological and immunological determinants of dengue epidemics *Proc. Natl. Acad. Sci. USA* , 103, 11802–11807.
- Weisstein, E.W. (2010). “*Kermack-McKendrick Model.*” *From MathWorld – A Wolfram Web Resource.* Retrieved from <http://mathworld.wolfram.com/Kermack-McKendrickModel.html>
- Welsh, R.M., & Selin, L.K. (2002). No one is naive: The significance of heterologous T-cell immunity. *Nature Reviews in Immunology*, 2, 417–426.
- Wikipedia contributors. Wikipedia, The Free Encyclopedia. *Provinces of Thailand.* Retrieved from [http://en.wikipedia.org/wiki/Provinces\\_of\\_Thailand](http://en.wikipedia.org/wiki/Provinces_of_Thailand)
- World Health Organization. (2009). *Dengue and Dengue Hemorrhagic Fever, Fact sheet 117.* Retrieved from <http://www.who.int/mediacentre/factsheets/fs117/en/>
- World Health Organization: Health statistics and health information systems (2010). *The global burden of disease: 2004 update*, ISBN 978 92 4 156371 0. Retrieved from [http://www.who.int/healthinfo/global\\_burden\\_disease/GBD\\_report\\_2004update\\_AnnexA.pdf](http://www.who.int/healthinfo/global_burden_disease/GBD_report_2004update_AnnexA.pdf)
- World Health Organization – Programs and Projects: Initiative for Vaccine Research (2011). *Vector borne infections.* Retrieved from [http://www.who.int/vaccine\\_research/diseases/vector/en/index1.html#virology](http://www.who.int/vaccine_research/diseases/vector/en/index1.html#virology)
- United Nations Population Division. (2011). *World Urbanization Prospects: The 2009 Revision Population Database.* Retrieved from <http://www.un.org/esa/population/unpop.htm>



# Acknowledgments

I would like to express my sincere gratitude to my supervisors, Nico Stollenwerk and Bob W. Kooi, for their patience, motivation, enthusiasm, and immense knowledge. Their guidance was essential during all the time of my research and I could not have imagined having better advisors and mentors for my Ph.D study.

My sincere thanks also go to my co-supervisor, Dr. Francisco Dionísio, who supported me from the initial to the final level and enabled me to finalize the PhD course at Science Faculty in Lisbon University. Special thanks to Sônia Diniz, who provided valuable experience and knowledge on dengue fever epidemiology. A special thanks also to Dr. Gabriela Gomes, who supported me as a scientist and gave me the opportunity to learn and love theoretical biology.

My sincere thanks to Prof. Dr. S.A.L.M. Kooijman for supporting me on the opportunity of the Double Doctorate Degree at Vrije Universiteit Amsterdam.

I also like to extend my thanks to Prof. Luis Sanchez for the scientific and organizational support at Centro de Matemática e Aplicações Fundamentais da Universidade de Lisboa.

I thank my colleagues from the Theoretical Epidemiology Group at the Gulbenkian Institute of Science and my colleagues in the Centro de Matemática e Aplicações Fundamentais, Lisbon University, for many discussions and calculations who motivated me and inspired me during my work on dynamical systems applied to infectious diseases, Prof. Scott Halstead, Bethesda, Maryland, and Dr. Francisco Lemos, Belo Horizonte, Minas Gerais for detailed information about dengue epidemiology.

I cannot forget to express appreciation to Prof. Bernard Cazelles, Ecole Normale Supérieure, France for providing the available DHF incidence data in Thailand. Prof. Yoshiro Nagao, Osaka University Graduate School of Medicine in Japan, and Prof. Katia Koelle, Biology Department of Duke University in the USA for providing the extended Thailand DHF incidence data.

Last but not the least, I would like to thank my beloved family: my husband and partner Nico and my beautiful daughter Iara, my parents Roseli and Mario and my sisters Daniela and Marina, who supported me in any respect during the completion of my PhD project.





# Curriculum vitae

Maíra Aguiar Freire dos Santos  
born October 31, 1980  
Belo Horizonte, Minas Gerais, Brazil  
*maira@ptmat.fc.ul.pt*



I studied biological sciences at Pontifícia Universidade Católica de Minas Gerais (PUC-Minas), Brazil, from 2000 to 2004. From 2002 to 2004 I worked at Fundação Ezequiel Dias (FUNED) at Divisão de Epidemiologia e Controle de Doenças (DECD), Dengue and Yellow Fever Laboratory, as a technician, performing serological diagnosis and epidemiological data analysis. In 2004, as a biologist, I was the responsible for the dengue and yellow fever laboratory at Serviço de Virologia e Riquetsioses (SVR) at FUNED. During this period, results of immunological testing were combined with epidemiological data to create a comprehensive database, which was made available to public health authorities in order to control the impact of epidemics, promote control strategies and optimize health care provision.

I followed a post graduation course in statistics applied to biology and health sciences at Lisbon University, Portugal (2006-2007) and worked on the Project “Reinfection Threshold and the Management of Recurrent Infections” at Gulbenkian Institute of Science (IGC), Portugal (2006-2009), under supervision of Dr. Nico Stollenwerk and Dr. Gabriela Gomes. During my PhD I worked on epidemic models development and data analysis. My research crosses the different epidemiological areas of infectious diseases, with special focus on the study of dengue fever and its dynamics in the social and political environment, by developing mathematical models which can be used by public health authorities as a tool to predict, understand the transmission of the disease and develop and evaluate the introduction of intervention strategies including vector control and vaccination.

## Publications in refereed international journals:

1. Massad, E., Ma S., Chen, M., Struchiner, J.C., Stollenwerk, N., & Aguiar, M. (2008). Scale-free network of a dengue epidemic. *Applied Mathematics and Computation*, 195, 376–381.
2. Aguiar, M., Kooi, B.W., & Stollenwerk, N. (2008). Epidemiology of Dengue Fever: A Model with Temporary Cross-Immunity and Possible Secondary Infection Shows Bifurcations and Chaotic Behavior in Wide Parameter Regions (see Chapter 2). *Math. Model. Nat. Phenom.*, 4, 48–70.
3. Aguiar, M., Stollenwerk, N., & Kooi, B.W. (2009). Torus bifurcations, isolas and chaotic attractors in a simple dengue model with ADE and temporary cross immunity (see Chapter 3). *International Journal of Computer Mathematics*, 86, 1867–1877.
5. Stollenwerk, N., van Noort, S., Martins, J., Aguiar, M., Hilker, F., Pinto, A. & Gomes, G. (2010). A spatially stochastic epidemic model with partial immunization shows in mean field approximation the reinfection threshold. *Journal of Biological Dynamics*, 4, 634–649.
6. Pinto, A., Aguiar, M., Martins, J. & Stollenwerk, N. (2010). Dynamics of epidemiological models. *Acta Biotheoretica*, 58, 381–389.
7. Aguiar, M. (2011). The effect of global warming on vector-borne diseases: Comment on "Modeling the impact of global warming on vector-borne" infections by E. Massad et al. *Physics of Life Reviews*, 8, 202–203.
4. Martins, J., Aguiar, M., Pinto, A., & Stollenwerk, N. (2011). On the series expansion of the spatial SIS evolution operator. *Journal of Difference Equations and Applications*, 17, 1107–1118.
8. Aguiar, M., Ballesteros, S., Kooi, B.W., & Stollenwerk, N. (2011). The role of seasonality and import in a minimalistic multi-strain dengue model capturing differences between primary and secondary infections: complex dynamics and its implications for data analysis (see Chapter 4). *Journal of Theoretical Biology*, 289, 181–196.
9. Aguiar, M., Stollenwerk, N. & Kooi, B.W. (2011). Scaling of stochasticity in dengue hemorrhagic fever epidemics (see Chapter 5). *under review*.
10. Aguiar, M., Stollenwerk, N. & Kooi, B.W. (2011). Irregularity in dengue fever epidemics: difference between first and secondary infections drives the rich dynamics more than the detailed number of strains (see Chapter 6). *submitted*.
11. Stollenwerk, N., Aguiar, M., Ballesteros, S., Boto, J., Kooi, B.W. & Mateus, & L. (2011). Dynamic noise, chaos and parameter estimation in population biology. *accepted to be published in Interface Focus*.

## Refereed conference contributions in scientific books:

1. Aguiar, M., Stollenwerk, N., & Kooi, B.W. (2008). Torus bifurcations, isolas and chaotic attractors in a simple dengue model with ADE and temporary cross immunity. *Proceedings of 8th Conference on Computational and Mathematical Methods in Science and Engineering, CMMSE*, ISBN 978-84-612-1982-7, edited by Jesus V.A. et al., Murcia, pp. 23–35.
2. Stollenwerk, N., Aguiar, M., & Kooi, B.W. (2009). Computational aspects in the investigation of chaotic multi-strain dengue models. *Proceedings of 9th Conference on Computational and Mathematical Methods in Science and Engineering, CMMSE*, ISBN 978-84-612-9727-6, edited by Jesus Vigo Aguiar et al., Gijón, pp. 995–1002.
3. Maíra Aguiar & Ezio Venturino. (2009). Symposium on Biomathematics. *AIP Conference Proceedings*, 1168, 1525–1526.
4. Aguiar, M., Kooi, B.W. & Stollenwerk, N. (2009). Multi-strain deterministic chaos in dengue epidemiology, a challenge for computational mathematics. *AIP Conference Proceedings*, 1168, 1555–1558.
5. Aguiar, M., Ballesteros, S., & Stollenwerk, N. (2010). The influence of seasonality on dengue epidemiology, modeling and data analysis. *Proceedings of 10th Conference on Computational and Mathematical Methods in Science and Engineering, CMMSE*, ISBN 978-84-613-5510-5, edited by Jesus V.A. et al., Almería, pp. 25–35.
6. Stollenwerk, N., Aguiar, M., Ballesteros, S., & Kooi, B.W. (2010). Certain uncertainties in population biology revisited. *Proceedings of 10th Conference on Computational and Mathematical Methods in Science and Engineering, CMMSE*, ISBN 978-84-613-5510-5, edited by Jesus V.A. et al., Almería, pp.840–48.
7. Aguiar, M., Ballesteros, S., & Stollenwerk, N. (2010). Two strain dengue model with temporary cross immunity and seasonality. *AIP Conference Proceedings*, 1168, 732–735.
8. Aguiar, M., Ballesteros, S., & Stollenwerk, N. (2010). Dynamic noise and its role in understanding epidemiological processes. *AIP Conference Proceedings*, 1168, 736–40.
9. Maíra Aguiar & Ezio Venturino. (2010). Symposium on Biomathematics. *AIP Conference Proceedings*, 1168, 709–11.
10. Maíra Aguiar & Ezio Venturino. (2011). Symposium on Biomathematics. *AIP Conference Proceedings*, 1389, 1204–1207.
11. Aguiar, M., Stollenwerk, N. & Kooi, B.W. (2011). The stochastic multi-strain dengue model: analysis of the dynamics. *AIP Conference Proceedings*, 1389, 1224–1227.

12. Aguiar, M., Ballesteros, S., Boto, J.P., Kooi, B.W., Mateus, L., & Stollenwerk, N. (2011). Parameter estimation in epidemiology: from simple to complex dynamics. *AIP Conference Proceedings*, 1389, 1248–1251.

### **Book chapters:**

1. Aguiar, M., Kooi, B.W. & Stollenwerk, N. (2011). Modeling infectious diseases dynamics: Dengue fever, a case study (see Chapter 1). *Epidemiology*, InTech, ISBN: 979-953-307-754-2.

### **Scientific meetings organized:**

1. Workshop DSABNS - Third Workshop Dynamical Systems Applied to Biology and Natural Sciences. Lisbon, Portugal (February 2012).

2. Mini-symposium at ICNAAM - Mini-symposium “Biomathematics” (September 2011).

3. Mini-Symposium at ECMTB - Mini-Symposium “Modeling dengue fever epidemiology” (June 2011).

4. Workshop DSABNS - Second Workshop Dynamical Systems Applied to Biology and Natural Sciences. Lisbon, Portugal (February 2011).

5. Mini-symposium at ICNAAM - Mini-symposium “Biomathematics” (September 2010).

6. Mini-symposium at CMMSE - Mini-symposium “Bio-Mathematics” (June 2010).

7. Workshop DSABNS - First Workshop Dynamical Systems Applied to Biology and Natural Sciences. Lisbon, Portugal (February 2010).

8. Mini-symposium at ICNAAM - Mini-symposium “Biomathematics” (September 2009).

9. Mini-symposium at CMMSE - Mini-symposium “Bio-Mathematics” (July 2009).